



LUND UNIVERSITY

Understanding the Role of Seed Particle Material on III-As Nanowire Growth

Sun, Rong

2018

Document Version:

Publisher's PDF, also known as Version of record

[Link to publication](#)

Citation for published version (APA):

Sun, R. (2018). *Understanding the Role of Seed Particle Material on III-As Nanowire Growth*. [Doctoral Thesis (compilation), Solid State Physics]. Lund University, Faculty of Engineering.

Total number of authors:

1

General rights

Unless other specific re-use rights are stated the following general rights apply:

Copyright and moral rights for the publications made accessible in the public portal are retained by the authors and/or other copyright owners and it is a condition of accessing publications that users recognise and abide by the legal requirements associated with these rights.

- Users may download and print one copy of any publication from the public portal for the purpose of private study or research.
- You may not further distribute the material or use it for any profit-making activity or commercial gain
- You may freely distribute the URL identifying the publication in the public portal

Read more about Creative commons licenses: <https://creativecommons.org/licenses/>

Take down policy

If you believe that this document breaches copyright please contact us providing details, and we will remove access to the work immediately and investigate your claim.

LUND UNIVERSITY

PO Box 117
221 00 Lund
+46 46-222 00 00



Understanding the Role of Seed Particle Material on III-As Nanowire Growth

RONG SUN

SOLID STATE PHYSICS | LTH | LUND UNIVERSITY



Understanding the Role of Seed Particle Material on III-As Nanowire Growth

Understanding the Role of Seed Particle Material on III-As Nanowire Growth

Rong Sun



LUND
UNIVERSITY

DOCTORAL DISSERTATION

by due permission of the Faculty of Engineering, Lund University, Sweden.
To be defended on 24th Aug 2018, at 13:00 in Rydbergsalen, Sölvegatan 14, Lund.

Faculty opponent

Dr. Lutz Geelhaar

Paul-Drude-Institut für Festkörperelektronik (PDI)

Organization LUND UNIVERSITY	Document name DOCTORAL DISSERTATION	
	Date of issue 2018-05-25	
Author Rong Sun	Sponsoring organization	
Title Understanding the Role of Seed Particle Material on III-As Nanowire Growth		
<p>Abstract</p> <p>III-V semiconductor nanowires have attracted extensive research interests over the past few decades due to their unique geometry and great potential for promoting new functionalities in future electronics, light-emitting diodes and solar cells. However, in order to push this technology beyond the laboratory level, it is essential to combine it with the current Si-based semiconductor industry for affordable production. The synthesis of III-As nanowires relies mostly on the use of Au as seed particle, which as a result of high diffusivity of Au in Si, limits the possibility to integrate III-As nanowires into Si devices.</p> <p>The purpose of this thesis is trying to get a better understanding of which properties might be desirable for a material to act as seed particle to assist nanowire growth.</p> <p>This thesis studies Sn-seeded growth of GaAs, InAs and InGaAs nanowires by MOVPE, and how the growth process can be controlled to tailor the nanowire morphology and crystal phase to some extent. The in-situ formation of Sn particles on various substrates has been investigated. The temperature range and the flow of growth precursors for Sn-seeded nanowire growth differ a lot from nanowire growth from Au seed particles. In contrast to Au-seeded nanowires, Sn-seeded GaAs and InAs nanowires mostly exhibit zincblende crystal phase. Furthermore, a big advantage of using Sn as seed material is the simultaneous incorporation of the particle material into the nanowire during growth, leading to nanowires with high n-type doping profile.</p>		
<p>Key words</p> <p>semiconductor materials, nanowire growth, catalyst, metal-organic vapor phase epitaxy, tin</p>		
Classification system and/or index terms (if any)		
Supplementary bibliographical information	Language English	
ISSN and key title	<p>ISBN</p> <p>978-91-7753-732-8 (print)</p> <p>978-91-7753-733-5 (pdf)</p>	
Recipient's notes	Number of pages	Price
	Security classification	

I, the undersigned, being the copyright owner of the abstract of the above-mentioned dissertation, hereby grant to all reference sources permission to publish and disseminate the abstract of the above-mentioned dissertation.

Signature



Date 2018.05.28

Understanding the Role of Seed Particle Material on III-As Nanowire Growth

Rong Sun



LUND
UNIVERSITY

Coverphoto and back coverphoto by Rong Sun

Copyright (Rong Sun)

Paper I © 2015 American Chemical Society, DOI: 10.1021/acs.nanolett.5b00276

Paper II © 2016 IOP Publishing Ltd, DOI: 10.1088/0957-4484/27/21/215603

Paper III © 2018, by the authors

Paper IV © 2018, by the authors


Solid State Physics
Department of Physics
Lund University
SE-22100 Lund
Sweden

ISBN 978-91-7753-732-8 (print)

ISBN 978-91-7753-733-5 (pdf)

Printed in Sweden by Media-Tryck, Lund University
Lund 2018



MADE IN SWEDEN 

Media-Tryck is an environmental-
ly certified and ISO 14001 certified
provider of printed material.
Read more about our environmental
work at www.mediatryck.lu.se

To my receding hairline

Table of Contents

Abstract	11
Popular Science	13
Acknowledgement.....	15
List of Papers.....	17
1 Introduction.....	19
1.1 Nanowires.....	19
1.2 Outline of the thesis	21
2 Epitaxial Growth by Metalorganic Vapour Phase Epitaxy	23
2.1 General concepts about MOVPE	23
2.2 Thermodynamic aspects of epitaxial growth	25
2.3 Physical processes occurring on the surface.....	27
2.3.1 Adsorption and desorption	27
2.3.2 Surface diffusion	27
2.4 Pyrolysis of the precursors.....	28
2.5 Kinetic aspects of epitaxial growth.....	29
3 Epitaxial Growth of Semiconductor Nanowires	31
3.1 Nanowire nucleation theory.....	32
3.2 The crystal structure of III-V nanowires.....	36
3.3 Alternative approaches for III-V nanowires growth.....	38
3.3.1 Selective area epitaxy and self-seeded nanowire epitaxy	38
3.3.2 Alternative foreign metal-seeded nanowires.....	40
3.3.3 Properties of Sn	42
4 III-As Semiconductor Nanowires	45
4.1 GaAs and InAs nanowires	45
4.2 InGaAs nanowires.....	49

5	Sn-Seeded Nanowire Growth.....	51
5.1	Sn-seeded GaAs nanowire growth (Paper I and II)	51
5.1.1	The formation of Sn particles on GaAs substrates	51
5.1.2	Growth of Sn-seeded GaAs nanowires dependency on temperature and V/III ratio	54
5.1.3	Properties of Sn-seeded GaAs nanowires	57
5.2	Sn-seeded InAs nanowire growth (Paper III and IV)	59
5.2.1	The formation of Sn particles on InAs substrates	59
5.2.2	Growth of Sn-seeded InAs nanowires dependent on temperature and V/III ratio	60
5.2.3	Properties of Sn-seeded InAs nanowires.....	62
5.3	Sn-seeded GaAs-InGaAs heterostructures.....	64
6	Summary and outlook	67
7	References	69

Abstract

III-V semiconductor nanowires have attracted extensive research interests over the past few decades due to their unique geometry and great potential for promoting new functionalities in future electronics, light-emitting diodes and solar cells. However, in order to push this technology beyond the laboratory level, it is essential to combine it with the current Si-based semiconductor industry for affordable production. The synthesis of III-As nanowires relies mostly on the use of Au as seed particle, which as a result of high diffusivity of Au in Si, limits the possibility to integrate III-As nanowires into Si devices.

The purpose of this thesis is trying to get a better understanding of which properties might be desirable for a material to act as seed particle to assist nanowire growth.

This thesis studies Sn-seeded growth of GaAs, InAs and InGaAs nanowires by MOVPE, and how the growth process can be controlled to tailor the nanowire morphology and crystal phase to some extent. The in-situ formation of Sn particles on various substrates has been investigated. The temperature range and the flow of growth precursors for Sn-seeded nanowire growth differ a lot from nanowire growth from Au seed particles. In contrast to Au-seeded nanowires, Sn-seeded GaAs and InAs nanowires mostly exhibit zincblende crystal phase. Furthermore, a big advantage of using Sn as seed material is the simultaneous incorporation of the particle material into the nanowire during growth, leading to nanowires with high n-type doping profile.

Popular Science

Modern life is full of semiconductors. The word ‘semiconductor’ sounds remote, but is actually something that is all round us. Our computers, mobile phones, LED lights and almost every modern device we use are all based on semiconductor components. As semiconductors have made our lives easier over the past 30 years, the semiconductor industry has also grown rapidly from USD 33 billion in 1987 to USD 409 billion in 2017.

Semiconductors have the ability to conduct electricity at some temperatures but not others. They occupy a space between conductors such as most metals, and insulators such as plastic, rubber and glass. More importantly, however, semiconductors can allow current to flow in only one direction and can also amplify a signal. Electrical current and voltage can be turned into light using semiconductors, allowing for the emission of light. This process also works in reverse.

The first semiconducting transistor was made in 1948 from germanium, but silicon quickly became, and remains, the predominant semiconductor material. One of the many advantages of silicon is its cost, with silicon being the second most abundant element in the earth’s crust, which is about 28% by mass. However, silicon does not convert light into electricity or turn electricity back to light very efficiently. Consequently, searching for new semiconductor materials is of great relevance.

III-V semiconductor materials are composed of elements from the group III and group V columns in the periodic table of elements. Their unique properties make them ideal for the application of optoelectronic devices. For example, GaAs is widely used in lasers, photodetectors and LEDs. There is a current trend towards making devices smaller in order to increase their speed and power. Scaling down the III-V materials leads to III-V nanowires. Nanowires are considered to be one-dimensional materials because their diameter is constrained to a few tens of nanometres. This can be compared to a strand of human hair, which has a diameter of about 80,000-100,000 nm; one hair is therefore comparable in diameter to 1000 nanowires.

There are a number of approaches to fabricate III-V nanowires. In this thesis, III-V nanowires are synthesized with the help from a catalytic seed particle. The seed particle could locally facilitate the chemical reaction and it also acts as a preferential collection point for the growth materials. When the growth materials are continuously accumulated inside the seed particle and reach a threshold point, the solid nanowire would simultaneously precipitates below the seed particle. The one-dimensional geometry of the nanowire relies on the anisotropic growth rates: a nanowire elongates in the direction with the highest growth rate, and other directions

with slower growth rates confine the diameter of the nanowire. The presence of seed particle facilitates this anisotropic growth.

To date, gold nanoparticles have been widely used in III-V nanowire growth. In this work, I have studied the feasibility of using alternative seed materials, in particular tin (Sn), as catalytic nanoparticles for the growth of III-V nanowires. Understanding the properties and the mechanisms of seed particles will allow us to tailor the nanowire growth to the characteristics and properties desired for potential device applications.

Acknowledgement

When I look back at the past five years, there are so many people whom have helped me and have shared a great time together. I will try my best to name and thank each of you, but if your name is not shown here, it might just have slipped away from my mind for the moment. I could never forget your contribution and this thesis would have not been possible without all your support.

The first person I want to thank without any doubt is my supervisor, Kimberly Thelander, who took me in and gave me the opportunity to start this Ph.D at the first place. I would like to thank you for the countless support and guidance during my Ph.D study. Your kind encouragements helped me tackle those hard times, especially when things were not smooth. Your patience and enthusiasm make my past five years a valuable memory in my life.

I would also like to thank my co-supervisors, Jonas Johansson and Reine Wallenberg. Jonas, you have always been very patient and kind to me and you have been helping me refresh my thermodynamic knowledge again and again. Reine, thanks for your introduction on TEM.

Sebastian Lehmann, you are an extra advisor for me. You are always willing to support me in the lab, help me with TEM. I am truly grateful for your constructive discussion, comments and input on the manuscripts.

It seems very lucky for me to join such a dynamic group with inspiring discussion and full support from the present and past group members: Luna Namazi, Robert Hallberg, Erik Mårtensson, Marcus Tornberg, Carina Babu Maliakkal, Daniel Jacobsson, Karl Winkler, Heidi Potts, Robin Sjökvist, Hanna Kindlund, Reza Zamani, Sepideh Gorji, Martin Ek, and Maria De la Mata. A special thanks to Daniel for guiding and assisting me in the lab when I started.

I am truly grateful to Claes Thelander, Malin Nilsson, I-Ju Chen and Karl Winkler for your work on electrical measurement. Thank you also for teaching and showing me how things work there.

I would like to extent my gratefulness to Neimantas Vainorius and Mats-Erik Pistol for the optical characterization and Sarah McKibbin and Rainer Timm for the STM work on my samples.

I want to thank Dan Hessman and Maria Huffman for being great mentors. Thank you for being open and sharing your life experiences and enthusiasm with me.

I appreciate the assistance and support from Nanolund lab staffs: Anders Kvennefors, Bengt Meuller, Peter Blomqvist, George Rydnemalm, Håkan Lapovski, Ivan Maximov, Mariusz Graczyk, Sara Attaran, Dmitry Suyatin, and

Søren Jeppsen. Thank you all for maintaining the lab and making it a great place to work in.

Thanks to the administrative and technical support staff of FTF: Dan Hessman, Anneli Löfgren, Heiner Linke, Anders Gustavsson, Line Lundfald, Abdul-Rehman Hakim, Mia Hedin, Charlotte Solberg, Gerda Rentschler, Loiuse Baldetorp, Johanna Mosgeller and Janne Mårtensson. Thank you for developing Nanolund and helping me with all the practical work.

I want to thank my (present and past) colleagues and friends at FTF: Maryam Khalilian, Luna Namazi, Chunlin Yu, Linus Ludvigsson, Neimantas Vainorius, Regina Schmitt, David Göransson, Killian Mergenthaler, Malin Nilsson, Xulu Zeng, Yang Chen, Laura Abariute, Frida Lindberg, Kushagr Punyani, Martin Josefsson, Zhaoxia Bi, Jonas Ohlsson, Zhen Li, Vishal Jain, David Lindgren, Alexander Berg, Fangfang Yang, Nicklas Anttu, Mingtang Deng...the list goes on and on! I am very grateful for the fun, road trip and chat that we have had together. Thank you for the memorable moments!

My life in Lund would not be so vivid and colourful without my friends in town: Feifei, Duoduo, Vincent, Duoia, Yuran, Ruixia, Suyun, Kena, Ruiyu, Xiaoting, Weimin, Yuchen, Hengfang...Thank you for hosting the get-togethers and for celebrating the many festivals together. You make me less homesick in Lund.

Last but not least, I would like to write a few sentences in Chinese to my beloved family.

感谢我的父亲母亲。感谢你们给与我的一切！感谢父亲对我的时时鞭策和鼓励；感谢母亲对我无尽的理解和包容。无论我在哪里，你们永远给我有一个温暖的家。

感谢我的先生，胡晓楠。感谢你多年来的陪伴。这一路走来，从分隔两地开始着实不易。感谢你不论在何时何地，都对我温柔以待，开导我，逗我开心，照顾好我的情绪。感谢你为了我，来到瑞典。和你在一起的每一天都让我看到除了眼前苟且以外的诗和远方田野。

Rong Sun 孙蓉

Lund, May 2018

List of Papers

- I. Sn-seeded GaAs nanowires as self-assembled radial p-n junctions
R. Sun, D. Jacobsson, IJ. Chen, M. Nilsson, C. Thelander, S. Lehmann and K. A. Dick
Nano Lett. 2015, 15, 3757–3762
I performed the growth and data analysis, and was actively involved in writing the paper.
- II. Sn-seeded GaAs nanowires grown by MOVPE
R. Sun, N. Vainorius, D. Jacobsson, M.-E. Pistol, S. Lehmann and K. A. Dick
Nanotechnology 2016, 27, 215603 (8pp)
I planned the project and performed the growth and part of data analysis, and I had the main role in writing the paper.
- III. Sn seeded defect-free zincblende InAs nanowires
R. Sun, K. Winkler, S. McKibbin, J. Johansson, R. Timm, S. Lehmann and K. A. Dick
Manuscript
I initiated and designed the project. I performed the nanowire growth and part of data analysis, and I had the main role in writing the paper.
- IV. Thermodynamic understanding on the effect of V/III ratio for the growth of Sn seeded InAs nanowires
R. Sun, J. Johansson, K. A. Dick
Manuscript
I initiated and designed the project. I performed the growth and I had the main role in writing the paper.

1 Introduction

Gordon Moore predicted in 1965 that the number of transistors on a microprocessor chip would double between every generation of about two years [1]. This has been the rule of thumb and also the driving force in the semiconductor industry behind improvements to the processing speed and capability of the chip. Despite the technological developments made in the structural design of transistors, looking for ways to develop new materials with nanoscale dimensions is one of the important challenges faced in terms of maintaining the pace of advancement in electronics performance and the semiconductor industry. The minimization on the size of materials can have significant effect on, for example, mechanical, electrical and optical properties. This minimization can also be found in different fields of science and technology where it could bring new effects into the field. For instance, the large surface-to-volume ratio of a nanostructure can increase the efficiency of a catalyst. Nanostructures can have various shapes and sizes and can be composed of different materials depending on the desired application. Nanowires are one of the many types of structures that have attracted much interest in the research community over the past few decades.

1.1 Nanowires

Nanowires are nanometre-sized rod shape materials that have a length many times that of their width. They are constrained in one dimension, with diameters in the order of tens of nanometres and lengths of up to a few micrometres. There are different types of nanowires made of various materials including metallic nanowires (e.g. Ni, Cu), oxide nanowires (e.g. ZnO, SnO₂), group IV nanowires (e.g. Si, Ge) and group III-V nanowires (e.g. GaAs, InGaAs). III-V nanowires are the focus of this thesis. They are binary or ternary compounds composed of elements from group III and group V of the periodic table. There are an enormous number of reports concerning III-V nanowire-based light emitting diodes [2][3][4], lasers [5][6] or solar cells [7][8] that indicate there is great potential for future novel applications.

The fabrication of III-V semiconductor nanowires is categorized in two general ways, namely ‘top-down’ and ‘bottom-up’. The top-down method uses bulk

material and removes most of the part with the help of lithographic and etching methods in order to leave behind the desired nanostructure. On the other hand, the bottom-up method builds up a nanostructure on the substrate from the source supply by selectively growing material from the bottom to the top. Bottom up methods of fabricating semiconductor nanowires could be a purely physical process like molecular beam epitaxy (MBE) or a more chemical process like chemical vapour deposition (CVD). Nanowires can be grown with or without a seed nanoparticle, depending on which properties are desired. This thesis will focus on the bottom-up method of fabricating III-V semiconductor nanowires with a seed particle using metalorganic vapour phase epitaxy (MOVPE) which is one type of CVD methods. A common bottom-up approach that is used to fabricate III-V semiconductor nanowires in MOVPE involves using a metal seed particle to initiate the nanowire growth, as shown schematically in Figure 1.1. The seed particles are first formed or deposited on the growth substrate. Next, the temperature is increased and the vapour source material for the growth is supplied. The seed particles then absorb elemental material species to the extent that they reach supersaturation and solid nanowires begin to precipitate at the interface of the seed particles and growth substrate. With a continuous supply of the growth material, nanowires will preferably continue to grow axially. Depending on the phase of the seed particle during nanowire growth, the process can be referred to as either vapour-liquid-solid (VLS) or vapour-solid-solid (VSS).

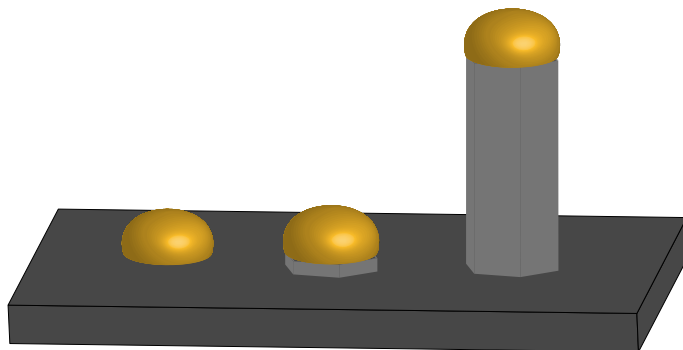


Figure 1.1 Schematic of a nanowire growth process with a seed particle.

Au has been used as the seed particle almost ever since this technique was developed. However, the ultimate goal is to combine the III-V nanowire with the low-cost Si to drive forward the advancement of the semiconductor industry. Au is one of the forbidden elements in the Si industry, since Au easily diffuses into Si and forms deep trap centres in Si, which will adversely affect the electronic property of Si [9][10]. Consequently, exploring alternative seed particle material for nanowire growth is highly relevant and important. In this thesis, I demonstrate the use of Sn

as the seed particle material for the growth of III-As nanowires. I believe that these results are not trivial and are indicative that Sn is an interesting material for initiating the growth of nanowires where high n-type doping is desired. Together with what have been reported on alternative metal-seeded nanowire growth, I hope this work can shed some light on which properties of the seed material are important for nanowire growth, and eventually this could lead to a better understanding on nanowire growth mechanism.

1.2 Outline of the thesis

This thesis focuses on exploring alternative seed particle, in particular Sn, for the synthesis of III-V semiconductor nanowires including GaAs, InAs and InGaAs material systems.

The structure of this thesis is as follows:

Chapter 2 provides an overview of the processes involved in the growth technique used in this thesis, namely metalorganic vapour phase epitaxy (MOVPE).

Chapter 3 describes the fundamental principles and the basic understanding of nanowire growth. It is followed by introducing the current progress made in the field towards achieving gold-free synthesis of nanowires.

Chapter 4 briefly introduces the properties and the growth of As-based material systems in nanowires including GaAs, InAs and InGaAs, which are relevant to my work in this thesis.

The results pertaining to the synthesis and properties of nanowires using Sn nanoparticles as a catalyst are presented in Chapter 5.

Finally, there is a discussion of the outlook for and the potential development of nanowire synthesis using alternative seed particles.

2 Epitaxial Growth by Metalorganic Vapour Phase Epitaxy

Epitaxy comes from the Greek origin ‘epi’ meaning above, and ‘taxis’ meaning in an ordered manner; thus, epitaxy is defined as ordered growth from atoms on a crystalline substrate. It is a widely used technique for depositing semiconductor materials. The orientation of the deposited layers is strongly dependent on the underlying substrate. The term homoepitaxy is used when the grown layers are the same material as the substrate; conversely, heteroepitaxy is used when they are not of the same material. This growth behaviour always comes with a phase transition from the supply phase to the solid crystal phase. The supply phase can be, for example, a solution, as in solution phase epitaxy, or a vapour, as in MOVPE, which is also the focus of this thesis.

In this chapter, I will first focus on concepts that are fundamental to MOVPE, then move on to the thermodynamic aspect of epitaxy. It will be followed by a discussion on the physical processes happening on the substrate surface and also the pyrolysis reaction of the precursors. Last but not least, I will discuss the kinetic aspects of epitaxy.

2.1 General concepts about MOVPE

MOVPE is a chemical vapour deposition technique using metalorganic compounds and hydrides as precursors to produce semiconductor crystals on the substrate. As its name indicates, this chemical deposition process occurs from vapour phase precursors to form solid phase crystals at moderate pressure, usually from 10 to 760 Torr [11]. It is now, together with molecular beam epitaxy (MBE), the predominant technique used to fabricate III-V semiconductor structures. MBE is a physical vapour deposition technique that is performed in a high or ultra-high vacuum environment, and the growth material is supplied in elemental form which is much purer than the metalorganic sources used in MOVPE. In this thesis, all the III-V nanowires are synthesized using MOVPE.

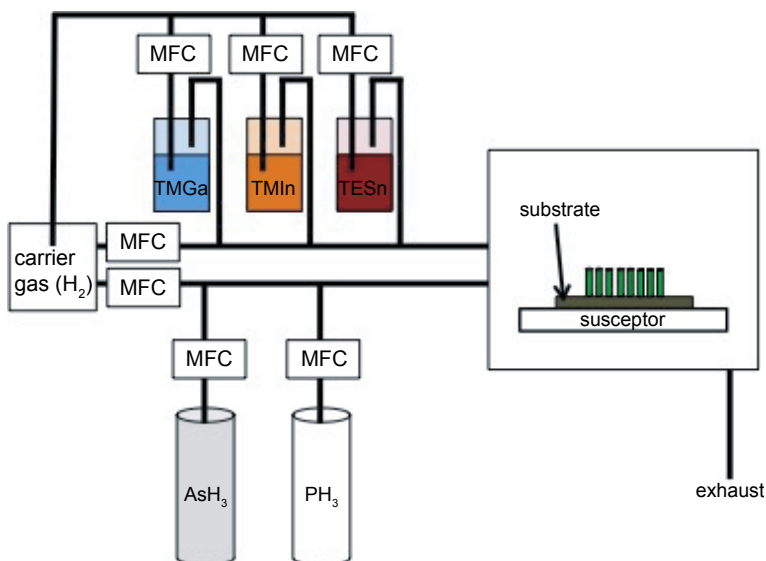


Figure 2.1 Schematic of a MOVPE setup.

A simplified schematic of a typical MOVPE setup is shown in Figure 2.1. The source materials are supplied in the form of metalorganic compounds and hydride precursors. Metalorganic compounds are often in a liquid state (like trimethylgallium TMGa) or sometimes in a solid state (like trimethylindium TMIn) at or below room temperature, which allows for convenient handling. They are kept in special containers that we call bubblers, which are kept in temperature-controlled baths. To generate metalorganic vapour, carrier gas flows into the bubbler through a pipe and is released below the liquid or solid surface of the metalorganics, causing bubbles within the metalorganic material. Since the vapour pressure of the metalorganic and the total pressure of the bubbler are not supposed to change at a set bubbler temperature within the container, abundant metalorganic vapour is mixed with carrier gas and transported via pipes into the reactor during growth. The molar flow of the metal organic sources is calculated as:

$$Q_{MO} = \left(\frac{1}{22.4 \left(\frac{1}{\text{mol}} \right)} \right) \times Q_{carrier} \times \frac{P_{MO}/P_b}{1 - P_{MO}/P_b} \quad (2.1)$$

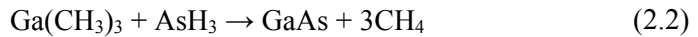
where $Q_{carrier}$ is the carrier gas flow in (*sccm*), in the setup used in this thesis it is the flow of H_2 . P_{MO} is the equilibrium vapour pressure of the metalorganic source at a set bubbler temperature, and P_b is the regulated bubbler pressure. A mass flow controller (MFC) and Epison are often used together in order to ensure that the different metalorganic precursor flows are at the desired values.

Hydride sources are stored in gas bottles in gaseous form and are controlled by different valves for open and close.

In a MOVPE system, the geometry of the reactor can vary, for instance a horizontal reactor or a vertical reactor. In the former geometry, gas precursors flow laterally with respect to the sample substrate, whereas in a vertical reactor, gas precursors flow from the top down to the sample substrate. Both types of reactor are used in the experimental part of this thesis. The sample substrate is placed on the susceptor inside the MOVPE reactor. During a growth run, the susceptor is heated to the desired growth temperature and the epitaxial growth then takes place on the substrate surface. The residual materials are pumped away through the exhaust pipe.

MOVPE growth of nanowires is a complicated process because it is sensitive to reactor pressure, substrate temperature, the flow of the carrier gas and surface chemistry. The growth process involves pyrolysis (decomposition) of the metalorganic precursors and the hydrides, substrate surface diffusion of the atoms, incorporation of the atoms into the seed particle and nucleation of the nanowire.

For instance, for GaAs nanowire growth, a group III atom such as Ga is bonded to three CH_3 molecules to form trimethylgallium (TMGa), while group V atom such as As can be supplied in either metalorganic form as tertiarybutylarsine (TBAs) or in hydride form as arsine (AsH_3). The latter As supply form is the one used in the experimental part of this thesis. Thus, the overall reaction for the growth of GaAs using TMGa and AsH_3 can be represented as:



2.2 Thermodynamic aspects of epitaxial growth

As mentioned above, there is always a phase transition in epitaxial growth. All the transitions or reactions move towards thermodynamic equilibrium where there is minimum Gibbs free energy (G).

Imagine there are two phases of a single substance coexisting in a closed system with a constant temperature and pressure, e.g. vapour and liquid. In this coexistence, the number of particles in the vapour phase is n_v , the number of particles in the liquid phase is n_l and the total number of particles for this substance is N , where $N = n_v + n_l$. The Gibbs free energy for vapour and liquid are a function of G_v and G_l respectively. Assuming that a number of Δn particles pass from the vapour phase to the liquid phase, where $\Delta n \ll n_v, \Delta n \ll n_l$, there will be a change in the Gibbs free energy (ΔG) in this closed system. The change in Gibbs free energy is expressed as:

$$\Delta G = \Delta G_v + \Delta G_l = G_v(n_v - \Delta n) - G_v(n_v) + G_l(n_l + \Delta n) - G_l(n_l) \quad (2.3)$$

Using Taylor expansion:

$$\Delta G = \frac{\partial G_v}{\partial n_v}(-\Delta n) + \frac{\partial G_l}{\partial n_l}(\Delta n) = -\left(\frac{\partial G_v}{\partial n_v} - \frac{\partial G_l}{\partial n_l}\right)\Delta n \quad (2.4)$$

For a vapour-liquid system at equilibrium, the change in Gibbs free energy of the system due to this fluctuation of the material should be 0, thus $\frac{\partial G_v}{\partial n_v} = \frac{\partial G_l}{\partial n_l}$.

If $\frac{\partial G_v}{\partial n_v} > \frac{\partial G_l}{\partial n_l}$, then $\Delta G < 0$, hence particles can change to liquid phase from the vapour phase.

If $\frac{\partial G_v}{\partial n_v} < \frac{\partial G_l}{\partial n_l}$, then $\Delta G > 0$, since all reactions go towards the direction where the Gibbs free energy is reduced, particles cannot enter the liquid phase from the vapour phase.

Thus, in non-equilibrium system, particles travel only from the vapour phase with the higher $\frac{\partial G_v}{\partial n_v}$ to the liquid phase with the lower $\frac{\partial G_l}{\partial n_l}$, where $\frac{\partial G}{\partial n}$ is the chemical potential.

Hence, chemical potential μ is defined as the incremental change in Gibbs free energy with the addition of material in a certain phase at a constant temperature and pressure: $\mu = \left(\frac{dG}{dn}\right)_{p, T}$

In addition, the difference in chemical potential $\Delta\mu$ between two phases is the driving force behind any reactions reaching equilibrium and can be defined as supersaturation. The supersaturation between two phases can also be expressed as:

$$\Delta\mu = RT \ln \frac{P_p}{P_{eq}} \quad (2.5)$$

where P_p and P_{eq} stand for the partial pressure and equilibrium vapour pressure of the same component.

In our nanowire system, in order to achieve growth, the chemical potential of the vapour phase gas precursors (μ_v) is kept the highest by constantly supplying the precursors, and that of the III-V crystals (μ_s) is the lowest, with the chemical potential of the liquid particle (μ_l) usually in between:

$$\mu_v > \mu_l > \mu_s \quad (2.6)$$

The process of nanowire growth will be discussed in detail in section 3.1.

To summarize, in order to determine the direction in which a reaction will go, one turns to the difference in chemical potential which is essentially the driving force behind any reaction.

2.3 Physical processes occurring on the surface

2.3.1 Adsorption and desorption

When a molecule reaches a surface from the vapour phase, it could be weakly bonded to the surface by van der Waals force, which is known as physisorption. The physisorbed molecule is usually free to move on the surface, so it can diffuse. After a while, the physisorbed molecule can either desorb from surface by gaining enough energy or it may become chemisorbed, with chemical bonds being formed with surface atoms. The bonds formed in chemisorption are much stronger than those of physisorption. These two types of adsorption commonly exist at the vapour-solid interface. The fraction of the incoming vapour molecules that remains adsorbed for the duration of the experiment is defined as the sticking coefficient, (S_c), which is usually represented as:

$$S_c = R_r/J_i \quad (2.7)$$

where R_r is the reaction rate for chemisorption and J_i is the flux of incoming molecules to the surface. The sticking coefficient is equivalent to the fraction of the incoming vapour molecules that becomes incorporated into the film. The rate of this desorption and adsorption is strongly affected by the substrate surface [12]; for example, molecules are bonded more strongly to atomic steps on atomic flat surfaces. The passivation of a silicon surface by a layer of H atoms will lead to weaker bonds with adsorbates.

2.3.2 Surface diffusion

Surface diffusion is a process where the physisorbed molecules are free to travel around on the surface before they desorb or become chemisorbed. The distance that molecules have travelled before desorption or chemisorption is the diffusion length (Λ),

$$\Lambda = a \sqrt{\frac{v_s n_a}{J_r}} e^{-E_s/2RT} \quad (2.8)$$

where a is the distance between adsorption sites, v_s is the pre-exponential factor, n_a is the number of adsorption sites per unit area, J_r is the deposition flux and E_s is the activation energy for diffusion. The diffusion length increases exponentially with T at a lower temperature range. However, when T is high enough, the desorption becomes dominant and the molecules are more likely to desorb from the surface than diffuse or incorporate into the film.

In the epitaxial growth of III-V nanowires, the predominant supply of group III elements comes from surface diffusion. For example, the diffusion length for Ga is in the order of a few tens of nanometres [13]. However, surface diffusion for group V elements is negligible and the supply of group V elements mostly comes from direct impingement from the vapour phase [14].

2.4 Pyrolysis of the precursors

In MOVPE, the transition of material from the vapour phase into a solid crystal phase is an essential process. The vapour phase materials consist of metalorganic compounds and hydrides and are transferred by a carrier gas such as hydrogen. Group III atoms are usually supplied in the form of low vapour pressure metalorganics, while group V atoms can be supplied in the form of either high vapour pressure hydrides or metalorganics. The process through which gas phase precursors dissociate thermally to supply the group III or group V elements is called pyrolysis.

The metalorganic materials are denoted using the format MR_n , in which M represents the element (e.g. Ga) used for MOVPE, R represents the alkyl (e.g. methyl, CH_3) and n is the number of alkyl radicals. The trimethyl- sources are most often used because of their higher vapour pressures and good stability for the purpose of storage. The pyrolysis of metalorganic compounds proceeds by the stepwise removal of the alkyl radicals. For example, the process of trimethylgallium (TMGa) pyrolysis starts with the removal of one methyl radical leading to dimethylgallium and then monomethylgallium, and eventually Ga. The pyrolysis of hydride takes place through the release of hydrogen radicals one at a time.

When pyrolysis occurs in the vapour phase, it is called a homogeneous reaction, whereas pyrolysis that happens at the interface between vapour and any other phase is called a heterogeneous reaction. In MOVPE, both homogeneous pyrolysis and heterogeneous pyrolysis should be considered.

The pyrolysis of unimolecules (involving a single molecule species) becomes more efficient with increasing temperature because thermal energy is needed to break the chemical bonds and also to overcome the energy barrier. The temperature at which

all molecules pyrolyze is referred to as complete pyrolysis. This temperature is usually much higher for group V materials in hydride form (e.g. AsH_3) than for group III materials in metalorganic form (e.g. TMGa) [15]. In a MOVPE reactor, there is usually more than one kind of molecule. The pyrolysis can often be enhanced by the presence of other molecules. For example, when both TMGa and AsH_3 are supplied to the reactor, the H radicals released from the hydrides will interact with the CH_3 group from the metalorganics to form relatively stable CH_4 . Thus, this reaction between TMGa and AsH_3 reduces the pyrolysis temperature for both precursors [15].

When III-V substrates are introduced into the MOVPE reactor, heterogeneous pyrolysis takes place and becomes predominant for the hydrides. In ref [16], it is reported that the pyrolysis temperature for decomposition of AsH_3 can be reduced drastically in the presence of a GaAs substrate.

2.5 Kinetic aspects of epitaxial growth

Aside from the thermodynamic driving force that allows a reaction to proceed, i.e. the supersaturation, kinetic factors determine the growth rate of the reaction. The final growth rate is limited by the slowest process in successive steps during epitaxial growth.

During epitaxial growth, there are many temperature-dependent processes, including the aforementioned pyrolysis of the precursors, the adsorption and desorption of the reactants, and the surface diffusion of the reactants. When a low temperature regime is used, the rate-limiting step could be the pyrolysis of one or more precursors due to this limiting the supply of certain growth species. Hence, the growth reaction rate should ideally increase linearly with temperature. This regime is referred to as a kinetically limited growth regime. The nanowire growth in this thesis is performed in this regime. In an intermediate temperature regime, the pyrolysis of precursors is more efficient than it is at a low temperature. The precursor decomposition is much faster than mass transport from the vapour source to the growth substrate. This regime is therefore called a mass-transport limited growth regime, and the growth rate here is almost independent of temperature. The epitaxial layer growth is performed in this regime. When the temperature increases further, desorption of the reactants from the substrate back to the vapour phase becomes more active. The growth reaction rate decreases in the regime.

For a kinetics-controlled reaction, the reaction rate (r) is expressed by the Arrhenius equation:

$$r = Ae^{-E_a/k_B T} \quad (2.9)$$

where A is the pre-exponential factor, which is usually temperature independent, k_B is the Boltzmann constant, and E_a is the activation energy. The activation energy is the energy barrier to overcome if a reaction is to proceed. Therefore, the rate of a chemical reaction is dependent on the temperature and the activation energy, and the ultimate growth reaction rate is dependent on the slowest process.

3 Epitaxial Growth of Semiconductor Nanowires

Wagner and colleagues first demonstrated the use of Au as a metal seed particle for initiating one-dimensional Si whisker growth in the 1960s [17]. Wagner proposed the VLS mechanism in order to explain the favourable one-dimensional crystal growth under the gold particle. The liquid particle acts as a collection site for the material and alloys with Si or Ge for the growth of group IV nanowires. A few decades later, in the early 1990s, Hiruma and colleagues demonstrated the synthesis of GaAs nanowires in MOVPE with diameters down to 10 nm [18][19]. Since then, many groups have explored the growth of III-V nanowires of different material systems using various growth techniques [20][21][22][23]. For particle-assisted III-V nanowire growth, a liquid droplet, usually gold, alloys with group III element, for example Ga or In atoms, for the growth of GaAs or InAs nanowires [24][25][26]. Aside from particle-assisted growth, a number of other methods, including selective-area epitaxy [27][28] and oxide-assisted growth [29][30], have been adopted and proposed in the last few years. Today, catalytic particle-assisted growth is still the predominant process used in the fabrication of III-V nanowires.

At present, the catalyst seed particle used to initiate III-V nanowire growth is almost exclusively gold. The universal reliance on and success of gold as an initiator for nanowire growth in this field could be attributed to its moderate melting point; it easily forms low-melting alloys with other materials like Ga; and its stability with exposure to oxygen. There is an interesting review paper discussing the properties of Au and the advantages of using Au to assist nanowire growth [31]. However, there is a big concern that Au will diffuse into the semiconductor nanowires and degrade the properties of the material. As early as 1965, Barns and Ellis reported the growth of GaAs and GaP whiskers using gold, palladium and platinum as the liquid seeds, which indicated that there could be various choices of seed particle material besides Au [32].

In this chapter, I will first introduce the theory of nanowire nucleation and crystal structures in nanowires. I will continue with a brief review of different methods for achieving Au-free nanowire growth. The properties of Sn, which is the chosen seed particle material in this thesis, will be discussed at the end.

3.1 Nanowire nucleation theory

Considering the case of vapour-solid deposition, where the supply phase is vapour, the chemical potential of the vapour phase is increased by, for example, supplying material. However, in thermodynamic equilibrium, where the system has its lowest total energy, the chemical potential of the vapour phase must be equal to that of the solid phase. The difference in chemical potential between the vapour phase and the solid phase is retained by continuously supplying material in the vapour which leads to a supersaturation ($\Delta\mu_{v-s}$). The supersaturation is the thermodynamic driving force behind atoms moving from the vapour phase to the solid phase, which can thus reduce the total energy of the system.

In classical nucleation theory, several atoms first diffuse and then come together to form a small nucleus. The minimum size this nucleus has to be in order to be stable and start growing bigger is called the critical radius. Assuming a spherical nucleus with a radius of r formed on a substrate in an ideal system, the total change in Gibbs free energy (ΔG) per nucleus is:

$$\Delta G = -\frac{4\pi}{3}r^3\frac{\Delta\mu}{V_m} + 4\pi r^2\gamma_f \quad (3.1)$$

where $\Delta\mu$ is the supersaturation between the two phases, V_m is the molar volume of the nucleus and γ_f is the interfacial energy (surface energy) between the nucleus and the vapour. The first term ($-\frac{4\pi}{3}r^3\frac{\Delta\mu}{V_m}$) is the volume term which causes a reduction in Gibbs free energy due to the formation of the nucleus, and the second term ($4\pi r^2\gamma_f$) is the interface term that increases the Gibbs free energy because of the newly formed interface of the nucleus. The critical radius (r^*) is achieved when ΔG has the maximum and $\frac{d(\Delta G)}{dr} = 0$. Thus, we obtain

$$r^* = \frac{2\gamma_f V_m}{\Delta\mu} \quad (3.2)$$

The critical radius is dependent on the surface energy, molar volume of the nucleus as well as supersaturation. As shown in Figure 3.1, the surface energy term is dominant for a small nucleus. As the nucleus grows, ΔG will increase, which is not thermodynamically favourable. The nucleus is not stable in this regime, and the size of nucleus could shrink. Beyond the critical radius (r^*), the first volume term becomes dominant. Further growth of the nucleus can lower the Gibbs free energy, and the nucleus becomes stable. Once a stable nucleus is formed, it will act as a preferential collection site for the material and will start to grow bigger. The Gibbs free energy at the critical radius (ΔG^*) is the energy barrier to overcome for nucleation to occur.

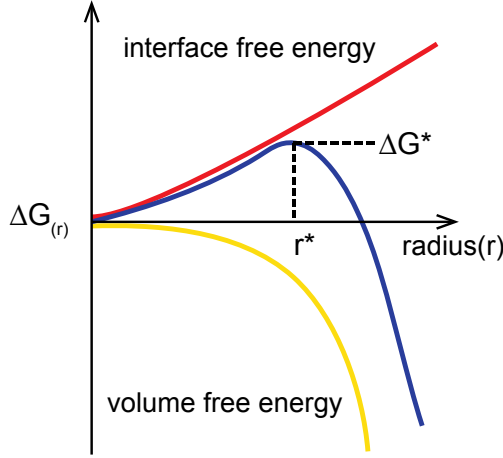


Figure 3.1 Total change in Gibbs free energy for a nucleus to form. The red line represents the interface term and the yellow line represents the volume term. Once the critical radius (r^*) is achieved, the nucleus will be stable and will continue to grow.

In the case of particle-assisted nanowire growth, a liquid seed particle, usually Au, is introduced to the system. Two relative supersaturations should be considered, the supersaturation between vapour and liquid ($\Delta\mu_{v-l}$) and the supersaturation between liquid and solid ($\Delta\mu_{l-s}$). When the system reaches steady-state growth $\Delta\mu_{v-s} = \Delta\mu_{v-l} + \Delta\mu_{l-s}$. In order to maintain the right direction for nanowire growth, i.e. that materials are accumulating inside the liquid seed particle from the vapour and nanowires are solidifying and precipitating below the liquid particle, $\Delta\mu_{v-l}$ and $\Delta\mu_{l-s}$ have to be positive. Thus $\Delta\mu_{v-s} > \Delta\mu_{l-s}$, which implies that the vapour-solid growth should be favoured over particle-assisted nanowire growth. However, if the nucleation barrier and thus the critical radius for a nucleus to form at the particle nanowire interface are smaller than that for a nucleus to form on a substrate, the particle-assisted nanowire growth will be favoured. In Eq. 3.2, besides supersaturation, the surface energy term of the nucleus can affect the size of the critical nucleus.

Consider three different cases in Figure 3.2, marked as A, B and C, respectively. A represents a nucleus forming on substrate, whereas B represents a nucleus forming at the interface between the particle and nanowire and C represents a nucleus forming at the triple phase boundary (where vapour, liquid particle and nanowire meet). Assuming that the three nuclei have the same crystal structure and composition as the substrate and the nanowire, the top facets of the nuclei are therefore equivalent to the surfaces' facets before the nuclei were formed. So, only the side facets of nuclei will contribute to the total Gibbs free energy.

Assuming the nuclei have the same height (h) and a perimeter length (p), for nucleus A, which is formed on substrate, the increase in Gibbs free energy from the creation of newly formed surfaces is:

$$ph\gamma_{vs} \quad (3.3)$$

For nucleus B, which is formed at the interface between particle and nanowire, the increase in Gibbs free energy is:

$$ph\gamma_{ls} \quad (3.4)$$

For nucleus C, which is formed at the triple phase boundary, the fraction of side facets that is exposed to vapour phase is represented as x and the contact angle of droplet is β . The increase in Gibbs free energy for nucleus C is:

$$ph\gamma_{ls}(1-x) + phx\gamma_{vs} - phx\gamma_{vl}\sin\beta \quad (3.5)$$

Here, the interfacial energies are the vapour-solid, (γ_{vs}), the vapour-liquid, (γ_{vl}) and the liquid-solid, (γ_{ls}). Considering the Young's equation at the particle nanowire interface, for a stable liquid particle sitting at the tip of the nanowire, the horizontal components of the surface forces need to be balanced:

$$\gamma_{ls} = -\gamma_{vl}\cos\beta \quad (3.6)$$

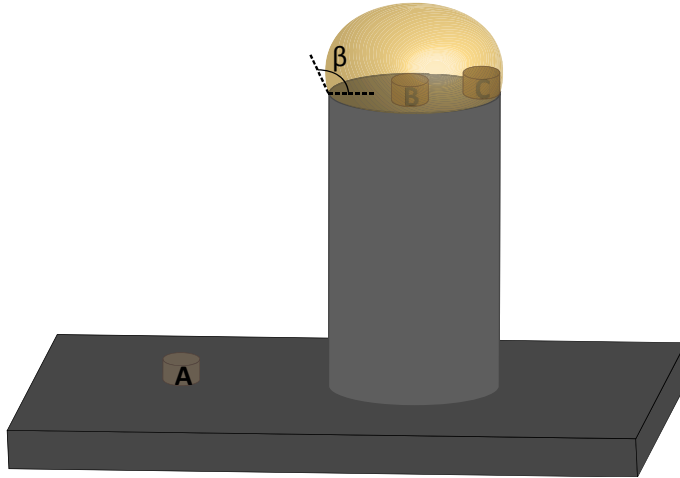


Figure 3.2 Geometry of nuclei in three different positions for nanowire growth with contact angle β for the seed particle. A. on substrate; B. at the interface between seed particle and nanowire; C. at the triple phase boundary.

Typical wetting angles of 100–130 degrees for GaAs nanowire growth are observed in the in-situ experiment [33], thus $\gamma_{ls} < \gamma_{vl}$. For Au-seeded GaAs nanowires, γ_{vs} is 1.3–2.2 J/m² depending on the facet [34]. The seed particle is assumed to be a binary liquid alloy consisting of Au and Ga. Since the low surface energy

component of a binary alloy tends to segregate to the surface in order to minimize the energy of the alloy, it is reasonable to assume that γ_{vl} should be between 1.15 J/m² and 0.72 J/m² [35]. Therefore, it can be assumed that $\gamma_{vl} < \gamma_{vs}$, and overall, it can be assumed that in most cases $\gamma_{ls} < \gamma_{vl} < \gamma_{vs}$.

Now we can go back to the three cases in Figure 3.2. Nucleus A has the highest increase in Gibbs free energy. It therefore has the highest nucleation barrier to overcome and thus the slowest growth rate. Compared to nucleus A, nucleus B has a smaller increase in Gibbs free energy due to the replacement of γ_{vs} with γ_{ls} , resulting in a faster growth rate for the particle-assisted nanowire growth.

In case C, the increase in Gibbs free energy is smaller than that in case B. Because the increase in Gibbs free energy due to the creation of the vapour-solid interface is compensated by removal of a part of the liquid-solid and the vapour-liquid interface. Thus the formation of a nucleus at the triple phase boundary is favoured over the formation of a nucleus at the centre of the interface between particle and nanowire.

After a stable nucleus is formed, the nanowire will grow in a step flow mechanism and a layer of the material will precipitate at the interface between the liquid particle and the nanowire growth front [36].

Recently, it has been shown through direct observation of GaAs nanowire growth by in-situ transmission electron microscopy (TEM) that a truncation appears at the triple phase boundary of the zincblende nanowire, which is rapidly filled with nanowire step flow [33]. The supersaturation within the seed droplet will be reduced during the step growth but will increase again until the next layer starts to nucleate.

Apart from the VLS mechanism, nanowire growth has also been reported to occur through a VSS mechanism. In VSS growth, a solid metal seed particle is responsible for initiating nanowire growth. The particle is in solid phase due to the melting temperature of the metal material being higher than the growth temperature or because no low-temperature eutectic alloy exists at certain compositions. Compared to the traditional VLS mechanism, VSS growth usually has a relatively low growth rate, which could be probably due to the lower solubility and diffusivity of the growth species in a solid seed particle. In 2007, Kodambaka and colleagues demonstrated Ge nanowire growth assisted by Au particles with in-situ TEM. They observed that Ge nanowires can be grown from Au particles in both liquid and solid states under identical growth conditions, while growth via the VSS mechanism has a much lower growth rate than that of the VLS growth [37]. It has also been suggested that nanowires grown by the VSS mechanism often lack epitaxial alignment with the growth substrate, which could be due to the interface between the solid seed particle and the nanowire growth front. However, the limited solubility of the growth species in the solid seed particle could also be beneficial in terms of growing nanowire heterostructures with atomically sharp interfaces [38][39]. In summary, although the VSS mechanism has drawbacks in terms of its

slower growth rate and the unstable interface between the particle and nanowire growth front, it can still be beneficial to achieve sharp interface in the growth of axial heterostructure nanowire which makes it a complement to the well-established VLS mechanism.

3.2 The crystal structure of III-V nanowires

In an ideal crystal, the atoms are arranged periodically in three dimensions. The smallest group of atoms that the entire crystal can be built from is called a unit cell. The unit cell determines the symmetry and structure of the crystal lattice. III-V semiconductor materials are usually found in a zincblende (ZB) crystal structure in bulk, with one exception being that when the group V element is nitrogen, the bulk material exhibits in a wurtzite (WZ) structure. However, in III-V nanowires, crystal structures ranging from pure ZB to pure WZ, with mixed compositions such as ZB/WZ or randomly and periodically twinned ZB have been observed. III-V nanowires are usually grown in a $\langle 111 \rangle$ direction for ZB and an equivalent $\langle 0001 \rangle$ direction for WZ structures.

The differences between the ZB and WZ crystal structures are the shape of their unit cells and their stacking sequences. In the case of WZ structures, the unit cell has a hexagonal shape and the atomic planes are arranged in the $\langle 0001 \rangle$ direction as ...ABAB..., where every second bilayer is repeated. In the case of ZB structures, the unit cell has a cubic shape and the atomic planes are arranged in the $\langle 111 \rangle$ direction as ...ABCABC..., where every third bilayer is repeated. ZB and WZ are both close-packed crystal structures. The stacking sequences in the close-packed direction for ZB and WZ are shown schematically in Figure 3.3a and b. ZB and WZ crystal structures are demonstrated along the $\langle 110 \rangle$ and $\langle 11-20 \rangle$ direction in Figure 3.3c and e, respectively. In the Ramsdell notation system, WZ is called 2H, denoting two bilayers repeating with hexagonal stacking, whereas ZB is called 3C, representing three bilayers repeating with cubic stacking. A longer repetitive segment in the crystal structure can be denoted as the number of bilayers and a letter representing the crystal system they belong to. For instance, a 4H structure has been observed in Cu-seeded nanowires and this has the stacking order of ...ABACABAC... . Since the only difference between these crystal structures is the stacking sequence of the bilayers, they are examples of polytypes that can be observed in nanowires.

Rotational twin is one of the common crystal defects observed in nanowires with a ZB structure. The rotational twin is considered to be a segment of ZB crystal structure rotated 60 degrees around the $\langle 111 \rangle$ direction, as shown in Figure 3.3c and d. Therefore, the stacking sequence changes from ...ABCABC... to, for instance, ...CBACBA... . The plane that separates two twinned segments is called the twin plane.

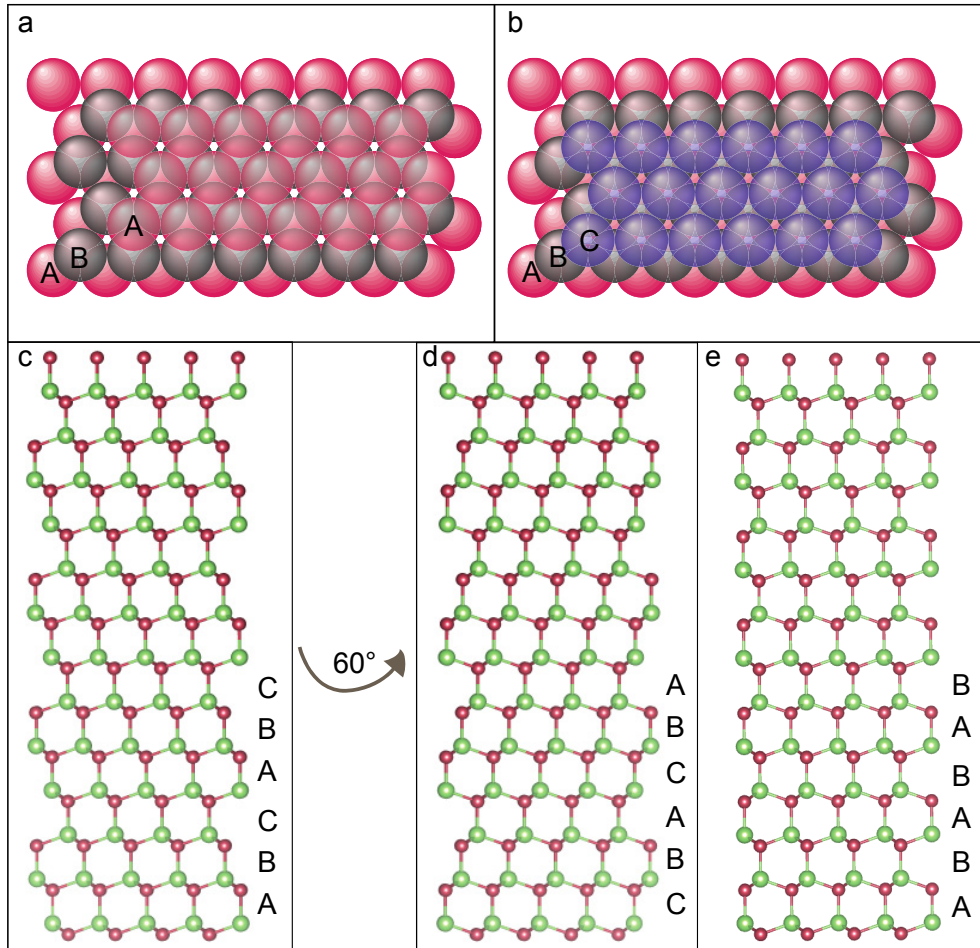


Figure 3.3 Schematic demonstration of the close-packed stacking sequences in a) wurtzite and b) zincblende. ZB crystal structure viewed along the $\langle 110 \rangle$ direction in c). Twin formed by rotation along the $\langle 111 \rangle$ direction in d). WZ crystal structure viewed along $\langle 11-20 \rangle$ direction.

The ZB crystal structure has two opposite polarities when considering the $\{111\}$ and $\{-1-1-1\}$ plane families, where the former planes are terminated by group III atoms and are called the (111)A planes, and the latter planes are terminated by group V atoms and are called the (111)B planes. These planes with different polarities have different properties, for example surface energy, which could affect the nanowire growth. It has been reported that substrate orientation can lead to difference in crystal quality for GaAs nanowires [40].

The interfacial energies considered in the formation of a new nucleus determine whether it is a ZB or WZ nucleus. Consider case C in Figure 3.2, where the nucleus forms at the triple phase boundary. The vapour-solid interfacial energy (γ_{vs}) should

be considered when calculating the total change in Gibbs free energy for the nucleus to form using Eq. 3.5. The vapour-solid interfacial energy is facet dependent and WZ generally has a lower interfacial energy (surface energy) than ZB. Thus the nucleation in WZ could be favoured at the triple phase boundary. The interfacial energy also depends on the vapour environment which might lead to surface reconstruction of the facet [41]. In Eq. 3.5, the vapour-liquid interfacial energy (γ_{vl}) should also be considered during nucleation. It has been suggested that the surfactant effect of group V material could decrease γ_{vl} , which promotes ZB formation [42]. The use of dopant has been reported to promote both ZB and WZ formation under different conditions [43][44].

3.3 Alternative approaches for III-V nanowires growth

3.3.1 Selective area epitaxy and self-seeded nanowire epitaxy

Selective area epitaxy (SAE) is a growth technique that uses a lithographically designed dielectric mask with openings on substrate. The concept of selective area was proposed in as early as 1960s for Si deposition [45]. It has subsequently been successfully developed to grow III-V nanowires by well-controlled growth conditions that favour axial growth but reduce the lateral overgrowth. The nucleation and growth of nanowires are restrained within the pre-defined openings.

Motohisa and colleagues demonstrated uniform selective area epitaxy grown GaAs and InGaAs nanowires on (111)B III-V substrates, high aspect-ratio nanowires can be achieved by optimizing the pre-patterning of the openings [46]. Later in 2007, Ikejiri and colleagues discovered that in selective area epitaxy, the nanowire growth rate is exclusively dependent on the growth conditions favouring the formation of specific facets and enhancing only axial growth [47]. Tomioka and colleagues demonstrated the selective area growth of Si-doped InGaAs nanowires and InGaAs/InP/InAlAs/InGaAs radial heterostructures on Si substrate and their application as high-performance vertical transistors [48]. This method allows the implementation of III-V nanowires directly onto a Si substrate, which offers great potential to allow the fabrication of cheaper Si-based III-V devices. SAE nanowire-based solar cells have also been demonstrated [49]. However, this technique involves expensive and complicated substrate preparation and the one-dimensional growth of nanowires is entirely reliant on selected growth parameters at a relatively higher growth temperature. This makes the suitable growth parameter window narrower compared to other techniques. The crystal phase control in nanowires is generally challenging in this technique, since high growth temperature is usually associated with twins or defects in the formation of nanowires [50]. Furthermore,

the radial growth on the side facets is never entirely suppressed, and the aspect ratio is thus limited.

III-V nanowires can also be grown with the low melting point group III material (Ga or In) that comprises the III-V nanowire as the seed particle. This method is called self-seeded growth as there is no foreign element used to initiate growth. In this growth mechanism, a relatively high group III flow is normally used to form liquid droplets prior to the nanowire growth. Since the seed particle material is one component of the nanowire, it is gradually consumed during nanowire growth. As a result, the growth parameters like V/III ratio and temperature need to be carefully controlled during nanowire growth in order to maintain the stability of the seed droplet. In much of the literature concerning self-seeded nanowires, the role of a thin oxide layer on the substrate cannot be neglected [51][52]. Essentially, it is suggested that the oxide layer facilitates the formation of Ga droplets [53]. Therefore, fine treatment of the substrate prior the growth is of great importance to initiating the droplet formation and thus the nanowire growth in self-seeded nanowire growth.

One of the first reports on In-seeded nanowires in MOCVD was published in 2005 by Novotny and colleagues [54]. They showed that with an important annealing step prior to nanowire growth, vertically aligned single crystalline InP nanowires can be achieved on InP substrate. In 2010, Yu and colleagues demonstrated the implementation of InP nanowires directly growing on Si substrate with the use of In droplets [55]. In the same year, self-seeded InAs nanowire growth directly on Si with a thin oxide layer was realized [56]. It has also been demonstrated that it is possible to observe the formation of ZB, 4H, and WZ crystal structures in InSb nanowires by controlling the V/III ratio [57]. Furthermore self-seeded ternary nanowires including $\text{InAs}_{1-x}\text{P}_x$, $\text{InAs}_{1-x}\text{Sb}_x$ and $\text{InP}_{1-x}\text{Sb}_x$ have also been reported [58][59][60].

Together with In, Ga droplets have also been used for the growth of Ga-assisted nanowires. Ga has been used for the growth of highly controlled GaAs nanowires, mostly in MBE [61][62][63]. Pure ZB phase and pure WZ phase can be observed in self-seeded GaAs nanowires through fine control of the growth conditions [61][64]. Ternary Ga-seeded $\text{GaAs}_{1-x}\text{Sb}_x$ nanowire growth with a wide range of composition tunability and a high crystal phase purity has been reported [65].

It is generally very challenging and complex to adapt self-seeded growth for an axial heterostructure system in which the group III species is changed. Maintaining a group III droplet with a stable size and composition over time by balancing the consumption and accumulation of group III material is crucial to achieving homogeneous nanowire growth. This process is challenging as it is determined exclusively by the growth conditions, thus any change in the growth parameters

would affect the nanowire growth. For example, reverse tapered morphology in GaAs nanowires is observed with an increase in the size of the Ga seed droplet [66].

3.3.2 Alternative foreign metal-seeded nanowires

Selective area epitaxy and self-seeded epitaxy are well-developed methods for the growth of III-V nanowires that can offer great advantages in terms of the cleanliness and purity of the resulting material. In principle, however, these two techniques have relatively narrow growth windows for favouring one-dimensional growth or retaining the stability of the liquid seed droplet. If foreign metal seed particles are considered as a whole group, the suitable parameter space is thus much broader compared to other techniques. In recent years, III-V nanowire growth with non-gold foreign metal seed particles has been explored using, for example, Cu, Pd, Ag, and Mn [67][68][69][70]. Instead of the traditional VLS mechanism, VSS growth is often proposed in alternative foreign metal-seeded nanowire growth. As previously mentioned in section 3.1, in VSS growth, a solid metal seed particle rather than a liquid droplet is responsible for initiating nanowire growth.

In order to achieve high-performance nanowire-based devices and study different polytypic structures, the crystal phase control of III-V nanowires needs to be investigated. As discussed in section 3.2, aside from the thermodynamic equilibrium phase ZB, the WZ phase is also commonly observed in nanowire systems. A highly controlled crystalline phase has been achieved with Au-seeded nanowires [71][72]. There are also indications that alternative foreign metal seed materials have the ability to tune the crystal phase in the resulting nanowires. For instance, several groups have proposed that the nanowire crystal structure is strongly dependent on the state of the metal seeds. Han and colleagues proposed that GaAs nanowires possess a ZB structure when the seed particle is cubic NiGa, while WZ GaAs nanowires are associated with hexagonal Ni₂Ga₃ seed particles [73]. Oliveira and colleagues observed that InP nanowires adopt the pure WZ crystal phase with Ag seed particles at higher temperatures and In precursor flow, where growth via the VLS mechanism is expected; whereas, at lower temperatures and In precursor flow, InP nanowires have mixed WZ/ZB segments, which the authors claimed are similar to self-seeded InP nanowires [74]. Moreover, alternative metal seed particles could lead to unique polytypism. For example, although a short segment of 4H crystal phase has been observed in nanowires [57], Hillerich and colleagues observed a 4H polytypism segment up to 100 nm in length in Cu-seeded InAs nanowire [75]. This long segment 4H structure has never been observed in any gold-seeded InAs nanowires.

Growth along the $[-1-1-1]$ direction is commonly observed in Au-seeded III-V nanowire growth. This growth direction is also associated with a high density of

stacking defects. There are a few factors that could affect the nanowire growth direction, for example substrate crystal direction, substrate surface chemistry, as well as the state and the surface energy of the seed particle [40][76]. Various growth directions have been observed for alternative foreign metal-seeded nanowires. Regolin and colleagues observed Fe-seeded GaAs nanowires along the $\langle 1\ 1\ 0 \rangle$ and $\langle 1\ 0\ 0 \rangle$ directions [77]. Heun and colleagues demonstrated Pd-seeded InAs nanowires growing in the $[1\ 1\ 1]$ direction [78]. It has been also proposed that the growth direction could affect the crystal structure of the resulting nanowire [79]. Lindberg and colleagues demonstrated that the use of Ag could initiate GaAs nanowire growth in both the $[-1\ -1\ -1]$ and the $[1\ 0\ 0]$ directions under identical growth conditions, with WZ nanowires being observed along the $[-1\ -1\ -1]$ direction, while ZB nanowires can be achieved along the $[1\ 0\ 0]$ direction [80].

The incorporation of foreign metal seed material into the nanowire is always expected at the growth temperature. Although a low concentration of Au has been detected in Si nanowires [81], Au is still considered detrimental to Si nanowires due to the deep traps that are formed [9][10]. Whether Au is also harmful to III-V nanowires is still under debate. However, there is strong evidence that Au degrades the optical and electrical properties of III-V nanowires [82][83]. Direct imaging of Au diffusion into III-V nanowires has also been reported [84]. Thus, by using alternative foreign metal seed particles, it is effectively possible to avoid Au diffusion into the nanowire. On the other hand, the use of alternative foreign materials allows exotic properties from the seed material to be introduced into the nanowire through the incorporation of the seed particle. For example, Mn is expected to act as a dopant in III-V nanowires and form ferromagnetic semiconductors, which is ideal for the study of spin-related physics [85]. Martelli and colleagues accomplished the growth of GaAs nanowires by using Mn seed particles in MBE and achieved p-type doped GaAs nanowires from Mn [86]. Their aim is to obtain a magnetic semiconductor through the incorporation of Mn atoms into the nanowires.

Historically, the use of alternative foreign metal seed particles in the growth of group VI nanowires (Si and Ge) has been investigated much more than it has in the growth of III-V nanowires. Most of the metal seed particles that have been reported being used in the growth of III-V nanowires, e.g. Cu, Ag, Mn, Sn, Ga and In, have also been demonstrated in the growth of group IV nanowires [87][88][89][90][91][92]. In addition to that, Ti, Al, Co and Sb as well as binary alloys consisting of two foreign metal materials like AlAu, AgAu, have also shown promising potential as seed materials for group IV nanowire growth [93][94][95][96][97][98].

In 2000, Kamins and colleagues demonstrated for the first time the growth of Si nanowires with alternative foreign metal seeds made of Ti. They also suggested that

Si nanowires were grown from solid TiSi₃, as the nanowire growth temperature is far below the eutectic temperature of bulk Ti and Si [93]. Later in 2009, Wen and colleagues demonstrated Cu-catalysed Si nanowires with in-situ TEM. They observed that the nanowire growth is via the VSS mechanism and that the nanowire growth is predominantly along the $\langle 110 \rangle$ direction but also that the growth is dependent on the alignment of the solid Cu particle on the substrate [38]. That same year, Wen and colleagues demonstrated an atomically sharp interface in the growth of Si/Ge heterostructure nanowires with AlAu alloy as the catalyst [39].

Furthermore, the potential for self-doping through the intentional incorporation of atoms into the group IV nanowires has been shown to be feasible. It has been demonstrated that the use of Al as a growth catalyst, instead of the usual gold, can yield an effective p-type doping in Si nanowires [94].

Sn nanoparticles have been used for the growth of Si and Ge nanowires for high performance battery applications [99][100]. It has also been shown that in the growth of Si nanowire with In-Sn binary alloy, Sn is incorporated into the nanowire during the growth [101].

The previous examples demonstrate that carefully choosing an alternative metal seed particle potentially allows the observance of unique polytypism and different growth directions in nanowires, which cannot otherwise be achieved by using Au. Ideally, the incorporation of different seed materials may also give the nanowire interesting properties such as magnetism and self-doping. However, the number of publications concerning these alternative seed particles is negligible compared to the huge number of publications from the nanowire community as a whole, where the use of Au as the catalyst seed particle is predominant. The lack of basic understanding of the role of specific metal materials in III-V nanowire growth and the properties they impart makes it difficult to predict which metal seed particle can be used to successfully grow III-V nanowires with the desired properties. However, the relatively enormous amount of work that has been done on alternative foreign metal seed particles assisting the growth of Si and Ge nanowires is not irrelevant here. It hints that there is great potential to extrapolate this to III-V nanowire growth. Thus, it is interesting to explore and investigate nanowire growth behaviour by using other metal materials as seed particles.

3.3.3 Properties of Sn

Sn is a group IV element and has low melting point (232°C). Thus, it is very likely to remain in the liquid phase during nanowire growth. It will, in principle, allow the VLS growth mode with a relatively high growth rate compared to the VSS mode in which the seed particle remains solid during the growth. Moreover, unlike most low-melting elements, Sn has relatively low vapour pressure, which is even comparable

to that of Ga and In, making it possible to easily form droplets at high temperatures. When the system is continuously supplied with Sn vapour material, the excess vapour material would prefer to condense and form liquid droplets in order to reach thermodynamic equilibrium. Sn is also a well-known dopant in III-V materials and could, in principle, be amphoteric, which means it can either be p-type or n-type dopant, depending on whether it occupies the position of group III or group V element. It would be interesting to see whether the type of dopant can be tuned by manipulating the growth parameters.

The metalorganic form of Sn commonly used in MOVPE systems is tetraethyltin (TESn, a Sn atom bonded to four CH_2CH_3), which is available as a dopant precursor. TESn has been used as dopants for GaAs layers in MOVPE [102]. Parsons and colleagues observed that the incorporation of Sn is not dependent on temperature in the range of 650°C to 700°C, but linearly on the molar fraction of TESn, which indicates that the complete pyrolysis of TESn happens in that range. In CBE systems, an increase in the free carrier concentration is reported up to 570°C, which suggests the decomposition temperature of TESn is estimated to be 570°C for a complete decomposition in CBE systems [103]. It has also been demonstrated that in MBE system, Sn can be deposited in the form islands on GaAs substrate at temperatures above 470 K [104]. Thus, we chose Sn as a promising candidate for III-V nanowire growth with the potential to form liquid droplets in-situ the MOVPE system.

4 III-As Semiconductor Nanowires

III-As-based semiconductor materials are composed of the group III elements, Al, Ga and In combined with As to form materials like AlAs, GaAs, InAs as binary materials, and InGaAs, AlGaAs, AlInAs as ternary materials. In this chapter, the focus of the discussion will be on three materials: GaAs, InAs and InGaAs.

4.1 GaAs and InAs nanowires

GaAs has a direct band gap which allows for efficient light-to-electricity conversion, and a higher electron mobility compared to Si. GaAs-based single junction solar devices exhibit the highest efficiency of about 28% [105]. GaAs nanowires have been extensively investigated in the past few decades for various applications including transistors, light emitting diodes, solar cells and lasers [4][5][8][106]. In order to achieve good quality and efficiency in the device applications, the morphology, crystal structure and doping profile of GaAs nanowires needs to be controlled through the growth process.

Au-catalysed GaAs nanowire synthesis has been a great success in different growth systems such as MBE and MOVPE [72][107][108]. For example, in MOVPE, GaAs nanowire growth can be obtained from at least 330°C to 575°C, with V/III ratios from as low as 0.6 to as high as 240 [50][72]. Au-seeded GaAs nanowires have been observed to exhibit a very strong preference to grow along the (111)B direction, while this direction has a tendency to form stacking defects. In addition to the commonly observed unidirectional nanowire growth, other growth directions have been observed and studied to a limited extent [40][76]. Transferable planar GaAs nanowires have also been demonstrated on (110) GaAs substrate [109]. Au-seeded GaAs nanowires can have mixed crystal structures, but controlled crystal structures from pure ZB to pure WZ have been achieved in Au-seeded GaAs nanowire growth using MOVPE [72]. It has been shown that pure WZ crystal phase is achieved within a limited V/III ratio range; beyond this range, a mixed crystal phase and a pure ZB phase could be obtained under selected conditions. Furthermore, an atomically sharp interface has been realized in ZB/WZ GaAs heterostructures with a precisely controlled length in each segment, allowing the study of band structure [110][111].

Adding external dopants during GaAs nanowire growth can induce artificial twinning superlattice structures [112].

InAs is a versatile material because it has a relatively narrow band gap (0.36 eV) and high electron mobility ($20000 \text{ cm}^2\text{V}^{-1}\text{s}^{-1}$) in bulk material compared to most other III-V materials. It is ideal for infrared detection, which is of great interest in photodetectors [113][114]. InAs is known to have a large g-factor which makes InAs nanowires a great candidate for the study of spin-related fundamental physics; for instance, it has been used for the study of Majorana fermions [115]. The growth of Au-seeded InAs nanowires has been extensively investigated. As with Au-seeded GaAs nanowires, crystal phase control has been achieved on Au-seeded InAs nanowires. Everything from pure ZB to pure WZ, as well as designed twin-plane superlattices are observed in Au-seeded InAs nanowires in MOVPE [41][116]. It has been found that the crystal structure of InAs nanowires is strongly dependent on the nanowire diameter. Achieving a pure ZB crystal phase in InAs nanowires with small diameters has been shown to be challenging [116]. There are very few reports in the literature of Au-seeded InAs nanowires growing in directions other than the predominant $[-1-1-1]$ direction. However, there are exceptions indicating that InAs nanowires growing along $\langle 001 \rangle$ directions possess a twin-free ZB crystal phase [117][118]. Furthermore, high doping in InAs nanowires always comes along with significant changes in the size and shape of the nanowires [119]. The crystal structure could also become more defected together with the simultaneous doping which is undesired for optical and electronic applications [120][121][122].

Gold-free synthesis of GaAs and InAs nanowires has been investigated in order to combine the III-V material with conventional Si-based technology. However, as previously mentioned in section 3.3.1, the intrinsic limitation of the growth mechanisms does not allow the nanowires to grow in a wide range of parameter windows. The yield of nanowires is also strongly dependent on the substrate preparation. Alternatively, there has been quite some effort in the field to explore alternative metal seeds for the growth of GaAs and InAs nanowires. The properties of various metal materials that people have used are listed in Table 4.1 along with Au for comparison. I will next discuss the effect of melting temperature and surface energy and then briefly review some examples.

As mentioned in section 3.1, nanowire growth occurs predominantly via the VLS mechanism. For VLS growth to occur, the seed particle material should either have a low melting temperature or have a low eutectic point with either of the growth species. Table 4.1 lists the melting points for various metallic elements. Most of the metals have a high melting point, except for Bi and Sn. The binary phase diagrams of Au-Ga and Au-In [123][124] show that Au has a low eutectic point with both Ga (341°C) and In (450°C), which makes it ideal for VLS growth. In addition to Au, Ag has a eutectic mixture with As at a temperature of 540°C [125], which is still

within the suitable temperature range for nanowire growth. On the other hand, the other metals in Table 4.1 that have a relatively high melting temperature do not have any low eutectic point with either group III or group V. For example, Fe does not have any eutectic mixture with group III element but Fe does have a eutectic point with As at 838°C [126]. However, this temperature is beyond the suitable temperature range for III-As nanowire growth. Hence, these metals are more likely, in principle, to induce nanowire growth via the VSS mechanism.

Note that the group III species Ga and In are both low melting point post-transition metals and are commonly used for the formation of low melting point alloy [127]. The phase diagram shows that the melting temperature of the metals drops drastically with increasing group III content in the mixture. For example, in the binary phase diagram for Cu-Ga, when the Ga composition in the mixture is 70%, the melting temperature of the alloy is reduced to about 500°C [128]. This indicates that the accumulation of group III species in the metal particles could lower the melting point of the mixture and induce nanowire growth via a VLS mechanism.

Table 4.1 Properties of the metal materials that have been used as seed particles for nanowire growth.

Material	Metal melting point (°C) [129]	Surface energy (J/m ²) [35]	III-As nanowire growth	remarks
Gold (Au)	1064	1.15	GaAs/ InAs/ InGaAs	
Silver (Ag)	962	0.92	GaAs/ InAs/ InGaAs	
Bismuth (Bi)	271	0.38	GaAs/ InAs	SLS
Copper (Cu)	1085	1.3	InAs	
Iron (Fe)	1538	1.8	GaAs	
Manganese (Mn)	1246	1.1	GaAs/ InAs	
Nickel (Ni)	1455	1.8	GaAs/ InAs	dual-zone tube furnace
Palladium (Pd)	1555	1.46	GaAs/ InAs	
Tin (Sn)	232	0.55	GaAs/ InAs	

The discussion of nanowire nucleation in section 3.1 indicates that the surface energy of the seed particle plays an important role in assisting stable nanowire growth. Nebol'sin and Shchetinin have predicted that in order to maintain the stability of seed particles on the tip of nanowires, the contact angle of the seed particle should be larger than 90° [130]. They also predicted that metal materials with a low surface energy are not plausible for stable Si nanowire growth. However, their work is only based on a geometric model but not considering the nanowire nucleation process. Recall that in Figure 3.2, there are two possible nucleation sites B and C, which are the centre nucleation and the triple-phase boundary nucleation. Cirlin and colleagues proposed that for the growth of self-seeded GaAs nanowires, triple-phase boundary nucleation is suppressed due to the much lower surface energy of Ga compared to the AuGa compound [62]. The formation of a ZB crystal

structure is favoured when the nucleation happens at the particle nanowire interface. Hence metal materials with a low surface energy could in principle, also be used to assist nanowire growth and promote a ZB crystal phase in nanowires.

Ag has been used to assist the growth of several III-V materials including both GaAs and InAs nanowires in MBE. Lindberg and colleagues have demonstrated that both high quality WZ- and ZB-structured GaAs nanowires can be achieved by choosing GaAs substrate orientations [80]. They cannot ascertain whether the growth is via the VLS or VSS mechanism because both mechanisms are possible at their growth conditions. InAs nanowires assisted by Ag nanoparticles has been realized on a Si (111) substrate [69]. Pan and colleagues achieved pure WZ InAs nanowires that are free of defects and twin planes down to 10 nm. They did not discuss the possible growth mechanism in their work, but from ex-situ characterization, they found that the Ag seed particle consists of around 14% In and 86% Ag.

Fe was used for the growth of GaAs nanowhiskers via the VSS mechanism, with an FeAs phase detectable inside the particle [77]. Mn was reported as a catalytic seed particle for the growth of both GaAs and InAs nanowires in MBE. The authors concluded that the particle remains solid for InAs nanowire growth, while for GaAs nanowire growth, the growth mechanism is very likely to be VLS [86][70]. Ni has been used for the growth of both GaAs and InAs nanowires where the seed particle remains solid during nanowire growth [131][132].

It has been proposed that Cu and Pd assist nanowire growth through both the VLS and VSS mechanisms. Cu-seeded InAs, Pd-seeded GaAs and InAs nanowires showed the coexistence of liquid and solid particles on a single substrate with the same growth conditions [75][68][133]. The authors proposed that the particle with a rich group III content remains in the liquid phase during growth, which is consistent with what I have previously discussed about the melting temperature of binary alloy.

Bi has been used for the synthesis of GaAs and InAs nanowires via the solution-liquid-solid (SLS) mechanism where the authors always observed a predominantly ZB crystal phase [134]. Lewis and colleagues have also suggested that Bi acts as surfactant due to its low surface energy, which could induce InAs nanostructure growth on the sidewall of GaAs nanowires. They proposed that Bi could potentially be used for future self-assembled quantum structure engineering [135].

In summary, alternative foreign metal-seeded GaAs and InAs growth has been reported as proceeding mostly via the VSS mechanism. This is due, on one hand, to the high melting point of the metal materials and, on the other hand, to the lack of a liquid binary phase between these metal materials and one of the nanowire growth species. In the rare cases where the growth is via the VLS mechanism, there is usually a substantial amount of group III material in the seed droplet. The solid

phase of the seed particle is usually associated with low diffusivity and solubility of the growth species, which affects the nanowire growth rate. It is worth noting that alternative metal seed materials can result in different particle/nanowire interfaces, which will, in turn, determine the nanowire growth direction and crystal structure. The aforementioned examples show that the selection of seed particle material does have a direct impact on the resulting properties of the nanowires. The use of alternative metal seed materials remains an underexplored area to study.

4.2 InGaAs nanowires

Ternary nanowires are less studied than the binary system because they are more complicated given the competition between the growth species and different diffusion coefficients for each species. This complexity leads to inhomogeneity in composition and crystal structure. However, ternary nanowires are of great interest and importance since desired band gap tunability is possible by simply changing the composition fraction of the ternary compound. $\text{In}_x\text{Ga}_{1-x}\text{As}$ is a ternary compound material that possesses a direct band gap that can be tuned for optoelectronic applications by changing the material composition, which is ideal for tuning the optical emission wavelength.

Many groups have reported Au-seeded InGaAs nanowire growth directly from the substrate [136][137][138]. The two group III elements, Ga and In, have different properties in terms of substrate surface diffusion length, solubility in the seed particle, incorporation mechanism and affinity with respect to the seed material [139]. Au-seeded InGaAs nanowires usually have a very inhomogeneous composition and a tapered morphology [136]. Direct epitaxy of Au-seeded InGaAs nanowires on Si substrate has also been reported, but does not allow thorough control of the nanowire morphology and crystal phase [140]. Although a uniform composition and controlled crystal phase have recently been reported for Au-seeded InGaAs nanowires under optimized growth conditions [141], in general the growth of InGaAs nanowire is still complex and needs further work.

Self-seeded InGaAs nanowire growth has so far only been demonstrated by using Ga droplets [142][143]. The incorporation of In into the InGaAs nanowire is limited to around 5% with substantial In-rich radial shell growth [143], which results in a limited range of compositional tunability and a tapered nanowire morphology.

Selective area epitaxy of InGaAs nanowires has been a great success, and this allows direct epitaxy of InGaAs nanowires on a Si substrate for device applications [48][144][145]. However, the nanowire diameter increases with growth time due to

the unavoidable radial growth, which makes it almost impossible to achieve high aspect ratio InGaAs nanowires.

Moreover, doping in InGaAs nanowires has been investigated only rarely, with one exception being the study to my best knowledge that found Mn-doped InGaAs nanowires demonstrate ferromagnetic properties [146]. However, there is no epitaxial alignment of the nanowire with respect to the growth substrate. This is a complicated mechanism given the interaction and competition between the five elements for Au-seeded InGaAs with dopants. Thus, it would be easier if ternary nanowire doping can be achieved through the incorporation of the seed particle.

To the best of my knowledge, Ag is the only alternative foreign metal material that has been reported as being used for the growth of ternary nanowires [147][148]. Although the resulting InGaAs nanowires lack epitaxial alignment with respect to the growth substrate, Ag induces a more uniform nanowire morphology without substantial tapering, as has been observed for Au-seeded InGaAs nanowires.

In summary, the growth of InGaAs nanowires has been investigated for over a decade with some control having been achieved over the nanowire composition, crystal structure and morphology. Further research into the growth of InGaAs nanowires is essential in order to achieve complete control of the composition, crystal phase, morphology and tapering. Alternative metal seed material could potentially provide new insights into the growth of InGaAs nanowires as Ag has been demonstrated to be effective in reducing InGaAs nanowire tapering. By using alternative foreign metals, group III elements might have a different solubility and affinity, which could lead to growth behaviours that are very different from that of Au-seeded or Ga-seeded InGaAs nanowire growth. Furthermore, by selecting a foreign metal material, one can expect the incorporation of the metal material into InGaAs nanowires, which might lead to interesting properties being imparted to the nanowire.

5 Sn-Seeded Nanowire Growth

The work presented in this thesis focuses on the epitaxial growth of nanowires with in-situ formed Sn particles. Sn particles are deposited in the MOVPE reactor by flowing TESn with a small flow of AsH₃ as precursors at high temperatures. The formation of Sn droplets involves several steps including pyrolysis of the TESn precursor into elemental Sn and physical adsorption of the material onto the substrate surface, followed by the diffusion of Sn atoms on the substrate surface until they start to nucleate and grow into particles or desorb away from the surface. The nanowire growth is initiated by introducing a group III precursor (TMGa or TMIIn) and a group V precursor (AsH₃) at elevated temperature. The nanowire growth can be manipulated by varying the growth temperature as well as the molar flow of the precursors, thereby changing the nominal V/III ratio. The study of Sn-seeded GaAs nanowires is discussed in section 5.1. In section 5.2, the growth of Sn-seeded InAs nanowires is discussed. Finally, section 5.3 continues a discussion of the growth of GaAs-InGaAs heterostructure nanowires from Sn particles.

5.1 Sn-seeded GaAs nanowire growth (Paper I and II)

I have studied the formation of Sn particles on GaAs substrates, the growth of GaAs nanowires from Sn seed particles on GaAs (111)B substrate by varying fundamental growth parameters such as growth temperature, group V precursor flow and group III precursor flow, which is discussed in detail in Paper I and II. These results will be summarized in this section.

5.1.1 The formation of Sn particles on GaAs substrates

Figure 5.1 shows Sn particles formed on GaAs substrates under different conditions. Figure 5.1a shows the reference condition for Sn particle deposition on a GaAs (111)B surface at 550°C which is the standard condition used in Paper I and II. Sn particles with a homogeneous diameter and surface density are formed uniformly over the surface. Many processes are involved in reaching this very narrow size distribution. First Sn atoms decomposed from precursor TESn diffuse on the

substrate surface to preferential nucleation sites and grow into nuclei. With a continuous contribution of Sn atoms from the precursor flow, the nuclei will become stable and grow larger. In the meantime, small nuclei or particles will also form on the surface. However, due to the effect of Ostwald ripening and coalescence, the number of small particles could gradually decrease, resulting in increasing numbers of larger particles [149]. Over time, the effect of Ostwald ripening and coalescence would decrease the size distribution and give the Sn particles a more homogeneous size.

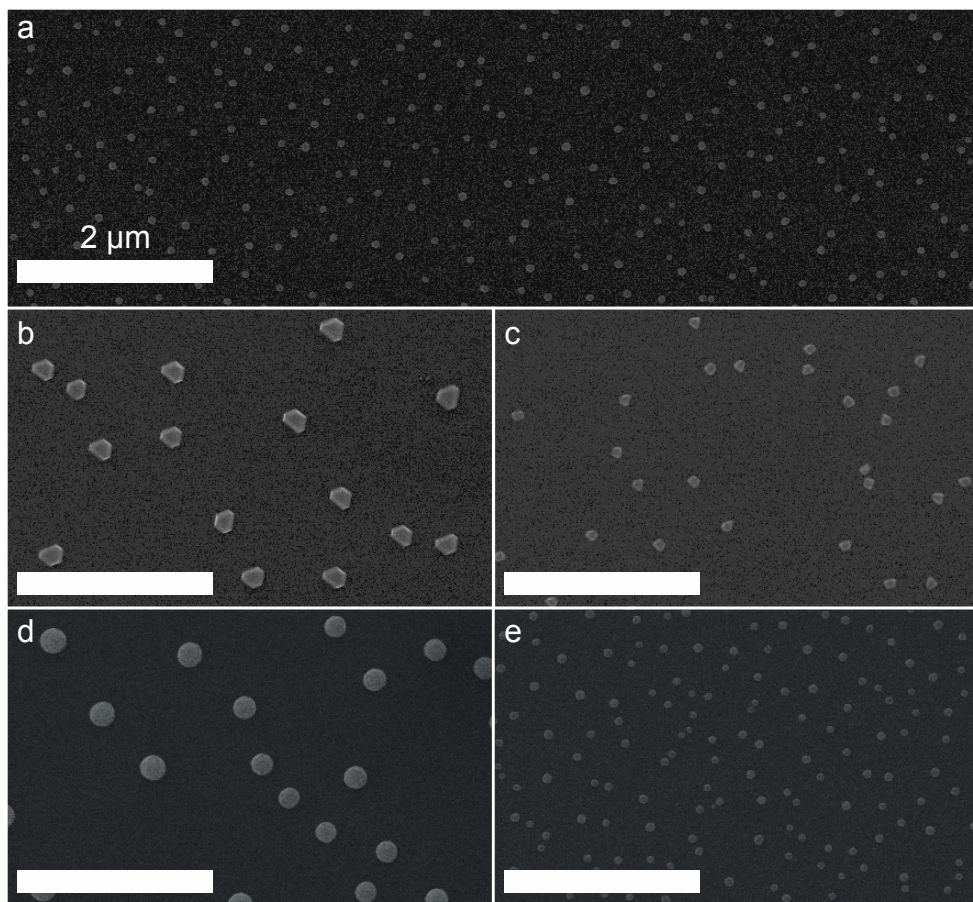


Figure 5.1 SEM micrographs of Sn particles formed on GaAs substrates under different conditions. a, reference condition for Sn particle formation on a GaAs (111)B surface with a low AsH_3 flow. b and c, Sn particles formed on GaAs (111)A and (111)B surfaces, respectively, with relatively high AsH_3 flow compared to the reference. d and e, Sn particles formed on GaAs (111)A and (111)B surfaces, respectively, without AsH_3 flow.

The temperature dependency of Sn particle formation on a GaAs (111)B substrate is studied elsewhere [150]. It has been suggested by investigating the particle diameter and density that the available amount of material for Sn particle formation increases with temperature.

In order to get some hints about the effect of AsH₃ flow on the mechanism of Sn particle formation, Figure 5.1 also compares Sn particles formed at relatively high AsH₃ flow (5.1c), low AsH₃ flow (5.1a) and no AsH₃ flow (5.1e) on a GaAs (111)B surface. It can be seen that the shape of Sn particles is more faceted in 5.1c and gradually changes to an intermediate condition in 5.1a, eventually becoming a round and smooth shape in 5.1e. It is very likely that the faceted Sn particles are associated with the formation of Sn-As compounds such as SnAs or Sn₄As₃ during cooling. This implies that AsH₃ incorporates into the droplets during the Sn particle formation step. The density of the Sn particles also changes with the AsH₃ flow. At a relatively high AsH₃ flow, as shown in Figure 5.1c, the density of the Sn particles is 2.6/μm². At a low AsH₃ flow, as in figure 5.1a, the density of Sn particles is 9.1/μm². When there is no AsH₃ flow during the particle formation step, the resulting density is 10.5/μm². The difference in particle density could be due to the completeness and morphology of the substrate. It is well known that GaAs substrate could decompose at high temperature and that the presence of AsH₃ could prevent this substrate decomposition [151]. The decomposition of the GaAs (111)B substrate would lead to defects or crystalline pits formed on the substrate surface, which could, in turn, act as preferential collection site for the diffusing material. Thus the substrate decomposition, which is more likely to occur under the no AsH₃ conditions, would result in larger particle density than under the high AsH₃ flow conditions, where the substrate could survive decomposition.

The polarity of the substrate surface also has a major impact on Sn particle formation. Figure 5.1 b and c show Sn particles formed at a relatively high AsH₃ flow on GaAs (111)A and (111)B surfaces, respectively. The density of Sn particles is 2.6/μm² on the (111)B substrate, which is higher than on the (111)A substrate (0.96/μm²). However, the size of the Sn droplets on the (111)A substrate is considerably larger than of those on the (111)B substrate. From a simple calculation of the surface area covered by the Sn droplets that assumes the droplets are circular, the percentage of the surface area covered by Sn particles on the (111)A substrate is 3.1%, which is much larger than the 1.9% of the (111)B substrate that is covered. Since the diameter of the particles on the (111)A surface is much larger than those on the (111)B surface, I speculate that they are also larger in height. This would imply that the volume of the coverage on the (111)A surface is even larger. There might be multiple factors that could possibly be responsible for this, for instance the decomposition rate of TESn precursor, the sticking coefficient for Sn, or the nucleation barrier for the nuclei.

In summary, the nucleation and formation of Sn particles is a process that involves many possible steps. The diameter, morphology and surface density of the in-situ formed Sn particles is dependent on many factors, including temperature, AsH_3 flow and substrate polarity.

5.1.2 Growth of Sn-seeded GaAs nanowires dependency on temperature and V/III ratio

The SEM image in Figure 5.2 shows the growth of GaAs nanowires in the temperature range of 475°C to 535°C . The temperature range for successful growth of GaAs nanowires from Sn particles is quite limited, which is from 487°C to 525°C at a fixed V/III ratio of 1.9. This is much narrower compared to GaAs nanowire growth from Au particles. Sn-seeded GaAs nanowire growth is very sensitive to and strongly dependent on the growth temperature. At a lower temperature, most of the nanowires are kinked, as shown in Figure 5.2a, and with increasing temperature, straight and vertical nanowires with tapered morphology are obtained, as shown in Figure 5.2b to e. At temperatures above 535°C , no obvious nucleation of the nanowires is observed, as shown in Figure 5.2f. The nanowire morphology is also related to the growth temperature. In the temperature range from 487°C to 525°C , when growth temperature rises, the length of the nanowires decreases and there is increasing radial growth; in addition, the side facets become rougher, as shown in Figure 5.2e, which is associated with the formation of rotational twin planes. The seed particle Sn remains at the tip of GaAs nanowire in the successful growth region.

Sn-seeded GaAs nanowires can be grown in a much narrower V/III ratio range compared to Au-seeded GaAs nanowires [72]. The effects of TMGa and AsH_3 precursors are investigated by varying the flow of each precursor while keeping the flow of the other constant.

Figure 5.3 shows the effect of TMGa precursor by presenting Sn-seeded GaAs nanowire growth with elevating TMGa precursor flow at a constant AsH_3 flow. As can be seen from the figure, the nanowire axial growth rate is strongly dependent on the supply of group III precursor. The nanowires adopt rough side facets with increasing TMGa flow, as shown in Figure 5.3 d and e as well as the insets, instead of the rather smooth side facets they take on at lower TMGa flows. These microfacets are correlated with multiple twin planes along the nanowires' growth axis.

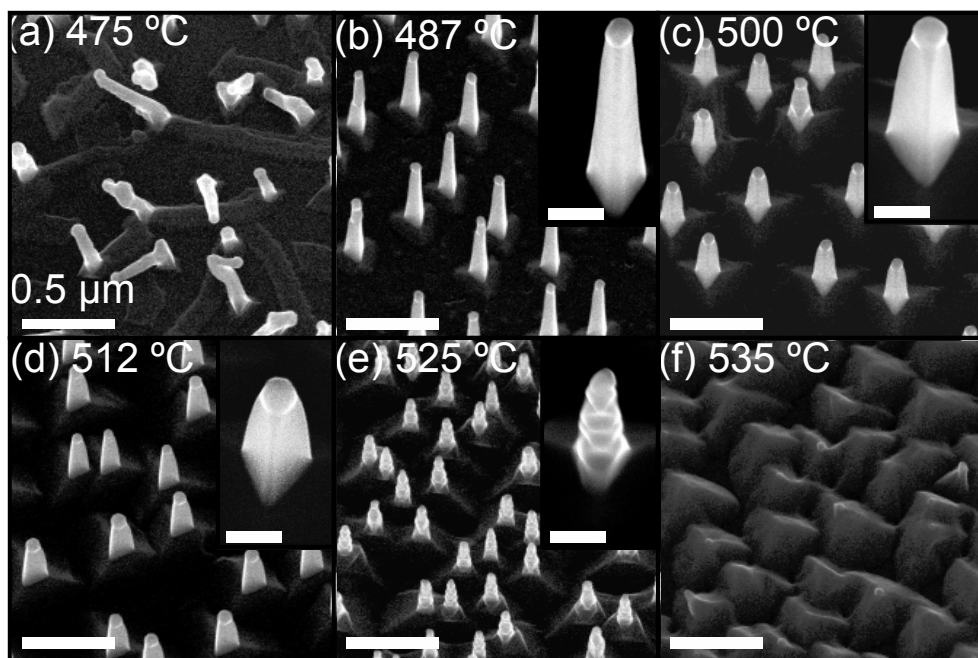


Figure 5.2 SEM images of Sn-seeded GaAs nanowires grown on a GaAs (111)B substrate at different temperatures with a fixed V/III ratio of 1.9.

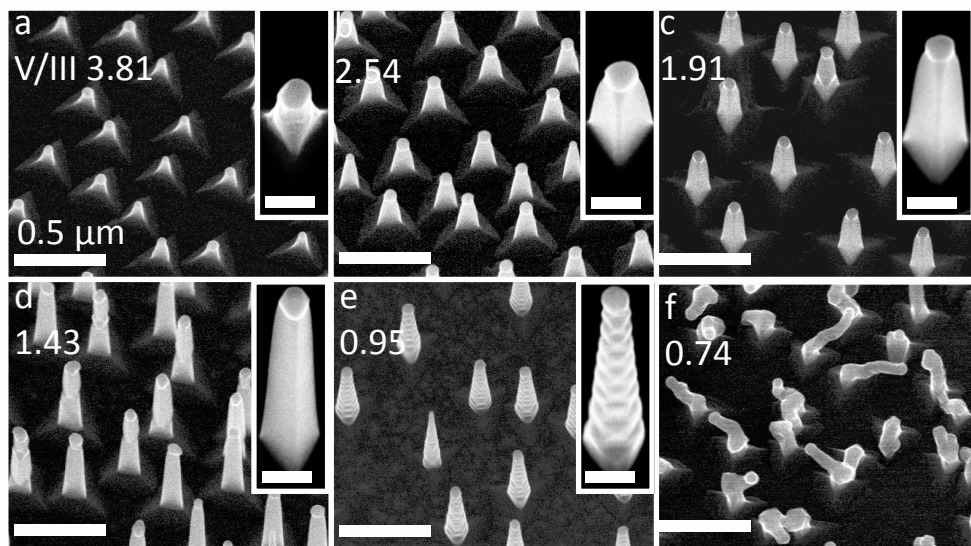


Figure 5.3 SEM images of Sn-seeded GaAs nanowires grown on a GaAs (111)B substrate with increasing TMGa precursor flow and constant AsH_3 flow at a fixed temperature of 500 °C.

Figure 5.4 shows the effect of AsH_3 precursor by presenting the growth of Sn-seeded GaAs nanowires with increasing AsH_3 precursor flow while keeping the TMGa flow constant. As illustrated in Figure 5.4a and the inset, nanowires have rough side facets at a low V/III ratio, and these are associated with twin planes perpendicular to the growth direction. This is consistent with what have been observed for the nanowires grown at a high TMGa flow, as shown in Figure 5.3e. The formation of twin planes in Sn-seeded GaAs nanowires is very likely caused by a relatively low V/III ratio, but not with the absolute precursor flows within the investigated V/III ratio range. Furthermore, a distinct trend in the rate of kinked nanowires associated with AsH_3 flow can be observed in Figure 5.4. At a V/III ratio of 3.34, around 6% of the nanowires kink into a non-vertical growth direction, as shown in Figure 5.4d. With increasing AsH_3 flow, and thus a higher V/III ratio, a larger number of kinked nanowires occur. Eventually, at a V/III ratio of 5.71, no straight and vertically aligned nanowires can be found, as shown in Figure 5.4f. The kinked nanowires with a high V/III ratio are similar to what has been observed with nanowire growth at a low temperature, as shown in Figure 5.2a, which could be due to incomplete pyrolysis of TMGa, resulting in a higher effective V/III ratio at the nanowire growth front.

By broadening the temperature window for Sn-seeded GaAs nanowire by gradually changing the TMGa flow and the growth temperature, vertical GaAs nanowires can be achieved at as low as 400°C . This implies the suitable growth temperature for Sn-seeded GaAs nanowires is closely connected to the V/III ratio.

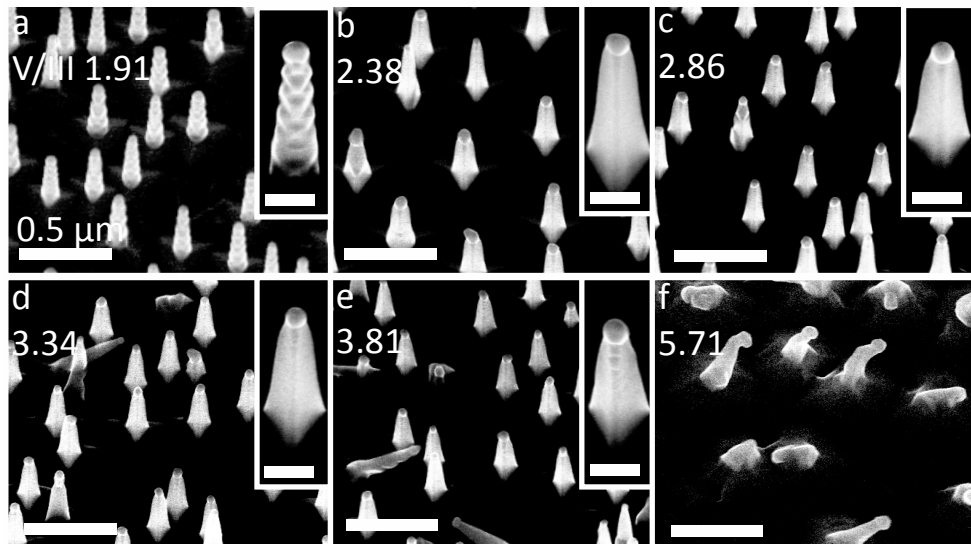


Figure 5.4 SEM images of Sn-seeded GaAs nanowires grown on a GaAs (111)B substrate with increasing AsH_3 precursor flow and constant TMGa flow at a fixed temperature of 500°C .

5.1.3 Properties of Sn-seeded GaAs nanowires

By analysing the nanowires in TEM, it has been found that the GaAs nanowires obtained using the investigated growth regime all have a pure ZB crystal structure or ZB with a few rotational twin planes; no WZ segment has ever been observed. A ZB crystal structure is stable and favourable in bulk GaAs material, whereas in nanowires, both a pure ZB and a pure WZ structure have been observed, but a mixture of the two is usually more common [42][152][153]. As shown in Figure 5.5a and b, the investigated GaAs nanowire is taken from the sample in Figure 5.2c, the nanowires have a pure ZB crystal structure without any rotational planes. Using energy-dispersive X-ray spectroscopy (XEDS), it is found that the seed particle remaining at the tip of the nanowire consists primarily of Sn, as shown in Figure 5.5g. It is also possible to find an As signal of up to 18 atomic % within the seed particle, which suggests that the solubility of As in a Sn particle is quite high and we might have a Sn droplet with a rich As content during nanowire growth. In Paper II, we also observe a long twin segment of up to 60 nm, as shown in Figure 5.5c, d and e, and we propose that the occurrence of rotational twinning planes along the nanowires is associated with a lower V/III ratio but not the absolute flow of either the group III or the group V precursor. For Au-seeded GaAs nanowires, the crystal structure is usually quite mixed between ZB and WZ phases and a gold particle with group III Ga component is usually detected with XEDS afterwards [110]. This indicates that the solubility of As in Au is much lower than that of Ga in Au, whereas As has a higher solubility and affinity in Sn than Ga. The ZB crystal structure in Sn-seeded GaAs nanowires could be due to the low surface energy of the Sn particle, as has been suggested for self-seeded GaAs nanowires where the Ga particle has a much lower surface energy than the AuGa compound [62].

One of the motivations for using alternative seed particles is the desire to investigate the interesting properties that the seed particle might bring into the nanowire system, for example self-doping or magnetism. In our experiment, the Sn seed particle is consumed and incorporated into the nanowire during growth. Figure 5.5f shows one extreme case where the Sn seed particles are completely consumed during growth. A weak Sn signal is detectable by XEDS along the GaAs nanowires, as shown in Figure 5.5g. However, the Sn content must be very high for this to have been detected at all as it is close to the detection limit of this technique, which is in the order of 1 atomic %. From electrical measurement, we find that the GaAs nanowires are highly n-doped, which can be attributed to the incorporation of Sn from the seed particles. Moreover, there is also a p-type shell on the nanowires, which we attribute to the incorporation of C into the simultaneous radial overgrowth. The nanowire works as a radial p-n junction in which band-to-band tunnelling is the dominant transport mechanism for both reverse bias and small forward bias and has a very high peak-to-valley current ratio. Photoluminescence (PL) measurement also

confirms the high doping level in the nanowires, with a strong Burstein–Moss shift, which increases the average recombination energy and broadens the PL spectrum. By characterizing nanowires grown under different conditions using electrical and optical approaches, we find that the incorporation of Sn and C into the GaAs nanowires can be controlled to some degree by varying growth temperature.

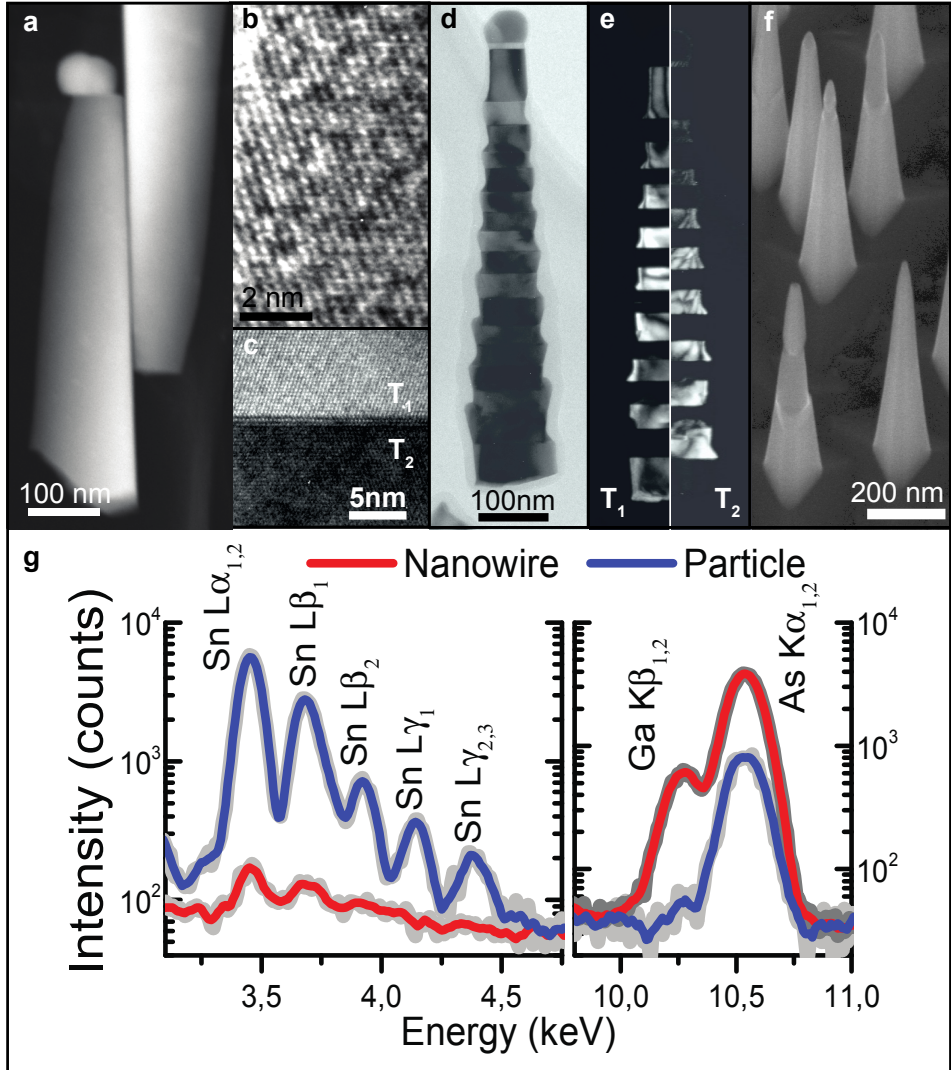


Figure 5.5 TEM images of Sn-seeded GaAs nanowires grown at different conditions where the pure ZB phase and multiple twin segments are observed in a, b, c, d and e. SEM image of Sn-seeded GaAs nanowires where the Sn particle is completely consumed in f. XEDS spectrum for the nanowire and particle in g.

5.2 Sn-seeded InAs nanowire growth (Paper III and IV)

Based on the project for Sn-seeded GaAs nanowire growth, I have also expanded the use of Sn to an InAs system as replacing the group III material Ga with In appeared to be a natural and intuitive continuation of this work. In this section, I will summarize the deposition and formation of Sn particles on InAs substrates, the growth of InAs nanowires from Sn seed particles on an InAs (111)A substrate by varying fundamental growth parameters including growth temperature and group III precursor flow. This part is discussed in detail in Paper III and IV.

5.2.1 The formation of Sn particles on InAs substrates

Figure 5.6 shows Sn particles formed on InAs substrates at different temperatures. The left column in Figure 5.6a, c, e and g, is what has been observed on an InAs (111)A surface, whereas the right column, b, d, f and h, shows Sn particles formed on an InAs (111)B surface.

The polarity of the substrate surface affects the formation of Sn particles. In Figure 5.6, the density of the Sn particles formed on a (111)B substrate is always larger than those formed on a (111)A substrate, regardless of the temperature at which they have been deposited. This is similar to the trend for the density of the Sn particles observed on GaAs substrates. Thus, similarly to what has been proposed for GaAs surfaces, there could be multiple reasons responsible for this such as the sticking coefficient of Sn atoms and the nucleation barrier for the nuclei to form.

It is also worth noting the opposite trends observed for the contact angle of the Sn particles. The contact angle of the particles on a (111)A surface increases from $49.7^\circ \pm 3$ at 490°C to $59.7^\circ \pm 2$ at 550°C , while on a (111)B surface, this decreases from $73.9^\circ \pm 1$ at 490°C to $60.6^\circ \pm 2$ at 550°C . The contact angle is obtained from a geometric model that we proposed in Paper III, which we believe is more accurate than the direct measurement from the image. It is interesting that the contact angle of Sn droplets on (111)A and (111)B substrates becomes consistent at a temperature of 550°C regardless of the opposite trend observed with increasing temperature.

The Sn particle formation under conditions identical to what is shown in Figure 5.6g, were used for the subsequent InAs nanowire growth.

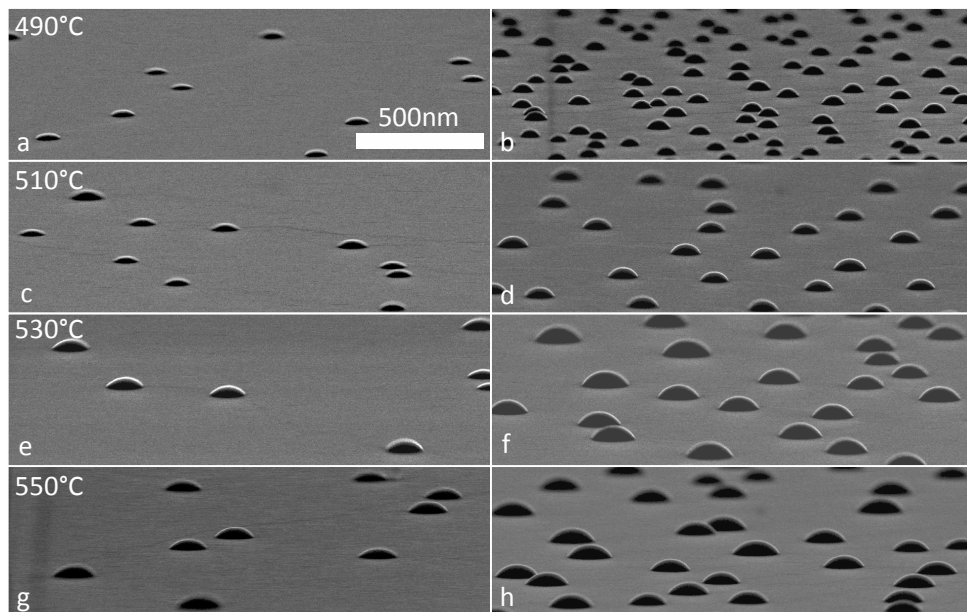


Figure 5.6 SEM images of Sn particles formed on InAs substrates at elevating temperatures.

5.2.2 Growth of Sn-seeded InAs nanowires dependent on temperature and V/III ratio

SEM images of InAs nanowire growth on an InAs (111)A substrate from Sn seed particles in the temperature range 455°C to 510°C are shown in Figure 5.7. Successful InAs nanowire growth is achieved when the nanowire is straight and vertically aligned on the InAs (111)A substrate. The temperature range for successful growth of InAs nanowires is quite limited, i.e. from 473°C to 500°C at a fixed V/III ratio of 91.6. The suitable temperature range for Sn-seeded InAs nanowire growth is much narrower than the range for Au-seeded InAs nanowires, which is from 380°C to 500°C [41][154]. We have also observed that there is a strong edge effect for nanowire growth. For example, Figure 5.7c shows InAs nanowires that have inhomogeneous length in the centre of the substrate, while homogeneous and longer nanowires are observed at the edge of the same substrate. This could be because the decomposition of precursors is enhanced at the edge of the substrate and more materials are involved in the growth process, whereas in the centre of the substrate the growth is limited by the available amount of material. Based on this assumption, the growth of InAs nanowires can be optimized by doubling the total flow of precursors while keeping the nominal V/III ratio and temperature constant, as shown in Figure 5.7f, where the nanowire growth rate increases and the length and the morphology become homogenous across the whole substrate.

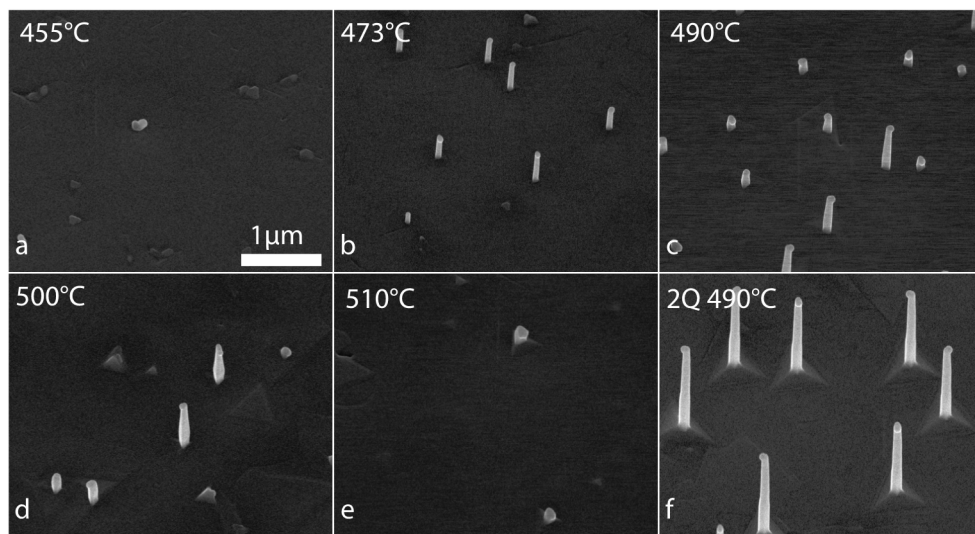


Figure 5.7 SEM images of Sn-seeded InAs nanowires grown on an InAs (111)A substrate at different temperatures with a fixed V/III ratio of 91.6 (a to e). InAs nanowire grown at optimized conditions (f).

The effects of nominal V/III ratio on InAs nanowire growth with Sn seed particles have been investigated. As shown in Figure 5.8, when the flow of TMIn precursor is varied while the AsH_3 flow is kept constant, the density of nucleated InAs nanowires increases dramatically with decreasing TMIn flow, thus the increasing V/III ratio. At a V/III ratio of 183.2 and higher up to 366.5, the nucleation rate from Sn particles is close to 100%, and we expect that a V/III ratio higher than 366.5 will also result in full nucleation of InAs nanowires from Sn particles. When increasing the TMIn flow results in a V/III ratio in the range of 91.6 to 122.2, the nucleation rate drops about 20%. Further increasing the TMIn flow into the reactor results in only 40% to 50% of the Sn droplets leading to successful nucleation of InAs nanowires. We have observed an identical trend when the AsH_3 flow is varied at a constant TMIn flow. At a lower AsH_3 flow, the nucleation of InAs nanowires is limited and very few nanowires can be observed. Increasing the AsH_3 flow improves the nucleation rate, yielding vertically aligned nanowires. It could be that successful nanowire nucleation from Sn droplets requires only a limited amount of In content in the particle is required. When there is a certain amount of In content in the Sn droplets, the surface energy of the Sn-In particle might be different from a Sn or even a Sn-As particle. The In content could also change the size of the seed particle. Thus, the stability of the Sn particle and the contact angle between the particle and the substrate might be changed. This change could hinder the nucleation of InAs nanowires and lead to surface island growth. A thermodynamic explanation of the growth mechanism is also proposed. The solubility of As in Sn particles decreases rapidly with increasing In content in the particle. This decrease in solubility is most

pronounced when there is a low In component, i.e. when In increases from 4% up to 20%. Thus, an increased amount of In can make it more difficult for As to incorporate or diffuse through the particle. The nanowire growth then becomes limited within this region.

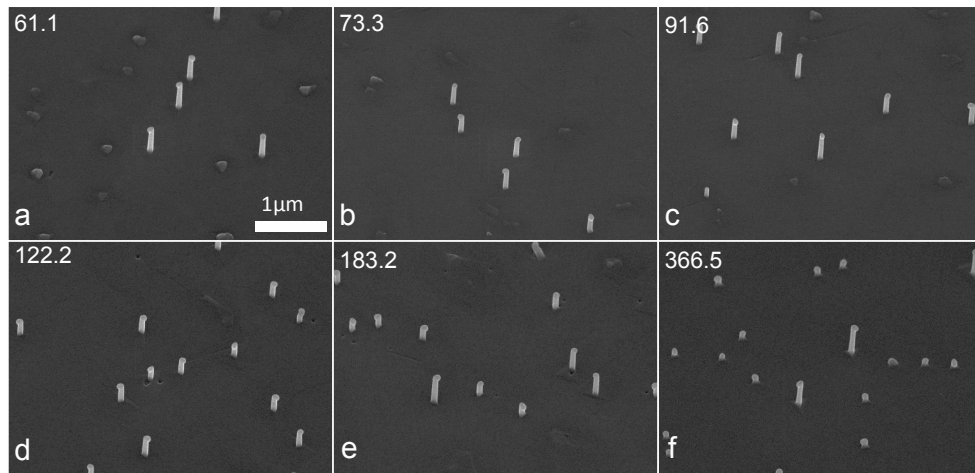


Figure 5.8 SEM images of Sn-seeded InAs nanowires grown on an InAs (111)A substrate with decreasing TMGa precursor flow and constant AsH₃ flow at a fixed temperature of 473°C

5.2.3 Properties of Sn-seeded InAs nanowires

By analysing the InAs nanowires in TEM, it has been found that under the investigated growth regime, the InAs nanowires obtained all have a pure ZB crystal structure with no rotational twin planes, a WZ segment has never been observed. A pure ZB crystal structure is usually difficult to achieve in Au-seeded InAs nanowires, especially in the temperature range that has been used here [41].

Figure 5.9 shows representative TEM images of a single InAs nanowire from Figure 5.7f. Figure 5.9c and the inset display pure ZB crystals. Figure 5.9b, d and e show how the Sn particle has slid down from the nanowire tip and has a tilted interface with the nanowire growth front. This happens during the cooling down process. The XEDS colour map in Figure 5.9e also shows that there is an As-rich Sn phase segregated from the Sn particle.

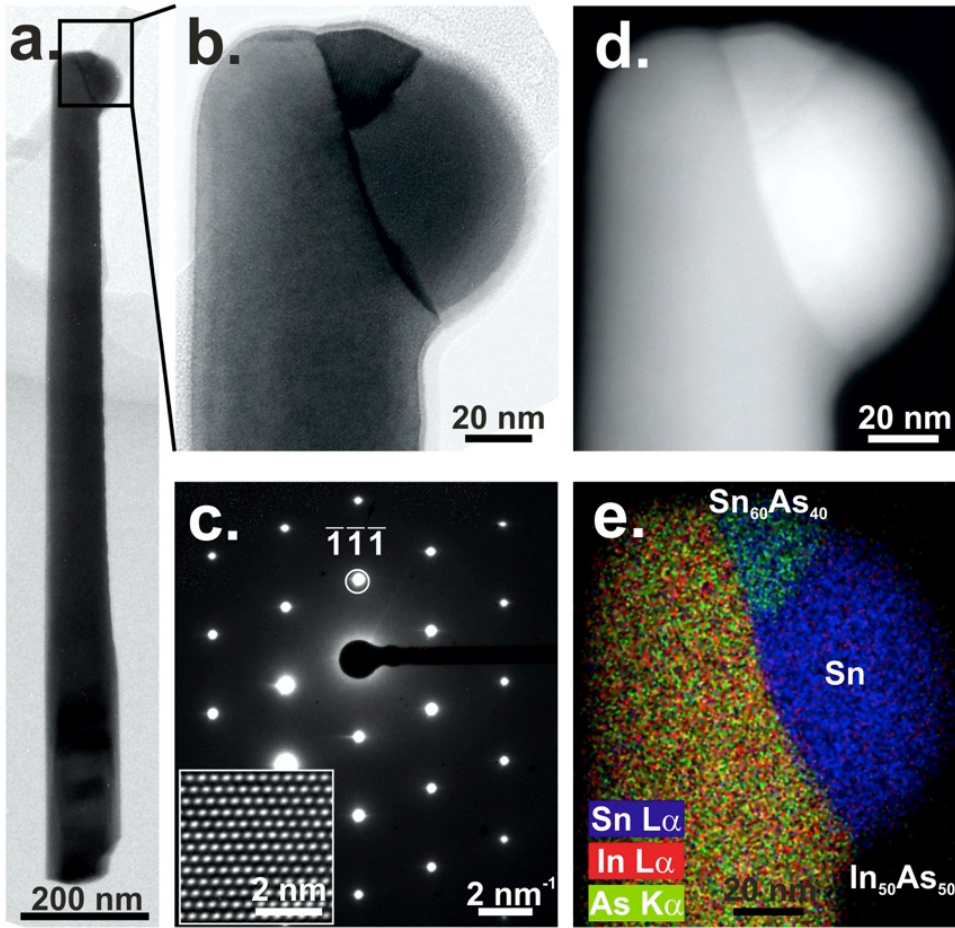


Figure 5.9 TEM images and diffraction pattern of Sn-seeded InAs nanowire with pure ZB crystal phase. XEDS colour map shows Sn particle at the tip of nanowire and the As-rich Sn phase.

Electrical characterization has been performed on Sn-seeded InAs nanowires. The resistivity of the nanowires is calculated based on the I-V characteristics, and is found to be much lower than that of intentionally doped InAs nanowires [119]. Back-gate measurements show n-type behaviour of the nanowires; however, the influence of the gate voltage is very low, which also confirms the high doping level. The doping profile in InAs nanowires comes from the simultaneous incorporation of the Sn seed particle into the nanowire during growth. The low resistivity of the nanowires proves that growth with Sn seed particles is a very efficient way to achieve high doping levels in InAs nanowires while achieving defect-free pure crystal phase compared to the intentional doping during growth using dopant precursors for Au-seeded nanowires.

In summary, Sn has been successfully employed as seed catalyst for the growth of GaAs and InAs nanowires. The resulting nanowires predominantly possess a ZB crystal phase, with rotational twin planes occurring occasionally in GaAs nanowires. This could be due to the low surface energy of Sn, which is even lower than that of Ga and comparable to that of In [35]. It has been proposed that for Ga-seeded GaAs nanowires on a Si substrate, the low surface energy Ga particle suppresses the triple phase boundary nucleation, which favours the ZB formation and makes the ZB phase formation less dependent on the growth parameters. In our case, where a low surface energy Sn particle is used, it might be the same scenario, i.e. that centre nucleation at the particle-nanowire interface is favoured over the triple phase boundary nucleation, resulting in the formation of the ZB crystal phase.

5.3 Sn-seeded GaAs-InGaAs heterostructures

After successful growth of Sn-seeded GaAs and InAs nanowires, an intuitive continuation of the project is to use Sn particles for the growth of ternary nanowires like InGaAs. As mentioned previously in section 4.2, no thorough study of the doping of InGaAs nanowires has yet been conducted. Based on what we have observed for GaAs and InAs nanowires, it would be beneficial for device applications if InGaAs could be doped by Sn particles with control over nanowire morphology and crystal phase.

As discussed in section 5.2.2, the nucleation and growth of Sn-seeded InAs nanowires are very sensitive to the particle composition. It is speculated that with the introduction of an extra element, Ga, to the growth system, direct nucleation of InGaAs from the substrate would become more complicated. Thus, in this work, a GaAs nanowire stem is used on a GaAs (111)B substrate, followed by InGaAs nanowire growth. The growth process involves firstly 10 min of GaAs stem growth (the reference GaAs stem is shown in Figure 5.10a), followed by InGaAs nanowire growth by introducing the TMIn precursor into the reactor for 20 min.

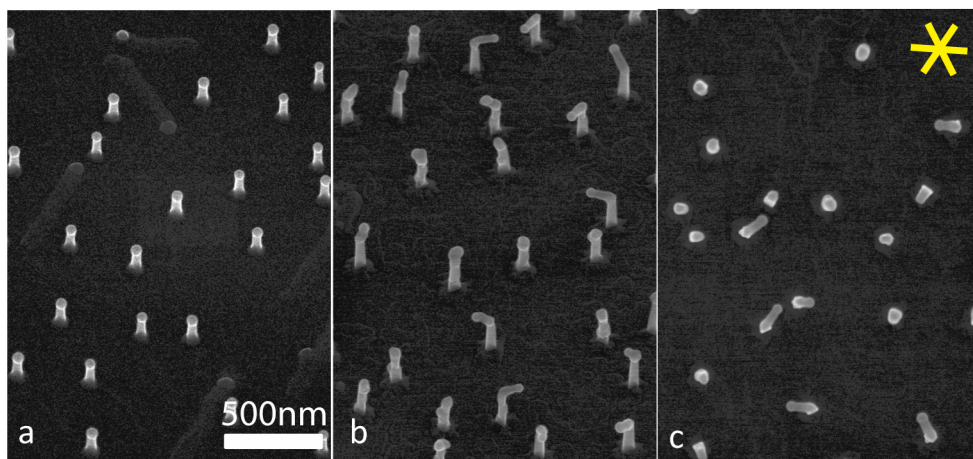


Figure 5.10 SEM images of Sn-seeded GaAs-InGaAs heterostructure nanowires. Tilted view of GaAs nanowire stem on a GaAs (111)B substrate in a, GaAs-InGaAs nanowires in b, and top view of GaAs-InGaAs nanowires in c.

Figure 5.10b and c show the preliminary results of InGaAs nanowires grown on GaAs nanowire stems at 455°C. The tilted view in Figure 5.10b shows that there are two clear nanowire segments: the bottom one is the GaAs nanowire stem and the top one is supposed to be the InGaAs segment. When In is introduced to the system, a number of nanowires kink to another direction. The top view image in Figure 5.10c shows that there are six directions for the kinked InGaAs nanowires. This implies that the InGaAs nanowires kink to $\langle 111 \rangle_A$ direction. In addition to the three equivalent $\langle 111 \rangle_A$ directions which should be observed on (111)B surface. The extra three directions might be due to the rotational twin formed in the GaAs nanowire stem. The six $\langle 111 \rangle_A$ directions are marked with coloured lines. The nominal V/III ratio ($As/(In+Ga)$) is 0.86, and the nominal In vapour concentration ($In/(In+Ga)$) is 0.014. It is quite interesting that an almost negligible amount of TMIIn can have a big impact on the nanowire growth and change the growth direction. Considering the many factors that could affect the growth of ternary nanowires, e.g. the different solubility into the particle and affinity with the particle as well as the different diffusion length of group III species, it is not straightforward to interpret what has been observed here and it definitely needs much more input into this work in order to achieve controlled growth and a thorough understanding of the system.

6 Summary and outlook

In recent decades, the growth and properties of III-V nanowires have been investigated intensively. A variety of nanowire-based electronic and optoelectronic devices have been demonstrated. With the increasing potential for device applications, there are greater demands for the ability to control nanowire properties such as crystal structure, doping profile, nanowire heterostructures as well as various nanowire-substrate combinations. To meet all these new demands, other growth techniques besides the traditional Au-seeded nanowire growth need to be explored. Selective area nanowire epitaxy and self-seeded nanowire growth have been developed a great deal and have become quite mature in terms of direct epitaxy from a Si substrate and the cleanliness and purity of the resulting nanowires. Nevertheless, the exploration of alternative foreign metal seed materials to assist III-V nanowire growth can potentially provide new insights into our understanding of and controlling over nanowire growth.

The intention of this thesis is to study alternative seed particle materials, in particular Sn, for the growth of III-V nanowires. First, the behaviour and properties of the in-situ formed Sn particles have been investigated. It is shown that the deposition and nucleation of the Sn particles are strongly dependent on the substrate material and polarity. Second, Sn-seeded growth of GaAs and InAs nanowires has been successfully demonstrated. It has been observed that the Sn particle is consumed and incorporated into the resulting nanowire. From electrical and optical characterization, one can see that Sn atoms become active n-type dopant in both GaAs and InAs nanowires. Sn-seeded nanowires predominantly possess a ZB crystal structure, which suggests that the seed particle material can strongly affect the crystal structure of the nanowire.

I hope that the investigation of Sn as seed particle material for the growth of III-V nanowires is not completely trivial and can make some contribution to our understanding of the essential properties of a suitable seed material. Although alternative foreign metal seed materials will never completely replace Au for the growth of III-V nanowires, they might be useful for growing nanowires with properties designed for specific application. For example, the fact that this thesis has demonstrated that the incorporation of Sn is an effective way to dope nanowires indicates that the approach of using in-situ formed Sn particles for nanowire growth could be promising for applications like electrical devices where a high n-doping

profile is required. However, due to the simultaneous consumption and incorporation of Sn particles into the nanowires, it is almost impossible to achieve intrinsic nanowires. For optoelectronic applications like solar cells or diode lasers, a designed p-n junction is essential for the device to function efficiently. Although a radial p-n junction has been shown in Paper I, this approach is still limited if an axial p-n junction is required, unless the Sn seed particle is completely consumed or removed before growing the p-doped section axially.

While research into alternative metal seed materials may not yet be able to answer all the questions that we have, there is still hope that in the future it will increase our general understanding of and control over nanowire growth and provide new approaches to the design of nanowire structures and properties that might be difficult to achieve in Au-seeded nanowires.

7 References

- [1] G. E. Moore, “Cramming more components onto integrated circuits (Reprinted from Electronics, pg 114-117, April 19, 1965),” *Proc. Ieee*, vol. 86, no. 1, pp. 82–85, 1998.
- [2] F. Qian, S. Gradec, and C. M. Lieber, “Core / Multishell Nanowire Heterostructures as Multicolor , High-Efficiency Light-Emitting Diodes,” 2005.
- [3] X. Duan, Y. Huang, Y. Cui, and J. Wang, “Indium phosphide nanowires as building blocks for nanoscale electronic and optoelectronic devices,” vol. 409, no. January, pp. 1999–2002, 2001.
- [4] K. Tomioka, J. Motohisa, S. Hara, K. Hiruma, and T. Fukui, “Light-Emitting Diodes on Si,” pp. 1639–1644, 2010.
- [5] D. Saxena, S. Mokkaapati, P. Parkinson, N. Jiang, Q. Gao, and H. H. Tan, “Optically pumped room-temperature GaAs nanowire lasers,” vol. 7, no. November, 2013.
- [6] G. K. and J. J. F. B. Mayer, D. Rudolph, J. Schnell, S. Morkötter, J. Winnerl, J. Treu, K. Müller, G. Bracher, G. Abstreiter, “nanowires up to Lasing from individual GaAs-AlGaAs core-shell nanowires up to room temperature temperature,” *Nat. Commun.*, vol. 4, p. 2931, 2013.
- [7] M. T. B. J. Wallentin, N. Anttu, D. Asoli, M. Huffman, I. Åberg, M. H. Magnusson, G. Siefert, P. Fuss-Kailuweit, F. Dimroth, B. Witzigmann, H. Q. Xu, L. Samuelson, K. Deppert, “InP Nanowire Array Solar Cells Achieving 13.8% Efficiency by Exceeding the Ray Optics Limit,” *Science (80-.)*, vol. 339, no. 2013, p. 1057, 2013.
- [8] P. Krogstrup, H. I. Jørgensen, M. Heiss, O. Demichel, J. V Holm, M. Aagesen, J. Nygard, and A. Fontcuberta, “Single-nanowire solar cells beyond the Shockley-Queisser limit,” vol. 7, no. April, 2013.
- [9] C. B. COLLINS, R. O. CARLSON, and C. J. GALLAGHER, “Properties of Gold-Doped Silicon,” vol. 105, no. 1953, pp. 1168–1173, 1957.
- [10] D. V. Lang, H. G. Grimmeiss, E. Meijer, and M. Jaros, “Complex nature of gold-related deep levels in silicon,” *Phys. Rev. B*, vol. 22, no. 8, pp. 3917–3934, 1980.
- [11] G. B. Stringfellow, “Overview of the OMVPE Process,” no. December 1998, 2000.
- [12] D. L. Smith, *Thin-film deposition: principles and practice*. International ed, McGraw-Hill, New York, 1995.
- [13] V. G. Dubrovski, N. V Sibirev, R. A. Suris, V. M. Ustinov, M. Tchernysheva, and J. C. Harmand, “The Role of Surface Diffusion of Adatoms in the Formation of Nanowire Crystals,” vol. 40, no. 9, pp. 1103–1110, 2006.

- [14] V. G. Dubrovskii, N. V. Sibirev, G. E. Cirlin, I. P. Soshnikov, W. H. Chen, R. Larde, E. Cadel, P. Pareige, T. Xu, B. Grandidier, J. P. Nys, D. Stievenard, M. Moewe, L. C. Chuang, and C. Chang-Hasnain, "Gibbs-Thomson and diffusion-induced contributions to the growth rate of Si, InP, and GaAs nanowires," *Phys. Rev. B - Condens. Matter Mater. Phys.*, vol. 79, no. 20, pp. 1–7, 2009.
- [15] C. A. Larsen, S. H. Li, N. I. Buchan, G. B. Stringfellow, and D. W. Brown, "Kinetics of the reaction between trimethylgallium and arsine," *J. Cryst. Growth*, vol. 102, no. 1–2, pp. 126–136, 1990.
- [16] R. LOCKERATH, P. TOMMACK, A. HERTLING, K. H.J, P. BALK, K. F. JENSEN, and W. RICHTER, "CARS IN SITU DIAGNOSTICS IN MOVPE: THE THERMAL DECOMPOSITION OF AsH₃ AND PH₃," vol. 93, pp. 151–158, 1988.
- [17] R. S. Wagner and W. C. Ellis, "Vapor-liquid-solid mechanism of single crystal growth," *Appl. Phys. Lett.*, vol. 4, no. 5, pp. 89–90, 1964.
- [18] K. Hiruma, M. Yazawa, K. Haraguchi, K. Ogawa, T. Katsuyama, and H. Kakibayashi, "GaAs free-standing quantum-size wires," vol. 3162, no. 1993, 2009.
- [19] K. Hiruma, M. Yazawa, T. Katsuyama, K. Ogawa, K. Haraguchi, M. Koguchi, and H. Kakibayashi, "Growth and optical properties of nanometer-scale GaAs and InAs whiskers," *J. Appl. Phys.*, vol. 77, no. 2, p. 447, 1995.
- [20] M. S. Gudiksen, L. J. Lauhon, J. Wang, D. C. Smith, and C. M. Lieber, "Growth of nanowire superlattice structures for nanoscale photonics and electronics," vol. 415, no. February, pp. 617–620, 2002.
- [21] M. Hilse, M. Ramsteiner, S. Breuer, L. Geelhaar, and H. Riechert, "Incorporation of the dopants Si and Be into GaAs nanowires," *Appl. Phys. Lett.*, vol. 96, no. 19, pp. 2008–2011, 2010.
- [22] P. Caroff, M. E. Messing, B. M. Borg, K. A. Dick, K. Deppert, and L. Wernersson, "InSb heterostructure nanowires : MOVPE growth under extreme lattice mismatch," 2009.
- [23] W. Seifert and J. Johansson, "Diameter-dependent growth rate of InAs nanowires," no. October, pp. 1–4, 2007.
- [24] M. Tornberg, K. A. Dick, and S. Lehmann, "Thermodynamic Stability of Gold-Assisted InAs Nanowire Growth," 2017.
- [25] M. Jeppsson, K. A. Dick, J. B. Wagner, P. Caroff, K. Deppert, L. Samuelson, and L. Wernersson, "GaAs / GaSb nanowire heterostructures grown by MOVPE," vol. 310, pp. 4115–4121, 2008.
- [26] E. Dimakis, L. Jonas, U. Jahn, M. Hilse, and L. Geelhaar, "Self-Assisted Nucleation and Vapor Å Solid Growth of InAs Nanowires on Bare Si (111)," no. 111, pp. 4001–4008, 2011.
- [27] J. Noborisaka, J. Motohisa, T. Fukui, J. Noborisaka, J. Motohisa, and T. Fukui, "epitaxy Catalyst-free growth of GaAs nanowires by selective-area metalorganic vapor-phase epitaxy," vol. 213102, no. 2005, 2005.
- [28] K. Tomioka, J. Motohisa, S. Hara, and T. Fukui, "Control of InAs nanowire growth directions on Si," *Nano Lett.*, vol. 8, no. 10, pp. 3475–3480, 2008.

- [29] W. S. Shi, Y. F. Zheng, N. Wang, C. S. Lee, S. T. Lee, W. S. Shi, Y. F. Zheng, N. Wang, C. S. Lee, and S. T. Lee, "Oxide-assisted growth and optical characterization of gallium-arsenide nanowires Oxide-assisted growth and optical characterization of gallium-arsenide nanowires," vol. 3304, no. 2001, pp. 1–4, 2011.
- [30] S. N. Mohammad, "Investigation of the oxide-assisted growth mechanism for nanowire growth and a model for this mechanism Investigation of the oxide-assisted growth mechanism for nanowire growth," vol. 1993, no. 2008, 2011.
- [31] M. E. Messing, K. Hillerich, J. Johansson, K. Deppert, and K. A. Dick, "The use of gold for fabrication of nanowire structures," *Gold Bull.*, vol. 42, no. 3, pp. 172–181, 2009.
- [32] R. L. Barns and W. C. Ellis, "Whisker Crystals of Gallium Arsenide and Gallium Phosphide Grown by the Vapor—Liquid—Solid Mechanism," vol. 2296, no. 1965, 2008.
- [33] D. Jacobsson, F. Panciera, J. Tersoff, M. C. Reuter, S. Lehmann, S. Hofmann, K. A. Dick, and F. M. Ross, "Interface dynamics and crystal phase switching in GaAs nanowires," *Nature*, vol. 531, no. 7594, p. accepted, 2016.
- [34] N. V Sibirev, M. A. Timofeeva, A. D. Bol, M. V Nazarenko, and V. G. Dubrovski, "Surface Energy and Crystal Structure of Nanowhiskers of III – V Semiconductor Compounds," vol. 52, no. 7, pp. 1531–1538, 2010.
- [35] K. C. Mills, Y. C. Su, K. C. Mills, and Y. C. Su, "Review of surface tension data for metallic elements and alloys : Part 1 – Pure metals Review of surface tension data for metallic elements and alloys : Part 1 – Pure metals," vol. 6608, 2013.
- [36] C. Wen, J. Tersoff, M. C. Reuter, E. A. Stach, and F. M. Ross, "Step-Flow Kinetics in Nanowire Growth," vol. 195502, no. November, pp. 1–4, 2010.
- [37] S. Kodambaka, J. Tersoff, M. C. Reuter, and F. M. Ross, "Germanium Nanowire Growth Below the Eutectic Temperature," vol. 316, no. May, 2007.
- [38] E. A. S. F. M. R. C.-Y. Wen, M. C. Reuter, J. Bruley, J. Tersoff, S. Kodambaka, "Structure , Growth Kinetics , and Ledge Flow during Vapor - Solid - Solid Growth of Copper-Catalyzed Silicon Nanowires," pp. 514–519, 2010.
- [39] C.-Y. Wen, M. C. Reuter, J. Bruley, J. Tersoff, S. Kodambaka, E. A. Stach, and F. M. Ross, "Formation of Compositionally Abrupt Axial Heterojunctions in Silicon-Germanium Nanowires," *Science (80-.)*, no. November, pp. 1247–1251, 2009.
- [40] B. A. Wacaser, K. Deppert, L. S. Karlsson, L. Samuelson, and W. Seifert, "Growth and characterization of defect free GaAs nanowires," vol. 287, pp. 504–508, 2006.
- [41] H. J. Joyce, J. Wong-leung, Q. Gao, H. H. Tan, and C. Jagadish, "Phase Perfection in Zinc Blende and Wurtzite III - V Nanowires Using Basic Growth Parameters," pp. 908–915, 2010.
- [42] S. Lehmann, J. Wallentin, D. Jacobsson, K. Deppert, and K. A. Dick, "A General Approach for Sharp Crystal Phase Switching in InAs, GaAs, InP, and GaP Nanowires Using Only Group V Flow," 2013.
- [43] J. Wallentin, M. Ek, L. R. Wallenberg, L. Samuelson, K. Deppert, and M. T. Borgstro, "Changes in Contact Angle of Seed Particle Correlated with Increased Zincblende Formation in Doped InP Nanowires," pp. 4807–4812, 2010.

- [44] J. Wallentin, K. Mergenthaler, M. Ek, L. R. Wallenberg, L. Samuelson, K. Deppert, M. Pistol, and M. T. Borgstr, "Probing the Wurtzite Conduction Band Structure Using State Filling in Highly Doped InP Nanowires," pp. 2286–2290, 2011.
- [45] B. D. Joyce and J. A. Baldrey, "Selective Epitaxial Deposition of Silicon," *Nature*, vol. 195, pp. 485–486, 1962.
- [46] J. Motohisa, J. Noborisaka, J. Takeda, M. Inari, and T. Fukui, "Catalyst-free selective-area MOVPE of semiconductor nanowires on (111)B oriented substrates," *J. Cryst. Growth*, vol. 272, no. 1–4, pp. 180–185, Dec. 2004.
- [47] K. Ikejiri, J. Noborisaka, S. Hara, J. Motohisa, and T. Fukui, "Mechanism of catalyst-free growth of GaAs nanowires by selective area MOVPE," *J. Cryst. Growth*, vol. 298, pp. 616–619, 2007.
- [48] K. Tomioka, M. Yoshimura, and T. Fukui, "A III–V nanowire channel on silicon for high-performance vertical transistors," *Nature*, vol. 488, no. 7410, pp. 189–192, 2012.
- [49] T. Fukui and M. Yoshimura, "Position-Controlled III – V Compound Semiconductor Nanowire Solar Cells by Selective-Area Metal – Organic Vapor Phase Epitaxy," vol. 41, no. Supplement 2, pp. 119–124, 2012.
- [50] H. J. Joyce, Q. Gao, H. H. Tan, C. Jagadish, Y. Kim, X. Zhang, Y. Guo, and J. Zou, "Twin-free uniform epitaxial GaAs nanowires grown by a two-temperature process.," *Nano Lett.*, vol. 7, no. 4, pp. 921–6, Apr. 2007.
- [51] M. H. Madsen, M. Aagesen, P. Krogstrup, C. Sørensen, and J. Nygård, "Influence of the oxide layer for growth of self-assisted InAs nanowires on Si (111)," pp. 1–5, 2011.
- [52] F. Matteini, G. Tütüncüoglu, H. Potts, F. Jabeen, and A. F. Morral, "Wetting of Ga on SiO₂," pp. 1–5, 2015.
- [53] A. Fontcuberta I Morral, C. Colombo, G. Abstreiter, J. Arbiol, and J. R. Morante, "Nucleation mechanism of gallium-assisted molecular beam epitaxy growth of gallium arsenide nanowires," *Appl. Phys. Lett.*, vol. 92, no. 6, pp. 10–13, 2008.
- [54] C. J. Novotny, P. K. L. Yu, C. J. Novotny, and P. K. L. Yu, "Vertically aligned , catalyst-free InP nanowires grown by metalorganic chemical vapor deposition Vertically aligned , catalyst-free InP nanowires grown by metalorganic chemical vapor deposition," vol. 203111, no. 2005, pp. 1–4, 2005.
- [55] S. Yu, G. Miao, Y. Jin, L. Zhang, H. Song, H. Jiang, Z. Li, D. Li, and X. Sun, "Growth and optical properties of catalyst-free InP nanowires on," *Phys. E Low-dimensional Syst. Nanostructures*, vol. 42, no. 5, pp. 1540–1543, 2010.
- [56] J.-P. Z. and G. A. G Koblmuller, S Hertenberger, K Vizbaras, M Bichler, F Bao, "Self-induced growth of vertical free-standing InAs nanowires on Si (111) by molecular beam epitaxy," no. 111, 2010.
- [57] B. Mandl, K. a Dick, D. Kriegner, M. Keplinger, G. Bauer, J. Stangl, and K. Deppert, "Crystal structure control in Au-free self-seeded InSb wire growth.," *Nanotechnology*, vol. 22, no. 14, p. 145603, 2011.

- [58] B. Mandl, M. Keplinger, M. E. Messing, D. Kriegner, R. Wallenberg, L. Samuelson, G. Bauer, J. Stangl, and K. Deppert, "Self-Seeded Axio-Radial InAs – InAsP Nanowire Heterostructures beyond 'Common' VLS Growth," *Nano Lett.*, no. 18, pp. 144–151, 2018.
- [59] W. Du, X. Yang, X. Wang, H. Pan, H. Ji, S. Luo, T. Yang, and Z. Wang, "The self-seeded growth of InAsSb nanowires on silicon by metal-organic vapor phase epitaxy," *J. Cryst. Growth*, vol. 396, pp. 33–37, 2014.
- [60] H. Zhou, M. Pozuelo, R. F. Hicks, and S. Kodambaka, "Self-catalyzed vapor – liquid – solid growth of InP 1 Å x Sb x nanostructures," vol. 319, pp. 25–30, 2011.
- [61] P. Krogstrup, R. Popovitz-biro, E. Johnson, M. H. Madsen, J. Nygård, and H. Shtrikman, "Structural Phase Control in Self-Catalyzed Growth of GaAs Nanowires on Silicon (111)," no. 111, pp. 4475–4482, 2010.
- [62] G. E. Cirlin, V. G. Dubrovskii, Y. B. Samsonenko, A. D. Bouravleuv, K. Durose, Y. Y. Proskuryakov, B. Mendes, L. Bowen, M. A. Kaliteevski, R. A. Abram, and D. Zeze, "Self-catalyzed , pure zincblende GaAs nanowires grown on Si (111) by molecular beam epitaxy," no. 111, pp. 1–6, 2010.
- [63] S. Plissard, K. a Dick, G. Larrieu, S. Godey, A. Addad, X. Wallart, and P. Caroff, "Gold-free growth of GaAs nanowires on silicon: arrays and polytypism.," *Nanotechnology*, vol. 21, no. 38, p. 385602, 2010.
- [64] S. Von Molna, "Evidence for Structural Phase Transitions Induced by the Triple Phase Line Shift in Self-Catalyzed GaAs Nanowires," 2012.
- [65] D. Ren, D. L. Dheeraj, C. Jin, J. S. Nilsen, J. Huh, J. F. Reinertsen, A. M. Munshi, A. Gustafsson, A. T. J. Van Helvoort, H. Weman, and B. Fimland, "New Insights into the Origins of Sb-Induced Effects on Self-Catalyzed GaAsSb Nanowire Arrays," 2016.
- [66] C. Colombo, D. Spirkoska, M. Frimmer, G. Abstreiter, and A. F. Morral, "Ga-assisted catalyst-free growth mechanism of GaAs nanowires by molecular beam epitaxy," no. March, pp. 2–6, 2008.
- [67] K. Hillerich, K. a Dick, M. E. Messing, K. Deppert, and J. Johansson, "Simultaneous growth mechanisms for Cu-seeded InP nanowires," *Nano Res.*, vol. 5, no. 5, pp. 297–306, May 2012.
- [68] R. T. Hallberg, S. Lehmann, M. E. Messing, and K. A. Dick, "Palladium seeded GaAs nanowires grown by MOCVD," vol. 46, no. 11, p. 2014, 2014.
- [69] D. Pan, M. Fu, X. Yu, X. Wang, L. Zhu, S. Nie, S. Wang, Q. Chen, P. Xiong, S. Von Molna, and J. Zhao, "Controlled Synthesis of Phase-Pure InAs Nanowires on Si(111) by Diminishing the Diameter to 10 nm," no. 111, 2014.
- [70] F. Jabeen, M. Piccin, L. Felisari, V. Grillo, G. Bais, S. Rubini, F. Martelli, F. Acapito, M. Rovezzi, F. Jabeen, M. Piccin, L. Felisari, V. Grillo, G. Bais, S. Rubini, and F. Martelli, "Mn-induced growth of InAs nanowires Mn-induced growth of InAs nanowires," vol. 478, 2010.
- [71] H. J. Joyce, Q. Gao, H. H. Tan, C. Jagadish, Y. Kim, M. a. Fickenscher, S. Perera, T. B. Hoang, L. M. Smith, H. E. Jackson, J. M. Yarrison-Rice, X. Zhang, and J. Zou, "High Purity GaAs Nanowires Free of Planar Defects: Growth and Characterization," *Adv. Funct. Mater.*, vol. 18, no. 23, pp. 3794–3800, Dec. 2008.

- [72] S. Lehmann, D. Jacobsson, and K. a Dick, "Crystal phase control in GaAs nanowires: opposing trends in the Ga- and As-limited growth regimes," *Nanotechnology*, vol. 26, no. 30, p. 301001, 2015.
- [73] N. Han, A. T. Hui, F. Wang, J. J. Hou, F. Xiu, T. Hung, and J. C. Ho, "Crystal phase and growth orientation dependence of GaAs nanowires on NixGay seeds via vapor-solid-solid mechanism," *Appl. Phys. Lett.*, vol. 99, no. 8, pp. 11–14, 2011.
- [74] D. S. Oliveira, M. Zavarize, L. H. G. Tizei, M. Walls, C. A. Ospina, and F. Iikawa, "Different growth regimes in InP nanowire growth mediated by Ag nanoparticles Different growth regimes in InP nanowire growth mediated by Ag nanoparticles," 2017.
- [75] K. Hillerich, D. S. Ghidini, K. A. Dick, K. Deppert, and J. Johansson, "Cu particle seeded InP-InAs axial nanowire heterostructures," *Phys. Status Solidi - Rapid Res. Lett.*, vol. 7, no. 10, pp. 850–854, 2013.
- [76] X. Yuan, P. Caroff, J. Wong-leung, L. Fu, and H. H. Tan, "Tunable Polarity in a III – V Nanowire by Droplet Wetting and Surface Energy Engineering," pp. 1–8, 2015.
- [77] I. Regolin, V. Khorenko, W. Prost, F. J. Tegude, D. Sudfeld, J. Kästner, G. Dumpich, K. Hitzbleck, and H. Wiggers, "GaAs whiskers grown by metal-organic vapor-phase epitaxy using Fe nanoparticles," *J. Appl. Phys.*, vol. 101, no. 5, pp. 1–5, 2007.
- [78] S. Heun, B. Radha, D. Ercolani, G. U. Kulkarni, F. Rossi, V. Grillo, G. Salvati, F. Beltram, and L. Sorba, "Pd-Assisted Growth of InAs Nanowires," *Cryst. Growth Des.*, vol. 10, no. 9, pp. 4197–4202, Sep. 2010.
- [79] J. Johansson, L. S. Karlsson, C. Patrik T. Svensson, T. Mårtensson, B. A. Wacaser, K. Deppert, L. Samuelson, and W. Seifert, "Structural properties of $\langle 111 \rangle$ B - oriented III–V nanowires," *Nat. Mater.*, vol. 5, no. 7, pp. 574–580, 2006.
- [80] C. Lindberg, A. Whitticar, K. A. Dick, N. Sköld, J. Nygård, and J. Bolinsson, "Silver as Seed-Particle Material for GaAs Nanowires—Dictating Crystal Phase and Growth Direction by Substrate Orientation," *Nano Lett.*, p. acs.nanolett.5b04218, 2016.
- [81] J. E. Allen, E. R. Hemesath, D. E. Perea, J. L. Lensch-falk, Z. Y. Li, F. Yin, M. H. Gass, P. Wang, A. L. Bleloch, R. E. Palmer, and L. J. Lauhon, "High-resolution detection of Au catalyst atoms in Si nanowires," vol. 3, no. March, pp. 1–6, 2008.
- [82] M. J. Tambe, S. Ren, and S. Gradec, "Effects of Gold Diffusion on n-Type Doping of," pp. 4584–4589, 2010.
- [83] T. Flissikowski, O. Brandt, H. T. Grahn, and L. Geelhaar, "Suitability of Au- and Self-Assisted GaAs Nanowires for Optoelectronic Applications," pp. 1276–1279, 2011.
- [84] M. Bar-sadan, J. Barthel, H. Shtrikman, and L. Houben, "Direct Imaging of Single Au Atoms Within GaAs Nanowires," 2012.
- [85] M. Galicka, R. Buczko, and P. Kacman, "Structure-Dependent Ferromagnetism in Mn-Doped III À V Nanowires," pp. 3319–3323, 2011.
- [86] F. Martelli, S. Rubini, M. Piccin, G. Bais, F. Jabeen, S. De Franceschi, V. Grillo, E. Carlino, F. D’Acapito, F. Boscherini, S. Cabrini, M. Lazzarino, L. Businaro, F. Romanato, and A. Franciosi, "Manganese-induced growth of GaAs nanowires.," *Nano Lett.*, vol. 6, no. 9, pp. 2130–2134, 2006.

- [87] J. Arbiol, A. Fontcuberta I Morral, S. Estradé, F. Peiró, B. Kalache, P. Roca I Cabarrocas, and J. R. Morante, "Influence of the (111) twinning on the formation of diamond cubic/diamond hexagonal heterostructures in Cu-catalyzed Si nanowires," *J. Appl. Phys.*, vol. 104, pp. 0–7, 2008.
- [88] S. Barth, J. J. Boland, and J. D. Holmes, "Defect Transfer from Nanoparticles to Nanowires," pp. 1550–1555, 2011.
- [89] J. L. Lensch-Falk, E. R. Hemesath, D. E. Perea, and L. J. Lauhon, "Alternative catalysts for VSS growth of silicon and germanium nanowires," *J. Mater. Chem.*, vol. 19, p. 849, 2009.
- [90] L. Yu, B. O'Donnell, J. L. Maurice, and P. Roca I Cabarrocas, "Core-shell structure and unique faceting of Sn-catalyzed silicon nanowires," *Appl. Phys. Lett.*, vol. 97, pp. 3–5, 2010.
- [91] S. Conesa-Boj, I. Zardo, S. Estradé, L. Wei, P. Jean Alet, P. Roca i Cabarrocas, J. R. Morante, F. Peiró, A. F. I. Morral, and J. Arbiol, "Defect formation in Ga-catalyzed silicon nanowires," *Cryst. Growth Des.*, vol. 10, pp. 1534–1543, 2010.
- [92] Y. Xiang, I. Zardo, L. Y. Cao, T. Garma, M. Heiss, J. R. Morante, J. Arbiol, M. L. Brongersma, and a Fontcuberta I Morral, "Spatially resolved Raman spectroscopy on indium-catalyzed core-shell germanium nanowires: size effects.," *Nanotechnology*, vol. 21, p. 105703, 2010.
- [93] T. I. Kamins, R. S. Williams, D. P. Basile, T. Hesjedal, and J. S. Harris, "Ti-catalyzed Si nanowires by chemical vapor deposition: Microscopy and growth mechanisms," *J. Appl. Phys.*, vol. 89, no. 2, pp. 1008–1016, 2001.
- [94] B. a. Wacaser, M. C. Reuter, M. M. Khayyat, C. Y. Wen, R. Haight, S. Guha, and F. M. Ross, "Growth system, structure, and doping of aluminum-seeded epitaxial silicon nanowires," *Nano Lett.*, vol. 9, pp. 3296–3301, 2009.
- [95] H. Y. Tuan, D. C. Lee, and B. a. Korgel, "Nanocrystal-mediated crystallization of silicon and germanium nanowires in organic solvents: The role of catalysis and solid-phase seeding," *Angew. Chemie - Int. Ed.*, vol. 45, pp. 5184–5187, 2006.
- [96] X. Sun, G. Calebotta, B. Yu, G. Selvaduray, and M. Meyyappan, "Synthesis of germanium nanowires on insulator catalyzed by indium or antimony," *J. Vac. Sci. Technol. B Microelectron. Nanom. Struct.*, vol. 25, p. 415, 2007.
- [97] F. M. Ross, C.-Y. Wen, S. Kodambaka, B. a. Wacaser, M. C. Reuter, and E. a. Stach, "The growth and characterization of Si and Ge nanowires grown from reactive metal catalysts," *Philos. Mag.*, vol. 90, no. 910412225, pp. 4769–4778, 2010.
- [98] Y. C. Chou, C. Y. Wen, M. C. Reuter, D. Su, E. a. Stach, and F. M. Ross, "Controlling the growth of Si/Ge nanowires and heterojunctions using silver-gold alloy catalysts," *ACS Nano*, vol. 6, no. 7, pp. 6407–6415, 2012.
- [99] A. Chockla and K. Klavetter, "Tin-Seeded Silicon Nanowires for High Capacity Li-Ion Batteries," *Chem. Mater.*, vol. 24, pp. 3738–3745, 2012.
- [100] E. Mullane, T. Kennedy, H. Geaney, C. Dickinson, and K. M. Ryan, "Synthesis of tin catalyzed silicon and germanium nanowires in a solvent-vapor system and optimization of the seed/nanowire interface for dual lithium cycling," *Chem. Mater.*, vol. 25, no. 9, pp. 1816–1822, 2013.

- [101] L. Yu, B. O'Donnell, P.-J. Alet, S. Conesa-Boj, F. Peiró, J. Arbiol, and P. R. I. Cabarrocas, "Plasma-enhanced low temperature growth of silicon nanowires and hierarchical structures by using tin and indium catalysts.," *Nanotechnology*, vol. 20, p. 225604, 2009.
- [102] J. D. Parsons and F. G. Krajenbrink, "TIN DOPING OF MOVPE GROWN GALLIUM ARSENIDE USING TETRAETHYLTIN J.D. PARSONS and F.G. KRAJENBRINK," vol. 66, pp. 60–64, 1964.
- [103] G. D. Sourcesmombe, C. B. E. M. Weyers, and I. The, "GASEOUS DOPANT SOURCES IN MOMBE/CBE M. WEYERS, J. MUSOLF, D. MARX, A. KOHL and P. BALK," vol. 105, 1990.
- [104] J. J. Harris, B. A. Joyce, J. P. Gowers, and J. H. Neave, "Physics A a .. Nucleation Effects During MBE Growth of Sn-Doped GaAs," vol. 71, pp. 63–71, 1982.
- [105] M. A. Green, K. Emery, Y. Hishikawa, W. Warta, E. D. Dunlop, D. H. Levi, and A. W. Y. Ho-baillie, "Solar cell efficiency tables (version 49)," no. November 2016, pp. 3–13, 2017.
- [106] S. Kasai and T. Asai, "Stochastic Resonance in Schottky Wrap Gate-controlled GaAs Nanowire Field Effect Transistors and Their Networks," 2008.
- [107] J. C. Harmand, G. Patriarche, L. Travers, F. Glas, J. C. Harmand, and G. Patriarche, "Analysis of vapor-liquid-solid mechanism in Au-assisted GaAs nanowire growth Analysis of vapor-liquid-solid mechanism in Au-assisted GaAs nanowire growth," vol. 203101, no. 2005, 2005.
- [108] L. T. and G. E. C. M Tchernycheva, J C Harmand, G Patriarche, "Temperature conditions for GaAs nanowire formation by Au-assisted molecular beam epitaxy," 2006.
- [109] S. A. Fortuna, J. Wen, I. S. Chun, and X. Li, "Planar GaAs Nanowires on GaAs (100) Substrates : Self-Aligned , Nearly Twin-Defect Free , and Transfer-Printable," no. 100, pp. 19–24, 2008.
- [110] D. Jacobsson, S. Lehmann, and K. A. Dick, "pss Zinc blend e-to-wurtzite interface improvement by group III loading in Au-seeded GaAs nanowires," vol. 859, no. 10, pp. 855–859, 2013.
- [111] N. Vainorius, D. Jacobsson, S. Lehmann, A. Gustafsson, K. A. Dick, L. Samuelson, and M. Pistol, "Observation of type-II recombination in single wurtzite / zinc-blende GaAs heterojunction nanowires," vol. 165423, pp. 1–8, 2014.
- [112] T. Burgess, S. Breuer, P. Caroff, J. Wong-Leung, Q. Gao, H. Hoe Tan, and C. Jagadish, "Twinning superlattice formation in GaAs nanowires," *ACS Nano*, vol. 7, no. 9, pp. 8105–8114, 2013.
- [113] R. R. Lapierre, M. Robson, and P. Kuyanov, "A review of III – V nanowire infrared photodetectors and sensors," 2017.
- [114] H. Fang, W. Hu, P. Wang, N. Guo, W. Luo, D. Zheng, L. Liao, A. Pan, X. Chen, and W. Lu, "Visible Light-Assisted High-Performance Mid-Infrared Photodetectors Based on Single InAs Nanowire," 2016.
- [115] A. Das, Y. Ronen, Y. Most, Y. Oreg, M. Heiblum, and H. Shtrikman, "Zero-bias peaks and splitting in an Al-InAs nanowire topological superconductor as a signature of Majorana fermions," *Nat. Phys.*, vol. 8, no. 12, pp. 887–895, 2012.

- [116] P. Caroff, K. a Dick, J. Johansson, M. E. Messing, K. Deppert, and L. Samuelson, "Controlled polytypic and twin-plane superlattices in iii-v nanowires.," *Nat. Nanotechnol.*, vol. 4, no. 1, pp. 50–5, 2009.
- [117] S. I. Nanowires, "Catalyst Orientation-Induced Growth of Defect-Free Zinc-Blende Structured $\langle 001 \rangle$ InAs Nanowires," 2015.
- [118] Z. Li, C. Möller, V. Migunov, M. Spasova, M. Farle, A. Lysov, C. Gutsche, I. Regolin, W. Prost, F. Tegude, P. Ercius, Z. Li, C. Mo, V. Migunov, M. Spasova, M. Farle, F. Tegude, and P. Ercius, "Planar-defect characteristics and cross-sections of $h\ 001\ i$, $h\ 111\ i$, and $h\ 112\ i$ InAs nanowires," vol. 1058, no. 2002, 2012.
- [119] C. Thelander, K. a Dick, M. T. Borgström, L. E. Fröberg, P. Caroff, H. a Nilsson, and L. Samuelson, "The electrical and structural properties of n-type InAs nanowires grown from metal-organic precursors.," *Nanotechnology*, vol. 21, no. 20, p. 205703, 2010.
- [120] M. D. Schroer and J. R. Petta, "Correlating the Nanostructure and Electronic Properties of InAs Nanowires," pp. 1618–1622, 2010.
- [121] K. Shimamura, Z. Yuan, F. Shimojo, A. Nakano, K. Shimamura, Z. Yuan, F. Shimojo, and A. Nakano, "Effects of twins on the electronic properties of GaAs," vol. 022105, no. 2013, pp. 1–5, 2017.
- [122] I. Nanowires, C. Thelander, P. Caro, A. W. Dey, and K. A. Dick, "Effects of Crystal Phase Mixing on the Electrical Properties of InAs Nanowires," pp. 2424–2429, 2011.
- [123] P. Villars and H. Okamoto, Eds., "Au-Ga Binary Phase Diagram 0-100 at.% Ga: Datasheet from 'PAULING FILE Multinaries Edition – 2012' in SpringerMaterials (https://materials.springer.com/isp/phase-diagram/docs/c_0907587).," Springer-Verlag Berlin Heidelberg & Material Phases Data System (MPDS), Switzerland & National Institute for Materials Science (NIMS), Japan.
- [124] P. Villars and H. Okamoto, Eds., "Au-In Binary Phase Diagram 0-100 at.% In: Datasheet from 'PAULING FILE Multinaries Edition – 2012' in SpringerMaterials (https://materials.springer.com/isp/phase-diagram/docs/c_0907021).," Springer-Verlag Berlin Heidelberg & Material Phases Data System (MPDS), Switzerland & National Institute for Materials Science (NIMS), Japan.
- [125] P. Villars and H. Okamoto, Eds., "Ag-As Binary Phase Diagram 0-100 at.% As: Datasheet from 'PAULING FILE Multinaries Edition – 2012' in SpringerMaterials (https://materials.springer.com/isp/phase-diagram/docs/c_0900006).," Springer-Verlag Berlin Heidelberg & Material Phases Data System (MPDS), Switzerland & National Institute for Materials Science (NIMS), Japan.
- [126] P. Villars and H. Okamoto, Eds., "As-Fe Binary Phase Diagram 50-100 at.% Fe: Datasheet from 'PAULING FILE Multinaries Edition – 2012' in SpringerMaterials (https://materials.springer.com/isp/phase-diagram/docs/c_0903449).," Springer-Verlag Berlin Heidelberg & Material Phases Data System (MPDS), Switzerland & National Institute for Materials Science (NIMS), Japan.
- [127] H. Ge, H. Li, S. Mei, and J. Liu, "Low melting point liquid metal as a new class of phase change material: An emerging frontier in energy area," *Renew. Sustain. Energy Rev.*, vol. 21, pp. 331–346, 2013.

- [128] P. Villars and H. Okamoto, Eds., “Cu-Ga Binary Phase Diagram 0-100 at.% Ga: Datasheet from ‘PAULING FILE Multinaries Edition – 2012’ in SpringerMaterials (https://materials.springer.com/isp/phase-diagram/docs/c_0907572).” Springer-Verlag Berlin Heidelberg & Material Phases Data System (MPDS), Switzerland & National Institute for Materials Science (NIMS), Japan.
- [129] “Melting Points of the Elements,” *Bull. Alloy Phase Diagrams*, vol. 7, no. 6, p. 602, 1986.
- [130] V. A. Nebol and A. A. Shchetinin, “Role of Surface Energy in the Vapor – Liquid – Solid Growth of Silicon,” vol. 39, no. 9, pp. 899–903, 2003.
- [131] N. Han, F. Wang, A. T. Hui, J. J. Hou, G. Shan, F. Xiu, T. Hung, and J. C. Ho, “Facile synthesis and growth mechanism of Ni-catalyzed GaAs nanowires on non-crystalline substrates,” *Nanotechnology*, vol. 22, no. 28, p. 285607, Jul. 2011.
- [132] A. C. Ford, J. C. Ho, Z. Fan, O. Ergen, V. Altoe, S. Aloni, H. Razavi, and A. Javey, “Synthesis, contact printing, and device characterization of Ni-catalyzed, crystalline InAs nanowires,” *Nano Res.*, vol. 1, no. 1, pp. 32–39, Jul. 2008.
- [133] S. Heun, B. Radha, D. Ercolani, G. U. Kulkarni, F. Rossi, V. Grillo, G. Salvati, F. Beltram, and L. Sorba, “Coexistence of vapor-liquid-solid and vapor-solid-solid growth modes in Pd-assisted InAs nanowires,” *Small*, vol. 6, no. 17, pp. 1935–41, Sep. 2010.
- [134] D. D. Fanfair and B. A. Korgel, “Bismuth Nanocrystal-Seeded III-V Semiconductor Nanowire Synthesis,” *Cryst. Growth Des.*, vol. 5, no. 5, pp. 1971–1976, 2005.
- [135] R. B. Lewis, P. Corfdir, H. Ku, U. Jahn, and O. Brandt, “Self-Assembly of InAs Nanostructures on the Sidewalls of GaAs Nanowires Directed by a Bi Surfactant,” 2017.
- [136] Y. Kim, H. J. Joyce, Q. Gao, H. H. Tan, C. Jagadish, M. Paladugu, J. Zou, and A. A. Suvorova, “Influence of Nanowire Density on the Shape and Optical Properties of Ternary InGaAs Nanowires,” 2006.
- [137] I. Regolin, V. Khorenko, W. Prost, F. Tegude, D. Sudfeld, J. Kästner, G. Dumpich, I. Regolin, V. Khorenko, W. Prost, and F. Tegude, “Composition control in metal-organic vapor-phase epitaxy grown InGaAs nanowhiskers Composition control in metal-organic vapor-phase epitaxy grown InGaAs nanowhiskers,” vol. 074321, no. 2006, 2012.
- [138] C. Zhou, X. Zhang, K. Zheng, P. Chen, W. Lu, and J. Zou, “Self-Assembly Growth of In-Rich InGaAs Core – Shell Structured Nanowires with Remarkable Near-Infrared Photoresponsivity,” 2017.
- [139] C. Zhou, “Unexpected formation of a hierarchical structure in ternary InGaAs nanowires via ‘one-pot’ growth,” pp. 16960–16967, 2017.
- [140] J. Cheol, D. Yang, A. Lee, H. Jin, J. Hun, W. Jun, H. Kim, and K. Jin, “Improving the composition uniformity of Au-catalyzed InGaAs nanowires on silicon,” *J. Cryst. Growth*, vol. 372, pp. 15–18, 2013.
- [141] A. S. Ameruddin, H. A. Fonseka, and P. Caroff, “In x Ga 1 – x As nanowires with uniform composition , pure wurtzite crystal phase and taper-free morphology,” 2015.

- [142] M. Hei, A. Gustafsson, S. Conesa-boj, F. Peir, J. R. Morante, and G. Abstreiter, "Catalyst-free nanowires with axial $\text{In}_x\text{Ga}_{1-x}\text{As}/\text{GaAs}$ heterostructures," 2009.
- [143] M. Heiss, B. Ketterer, E. Uccelli, and A. Fontcuberta, "In (Ga) As quantum dot formation on group-III assisted catalyst-free InGaAs nanowires," no. 001, 2011.
- [144] J. Treu, M. Speckbacher, K. Saller, X. Xu, H. Riedl, G. Abstreiter, and J. J. Finley, "Widely tunable alloy composition and crystal structure in catalyst-free InGaAs nanowire arrays grown by selective area molecular beam epitaxy," vol. 053110, no. 2016, 2017.
- [145] K. Chiba, K. Tomioka, A. Yoshida, J. Motohisa, K. Chiba, K. Tomioka, A. Yoshida, and J. Motohisa, "Composition controllability of InGaAs nanowire arrays in selective area growth with controlled pitches on Si platform Composition controllability of InGaAs nanowire arrays in selective area growth with controlled pitches on Si platform," vol. 125304, 2017.
- [146] K. J. Kong, C. S. Jung, G. B. Jung, Y. J. Cho, H. S. Kim, J. Park, and N. E. Yu, "Room-temperature ferromagnetism and terahertz emission of Mn-doped InGaAs and GaAsSb nanowires," pp. 1–7, 2010.
- [147] K. Sarkar, M. Palit, P. Banerji, S. Chattopadhyay, N. N. Halder, and P. Biswas, "Silver catalyzed growth of $\text{In}_x\text{Ga}_{1-x}\text{As}$ nanowires on Si (001) by metal – organic chemical vapor," *CrystEngComm*, vol. 17, pp. 8519–8528, 2015.
- [148] K. Sarkar, M. Palit, S. Guhathakurata, S. Chattopadhyay, and P. Banerji, "Single In x Ga 1 – x As nanowire / p-Si heterojunction based nano-rectifier diode," 2017.
- [149] C. G. Granqvist and R. A. Buhrman, "Size Distributions for Supported Metal Catalysts," *J. Catal.*, vol. 42, pp. 477–479, 1976.
- [150] M. Tornberg, E. K. Mårtensson, and R. R. Zamani, "Demonstration of Sn-seeded GaSb homo- and GaAs – GaSb heterostructural nanowires," 2016.
- [151] M. F. Millea and D. F. Kyser, "Thermal Decomposition of Gallium Arsenide," *J. Appl. Phys.*, vol. 38, pp. 308–313, 1965.
- [152] A. Biermanns, D. Carbone, S. Breuer, V. L. R. Jacques, T. Schulli, L. Geelhaar, and U. Pietsch, "Distribution of zinc-blende twins and wurtzite segments in GaAs nanowires probed by X-ray nanodiffraction," *Phys. Status Solidi - Rapid Res. Lett.*, vol. 7, no. 10, pp. 860–863, 2013.
- [153] H. J. Joyce, Q. Gao, H. H. Tan, C. Jagadish, Y. Kim, M. A. Fickenscher, S. Perera, T. B. Hoang, L. M. Smith, H. E. Jackson, J. M. Yarrison-rice, X. Zhang, and J. Zou, "Unexpected Benefits of Rapid Growth Rate for III - V Nanowires 2009," 2009.
- [154] J. Bolinsson, P. Caroff, B. Mandl, and K. a Dick, "Wurtzite-zincblende superlattices in InAs nanowires using a supply interruption method.," *Nanotechnology*, vol. 22, no. 26, p. 265606, 2011.

Paper I

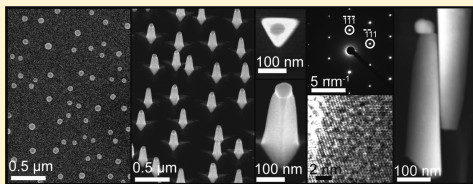


Sn-Seeded GaAs Nanowires as Self-Assembled Radial p – n JunctionsRong Sun,[†] Daniel Jacobsson,[‡] I-Ju Chen,[†] Malin Nilsson,[†] Claes Thelander,[†] Sebastian Lehmann,[†] and Kimberly A. Dick*,^{†,‡}[†]Solid State Physics and [‡]Center for Analysis and Synthesis, Lund University, S-221 00 Lund, Sweden

Supporting Information

ABSTRACT: The widespread use of Au as a seed particle in the fabrication of semiconductor nanowires presents a fundamental limitation to the potential incorporation of such nanostructures into electronic devices. Although several other growth techniques have been demonstrated, the use of alternative seed particle metals remains an underexplored but potentially very promising way to influence the properties of the resulting nanowires while simultaneously avoiding gold. In this Letter, we demonstrate the use of Sn as a seed particle metal for GaAs nanowires grown by metal–organic vapor phase epitaxy. We show that vertically aligned and stacking defect-free GaAs nanowires can be grown with very high yield. The resulting nanowires exhibit Esaki diode behavior, attributed to very high n -doping of the nanowire core with Sn, and simultaneous C-doping of the radial overgrowth. These results demonstrate that the use of alternative seed particle metals is a potentially important area to explore for developing nanowire materials with controlled material properties.

KEYWORDS: Nanowires, III–V semiconductors, vapor-phase epitaxy, GaAs, transmission electron microscopy, doping, p – n junction



Au is widely used as a seed particle in the growth of semiconductor nanowires. However, the incompatibility of Au with for example conventional silicon semiconductor processing has led to numerous efforts to find alternative techniques for nanowire growth.¹ Most common among these are self-seeded^{2,3} and selective-area^{4,5} nanowire growth, both of which avoid the introduction of any foreign catalyst material but have relatively narrow parameter space for tuning the resulting nanowire properties. An interesting alternative is to use a different foreign metal as a seed particle, specifically selected to yield properties of the nanowire different from those achieved with gold or alternative techniques. New properties may mean for example crystal structures or directions not observed with conventional growth techniques but may also mean designed material properties directly caused by incorporation of trace amounts of the foreign metal. This has been demonstrated for example in Al-seeded Si nanowires, where very high doping levels could be achieved by incorporation of Al atoms during Si nanowire growth.⁶ For III–V materials, there have to date been very few examples of seeded epitaxial nanowire growth using alternative seed metals,^{7–10} unlike Si and Ge nanowires, for which alternative seed particles have been extensively reported.¹ The potential for designing exotic materials is as yet virtually unexplored for III–V materials, with the notable exception of works by Martelli et al.¹¹ and Jabeen et al.,¹² who used Mn seed particles to induce magnetic properties in III–V nanowires.

In this Letter, we report the use of Sn as a seed material for GaAs nanowires grown by metal–organic vapor phase epitaxy (MOVPE). Sn is a potentially interesting material due to its low melting point (232 °C) and high boiling point (2602 °C),

which ensure that it can form liquid droplets over a wide potential growth temperature window without relying on the formation of specific low-temperature alloys (allowing for so-called vapor liquid solid, VLS, growth). In this way, it differs from nearly all other demonstrated alternative seed particle metals, which typically remain solid during nanowire growth (so-called vapor–solid–solid, VSS, growth).¹ Although VSS introduces certain possible advantages (such as potentially sharper heterojunction interfaces¹³), vertical alignment of the resulting nanowires is often more difficult due to the lack of a flat interface between the particle and the substrate.¹ Sn is therefore an interesting test case for exploring and developing the potential of alternative VLS seed metals.

Sn is a group-IV element and does not cause midgap electronic states in Si (making it potentially compatible with semiconductor processing). Several reports exist that demonstrate the use of Sn droplets for growth of Si nanowires using a variety of techniques.^{14–20} In III–V materials, it acts as a dopant; while in principle amphoteric, it is reported to act only as an n -dopant in GaAs.^{21,22} This makes it an advantageous choice compared to other group-IV dopants, as higher doping concentrations can in principle be achieved. However, doping of seeded nanowires remains challenging, and novel techniques for obtaining selected doping profiles are highly desirable.²³ In particular, n -doping of GaAs nanowires has proven difficult,²⁴ with most n -dopants incorporating preferentially in radial

Received: January 23, 2015

Revised: May 6, 2015

Published: May 19, 2015

overgrowth rather than into the nanowire itself, potentially limiting the flexibility of the obtained structures. Successful Sn-doping of GaAs nanowires has been reported using tetraethyltin (TESn) as an in situ dopant element during Au-seeded nanowire growth.²⁵ The authors report moderate doping levels with a narrow growth window, which they attribute to the difficulty for Sn atoms to pass through the Au seed particle. Here, we show that the use of Sn seed particles for GaAs nanowire growth results in high levels of self-doping; more remarkably, the nanowires show Esaki diode behavior with very high current levels. It is deduced that the nanowires exhibit self-assembled radial *p*–*n* junctions. The doping profile and nanowire dimensions are consistent with those predicted to be suitable for photovoltaics,²⁶ which make these structures potentially interesting for applications of this type. The Sn particles are formed in situ using TESn, which is a widely available doping source in conventional MOVPE. The resulting nanowires grown from Sn particles show epitaxial alignment with the substrate and pure zinc blende (ZB) crystal structure (free of stacking defects) under growth conditions that give high densities of stacking defects in Au-seeded GaAs nanowires.

Nanowire growth is performed using GaAs (111)B substrates placed in a horizontal-flow MOVPE reactor (Aixtron 200/4) for growth at 10 kPa in a hydrogen carrier gas flow of 13 L/min. Substrates are first heated to an annealing temperature of 630 °C in arsine (AsH₃) background with molar fraction 1.54×10^{-3} . Following 10 min annealing, samples are cooled to 550 °C in AsH₃. Once the temperature has stabilized, AsH₃ is changed to 7.69×10^{-5} , and a TESn flow with molar fraction 1.17×10^{-5} is introduced. Precision in mass flow is attained using Epison concentration measurements together with mass flow controllers. Note that two different mass flow controllers are used to cover the large flow range required for AsH₃. Following a 15 min deposition unless specified otherwise, TESn is turned off, and the samples are cooled to the desired growth temperature (in the range 475–535 °C) in AsH₃ ambient. Note that reactor temperature is calibrated using a LayTec setup for optical reflectance measurements of the Si–Al eutectic. Once growth temperature is attained, trimethylgallium (TMGa) is turned on with a molar fraction of 4.29×10^{-5} . Nanowires are grown for 10 min unless otherwise stated. The nanowires here are grown with a V/III ratio of 1.9, which is rather low compared to Au-seeded GaAs nanowires grown in MOVPE. However, we observed no growth of nanowires for V/III ratio of more than 4. It is at present unclear why such a low V/III ratio is necessary and how this is related to other parameters such as temperature. It should be noted that the use of a very low V/III ratio means the process used here resembles self-seeded growth.^{2,3}

Morphology is characterized by scanning electron microscopy (SEM; Hitachi SU8010 at 15 kV); structure is characterized with transmission electron microscopy (TEM; JEOL 3000F at 300 kV); and composition is characterized by X-ray energy dispersive spectroscopy (EDX) in high-angle annular dark-field scanning TEM (HAADF-STEM) mode. Samples are prepared for TEM analysis by mechanically breaking the nanowires near the base onto carbon film-coated Cu grids.

To confirm that the introduction of a high flow of TESn prior to nanowire growth results in Sn droplets on the surface, the sample shown in Figure 1, panel a was cooled down directly after a 15 min TESn deposition step without introducing TMGa. As shown, particles are formed on the surface with an

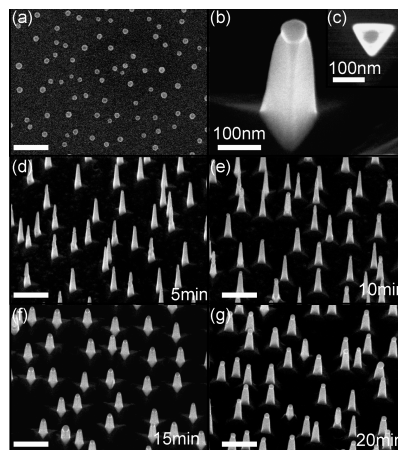


Figure 1. SEM images of (a) Sn particles formed on the substrate by exposure to TESn at 550 °C. (b) 30° tilted magnified view of a single nanowire grown from 15 min Sn particles and (c) top view of the same nanowire showing a triangular cross-section. 30° tilted view of GaAs nanowires grown from Sn particles deposited for (d) 5 min, (e) 10 min, (f) 15 min, and (g) 30 min. Scale bars are 500 nm unless otherwise specified.

average diameter of 59 ± 7 nm and surface density of $11 \pm 2/\mu\text{m}^2$. This size distribution is surprisingly narrow; it is for example much narrower than nanoparticles achieved using annealing of evaporated metal thin films and only moderately wider than colloidal or aerosol nanoparticles.²⁷ A narrow size distribution among metal droplets can be attributed to Ostwald ripening and is an indication that the surface diffusivity of Sn on these substrates is high at the temperatures used. Figure 1, panels b and c show a top view and 30° tilted view of a single nanowire grown from particles formed for 15 min (as in Figure 1a). The tips of the nanowires exhibit truncated spherical caps of average diameter 54 ± 7 nm, which may provisionally be identified as Sn seed particles. It is clear that the nanowires are relatively tapered toward the base, with smooth side facets and a triangular cross-section. Tapering may be an indication of radial growth in parallel with the Sn-seeded axial growth but may also be an indication that the Sn droplet is shrinking in diameter as the nanowire grows. Both of these possibilities will be discussed further. To determine the effect of TESn deposition time on nanowire growth, a series was grown with varied TESn deposition of 5 min, 10 min, 15 min, and 30 min (Figure 1d–g; nanowires were grown for 10 min in all cases). The nanowires grow homogeneously across the substrate in all cases. It is clear that, first, shorter deposition times lead to smaller Sn droplets and narrower nanowire diameter, and second, that nanowires grown following shorter deposition times have a higher growth rate. In particular, nanowires grown from 5 min particle deposition have a much higher aspect ratio than those grown following 15 min of Sn deposition.

To investigate the crystal structure of the nanowires and confirm the Sn-seeding mechanism, nanowires were next analyzed by TEM and EDX (Figure 2). Figure 2, panels b and c show TEM images of nanowires grown at the same conditions as in Figure 1, panel b, imaged in the $\{101\}$ zone

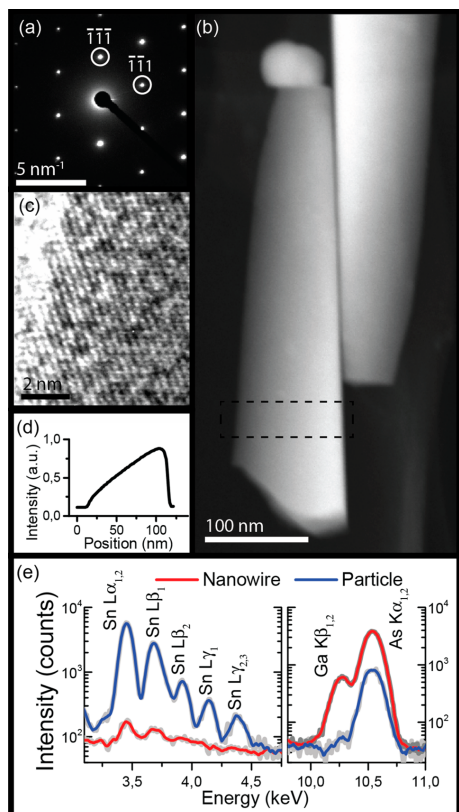


Figure 2. TEM analysis of a Sn-seeded GaAs nanowire, imaged in the $(\bar{1}01)$ zone axes. The diffraction pattern in panel a shows a pure ZB structure, which is also seen in the high-resolution TEM image in panel c. From the HAADF-STEM image in panel b, an (d) intensity line profile from the dashed area is used, in combination with panels a and c, to deduce the facet indices of the wire. The intensity line profile shows a triangular cross-section with one facet parallel to the beam. In panel e, two EDS spectra are overlaid: blue spectrum from the seed particle, clearly showing Sn- and As-related peaks, and red spectrum from the same area as the dashed box in panel b, showing a weak but detectable Sn signal.

axes. The nanowires exhibit ZB crystal structure without any stacking defects along the entire length of the nanowire. This is somewhat surprising since gold-seeded nanowires grown under identical conditions exhibit high densities of stacking defects. Defect-free ZB structure in GaAs nanowires is typically associated with either very low temperature,²⁸ high V/III ratio,^{29,30} or high total precursor flows.³¹ Clearly, the selection of seed particle material strongly influences the resulting crystal structure. The nanowires side facet orientation is identified as $\{112\}A$ by comparison of atomically resolved images and diffraction patterns with the HAADF intensity profiles (Figure 2a,c,d). The composition of the nanowires and seed particle were also investigated by EDX. The seed particle was found to consist primarily of Sn, with an average As content of up to 18

atomic % (and negligible postgrowth Ga content). Since the nanowires are cooled in AsH_3 , and the melting point of Sn lies below the growth temperature, the phase observed *ex situ* clearly is not indicative of the phase during growth. However, the presence of a Sn-rich particle confirms the Sn-seeded mechanism. A weak Sn peak is also observed in the EDX spectrum of the nanowire itself (see Figure 2e), which suggests Sn incorporation into the nanowire. This specific EDX spectrum was taken from the middle part the nanowire; EDX spectra from different parts of the nanowire are shown in Supporting Information S1. Since the sensitivity of the detection technique is on the order of 1 atomic %, it is difficult to accurately quantify the observed Sn content. However, to be detected at all levels, it must be very high. If this amount of Sn is incorporated into the nanowire, the doping level would be very high; however, such high Sn-doping of GaAs has been reported.³² On the other hand, it may also be that there is Sn present on the surface of the nanowire or in clusters that are not electrically active. Although we have not observed these effects, we cannot definitively rule them out.

The effect of temperature on the nanowire morphology is shown in Figure 3, panels a–f. At the lowest temperature investigated (475 °C), the nanowires exhibit a high probability of kinking, while nanowires grown at or above 487 °C exhibit perfect vertical alignment with a significant reduction in length with increasing temperature. Additionally, at higher temperatures, the nanowires exhibit rough side facets (Figure 3e), which TEM analyses show are associated with twinning (Figure 3g–j). It is interesting to note that, with the exception of occasional twin planes at high temperature, the nanowires are pure ZB over the entire temperature window, which indicates that the parameter window for obtaining defect-free crystal structure is much wider than for nanowires grown with gold.^{28–31} It is difficult to determine the reason for the very different crystal structure observed for Sn- and Au-seeded nanowires in the absence of comparative data from other seed nanoparticle materials, although we can speculate that differences in local supersaturation (due to different precursor solubility) or different interfacial energetics are likely to play a role. When the growth temperature is set to values higher than 535 °C, no nanowire growth is observed (Figure 3f). The temperature sensitivity of the growth system is on the order of 5 °C.

To combine the higher axial growth rate at lower temperature with the vertical alignment exhibited at higher temperature, we used a two-temperature approach similar to that previously demonstrated for growing vertically aligned gold-seeded nanowires at low temperatures.²⁸ The nanowires shown in Figure 4, panel a were nucleated at 500 °C for 3 min, followed by lowering the temperature to 475 °C and continuing the growth for an additional 7 min. Interestingly, these nanowires exhibit regularly spaced stacking defects, which are shown in Figure 4, panels b–e. The success of this two-temperature technique demonstrates that the nanowire growth itself is not limited to the temperature range shown in Figure 3, panels a–f; rather, it is the nucleation process that is temperature-limited (similar to Au-seeded nanowires).

Electrical characterization next was performed to investigate the properties and to confirm the hypothesis of Sn-doping. For electrical characterization, a high aspect ratio was required; nanowire growth was performed at 500 °C for 20 min following TESn deposition of 5 min to yield nanowires longer than 1 μm . Nanowires were deposited onto $Si(n++)/SiO_2(100\text{ nm})$

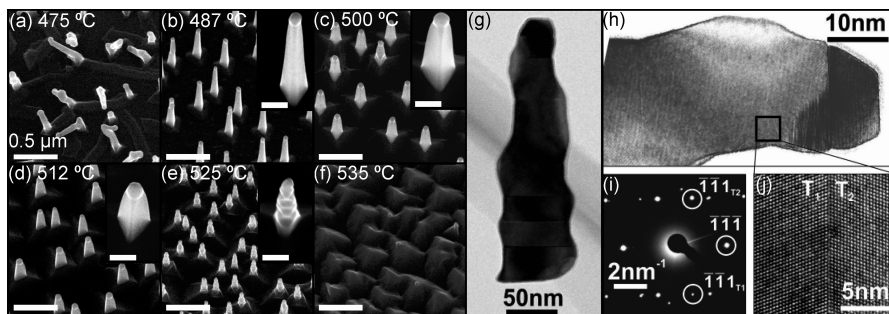


Figure 3. (a–f) 30° tilted SEM images of Sn-seeded GaAs nanowires grown at different temperatures with magnified single nanowire as insets in which scale bars are 100 nm. (g) Bright field overview TEM image of a single nanowire grown at 525 °C viewed along the $\langle 101 \rangle$ zone axes, with a higher magnification of the same nanowire shown in panel h. A twinned ZB crystal structure, 180° rotational twinning around a $\{101\}$ -type direction, of the nanowire can be recognized from the (i) characteristic diffraction pattern as well as from the (j) high resolution image. The latter displays an enlarged part of the nanowire shown in panels g and h.

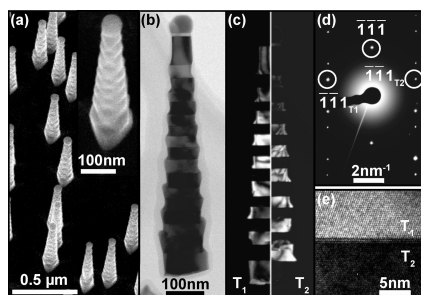


Figure 4. (a) 30° tilted view of nanowires grown with a two-temperature process with an inset showing a higher magnification of a single nanowire. (b) Bright-field overview TEM image of nanowire grown with a two-temperature approach viewed along the $\langle 101 \rangle$ zone axes. (c) Dark-field image of the same nanowire exhibits regularly spaced twin planes; twin 1 and twin 2 can be recognized from (d) characteristic diffraction pattern and also the (e) high-resolution image.

substrates and viewed in SEM using a low magnification. Contacts were fabricated using electron beam lithography, followed by 30 s oxygen plasma ashing, 15 s HCl/H₂O (1:10) etching, metal evaporation of Ni/Au (25/100 nm), and lift-off.

Two-probe electrical characterization, with contacts placed at the tip (source, S) and base (drain, D) of the nanowire (Figure 5a), revealed strongly nonlinear current–voltage (I_{DS} – V_{DS}) characteristics. A pronounced region of negative differential resistance was observed for positive V_{DS} applied to the base of the nanowires, see Figure 5, panel b. Such characteristics are typical for highly doped p – n junctions (Esaki diodes), where band-to-band tunneling is the dominant transport mechanism for reverse bias, and small forward bias. Without intentional doping, the devices exhibited surprisingly high peak-to-valley current ratios, up to 12 at $T = 295$ K and 18 at $T = 4.2$ K, and peak current densities of 2.5 kA/cm^2 .³³ To shed more light on where the doping is located along the length of the nanowire, devices with three contacts were also fabricated, see Figure 5, panel c. Electrical measurements of the top segment (contacts II–III) revealed close-to-linear I_{DS}/V_{DS} characteristics with a

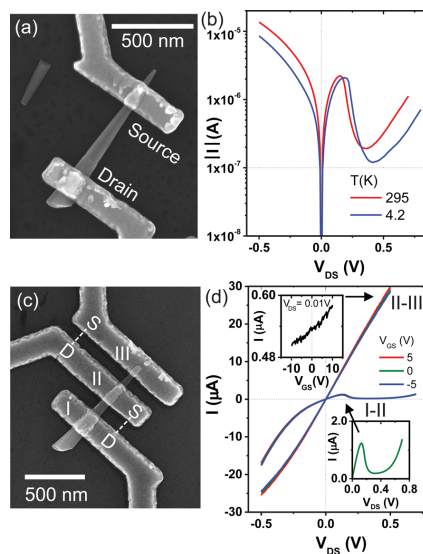


Figure 5. (a) SEM image of a contacted Sn-seeded GaAs nanowire grown at 500 °C. (b) Absolute drain current versus drain voltage, V_{DS} , applied to the base of the nanowire in panel a, at $T = 295$ K and 4.2 K. (c) SEM image of a nanowire from the same growth, with three contacts. (d) Electrical measurements of the bottom segment (I–II) and top segment (II–III) of the nanowire in panel c at 295 K. Top inset shows the back-gate dependence of the current in the upper segment, and the lower inset is a magnification of the peak associated with band-to-band tunneling in the lower segment.

low resistivity ($\rho = 2.9 \times 10^{-2} \Omega \text{cm}$). The positive slope for the back-gate voltage (V_{GS}) dependence of I_{DS} is a clear indicator that the dominant carrier type is electrons, a result of strong n -doping. The base of the nanowire (contacts I–II) shows the same electrical properties as the nanowire in Figure 5, panel a. From these measurements, we thus conclude that the p -doping is primarily located close to contact I in Figure 5, panel c, near

the base of the nanowire. Electrical measurements performed on nanowires grown at a lower temperature do not show this Esaki diode behavior (see Supporting Information S2) and have *n*-type conductivity up to five-times lower than the sample shown in Figure 5, which suggests that Sn incorporation can be controlled with temperature.

The formation of *p*–*n* junctions is somewhat surprising since the nanowires form in a single growth step. Sn is potentially an amphoteric dopant and may in principle act as either donor or acceptor in III–V materials. However, in GaAs, it is almost universally reported to act as an *n*-dopant. A simple explanation for the origin of the *p*–*n* junction is that the *n*-doping is a result of incorporation of Sn from the seed particle into the core of the nanowire during growth. This hypothesis is in agreement with the finding that the tip of the nanowire, where radial overgrowth is negligible, shows strong *n*-doping. It is interesting that the *n*-doping is so efficient despite the low V/III ratio, which might favor incorporation into As sites. However, it is consistent with previous studies of Sn in GaAs, which do not show amphoteric behavior regardless of growth conditions. Conversely, the *p*-doping we attribute to incorporation of background C from the metal–organic precursors into the radial overgrowth. It is well-documented that incorporation of C is low during axial III–V nanowire growth^{34–36} but that it can be used to *p*-dope radial overgrowth on GaAs nanowires.^{23,36} Although the high C incorporation necessary to produce the currents observed here is not typical of GaAs nanowires grown in MOVPE, Sn-seeded nanowires in this study are grown at unusually low V/III ratio compared to typical gold-seeded nanowires. Very low V/III ratio has been associated with formation of As vacancies and enhanced incorporation of parasitic C in GaAs layer growth.^{37,38} For the nanowires studied here, the overgrowth is primarily located around the base of the nanowires where the diameters are the largest and where the surfaces have been exposed to the C-containing vapor for the longest time. Very thin *p*-layers further up on the nanowire may also have been removed in the HCl etch during contact fabrication, which explains the very clear Esaki diode behavior observed. To confirm that the amount of Sn lost from the seed particle is indeed sufficient to provide the high doping levels observed, we have performed a simple order-of-magnitude calculation of the number of atoms (see Supporting Information S3). Also worth noting is that the small decrease in relative Sn content detected by EDX toward the base would be consistent with a shell that is not Sn-doped (see Supporting Information S1); however, since the Sn signal is barely detectable in EDX, this should be interpreted with caution.

Two control samples were grown and processed to confirm that the growth conditions used indeed would lead to strong *p*-type doping. Both samples were grown under conditions resulting in radial overgrowth. The first sample studied was based on Au-seeded GaAs nanowires grown under “normal” V/III conditions for MOVPE (V/III = 236), and the second on Au-seeded GaAs nanowires grown under conditions similar to the Sn-seeded nanowires, with a V/III ratio of 1.4. Electrical measurements of the first sample, Figure 6, panels a and b, showed very high two-probe resistivity ($\rho = 9 \times 10^4 \Omega\text{cm}$), partly explained by the formation of Schottky contacts due to a low carrier concentration. The back-gate dependence, with increasing conductivity for decreasing V_{GS} , is a signature of *p*-type doping. The second sample, however (Figure 6c,d), prepared under low V/III, showed several orders of magnitude

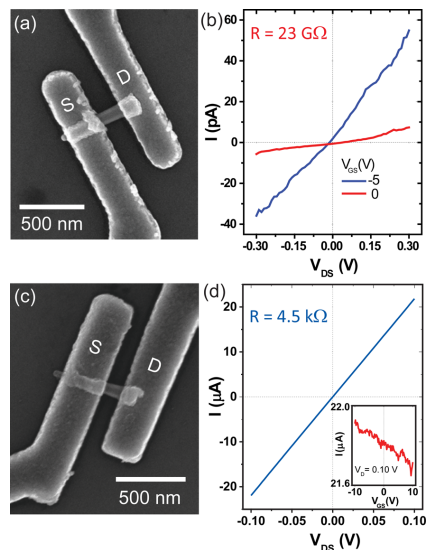


Figure 6. (a) SEM image of a contacted GaAs Au-seeded reference nanowire grown under V/III = 236. (b) Corresponding I – V_{DS} measurement, for two different V_{GS} , showing high resistive, *p*-type transport. (c) SEM image of a second Au-seeded GaAs reference nanowire grown under a lower V/III = 1.4. (d) Corresponding I – V_{DS} measurement showing a very low resistance, and the I_{DS} versus V_{GS} in the inset is indicative of *p*-type transport.

lower resistivity values ($\rho = 2 \times 10^{-2} \Omega\text{cm}$) and increasing conductivity with decreasing V_{GS} (inset of Figure 6d), indicative of strong *p*-type doping. Also worth noting is that the sample grown at higher V/III ratio exhibited defect-free ZB structure (similar to Sn-seeded nanowires), while the sample grown at low V/III ratio exhibited frequent stacking defects in a predominantly ZB structure. These results thus show that possible C incorporation in radial overgrowth is likely related to V/III ratio rather than to nanowire crystal structure.

In summary, we have demonstrated the use of Sn as a seed particle for GaAs nanowire growth, with Sn particles formed in situ using the standard metal–organic precursor tetraethyltin. The resulting nanowires exhibit uniform vertical alignment and defect-free ZB crystal structure for optimized growth temperature. Nanowires grown at high temperature exhibit low growth rate, but low growth temperature is associated with kinking. We demonstrate that straight nanowires with higher growth rate can however be achieved by a two-temperature approach, nucleating at higher temperature and growing at lower temperature. The nanowires in this work also exhibit Esaki diode behavior with high current levels despite the absence of intentional doping during nanowire growth. Electrical evaluation indicates that Sn primarily incorporates in the core of the nanowire, likely via the seed particle leading to strong *n*-doping, and that the *p*-doping is located in the radial overgrowth, where the high doping level is an effect of the low V/III ratio used during growth. Incorporation of both of these dopants is expected to depend on growth conditions: specifically, C-doping is anticipated to be very sensitive to V/III ratio, while Sn-dopant incorporation is known to be strongly temperature-

dependent. An important next step for future studies will therefore be to map the nanowire properties as a function of accessible growth parameters to determine the extent to which dopant levels can be controlled in Sn-seeded nanowires. In conclusion, this work demonstrates that the use of alternative seed particle materials is an interesting and potentially simple approach to introduce alternative properties and functions into semiconductor nanowires while at the same time avoiding the use of industrially incompatible gold.

■ ASSOCIATED CONTENT

■ Supporting Information

EDX analysis of Sn content as a function of position along the nanowire, electrical evaluation of nanowires grown at lower temperature, and comparison of Sn atoms in particle to degenerate doping nanowires. The Supporting Information is available free of charge on the ACS Publications website at DOI: 10.1021/acs.nanolett.5b00276.

■ AUTHOR INFORMATION

Corresponding Author

*E-mail: Kimberly.Dick@ftf.lth.se.

Author Contributions

The manuscript was written through contributions of all authors. All authors have given approval to the final version of the manuscript.

Notes

The authors declare no competing financial interest.

■ ACKNOWLEDGMENTS

The authors acknowledge financial support from the European Research Council under the European Union's Seventh Framework Programme (FP/2007-2013)/ERC Grant Agreement No. 336126; the People Programme of the European Union (Marie Curie Actions, FP7-People-2013-ITN) Grant No. n°608153; PhD4Energy; the Swedish Research Council (VR); the Knut and Alice Wallenberg Foundation (KAW); and the Nanometer Structure Consortium at Lund University (nmC@LU).

■ REFERENCES

- Dick, K. A.; Caroff, P. *Nanoscale* **2014**, *6*, 3006–3021.
- Fontcuberta i Morral, A.; Spirkoska, D.; Arbiol, J.; Heigoldt, M.; Morante, J. R.; Abstreiter, G. *Small* **2008**, *4*, 899.
- Grap, T.; Rieger, T.; Blomers, C.; Schapers, T.; Grutzmacher, D.; Lepsa, M. I. *Nanotechnology* **2013**, *24*, 335601.
- Tomioaka, K.; Motohisa, J.; Hara, S.; Fukui, T. *Nano Lett.* **2008**, *8*, 3475.
- Gao, Q.; Saxena, D.; Wang, F.; Fu, L.; Mokkapat, S.; Guo, Y.; Li, L.; Wong-Leung, J.; Caroff, C.; Tan, H. H.; Jagadish, C. *Nano Lett.* **2014**, *14*, S206–S211.
- Moutanabbi, O.; Ishei, D.; Blumtrit, H.; Senz, S.; Pippel, E.; Seidman, D. N. *Nature* **2013**, *496*, 78.
- Vogel, A. T.; de Boor, J.; Becker, M.; Wittemann, J. V.; Mensah, S. L.; Werner, P.; Schmidt, V. *Nanotechnology* **2011**, *22*, 015605.
- Hillerich, K.; Messing, M. E.; Wallenberg, L. R.; Deppert, K.; Dick, K. A. *J. Cryst. Growth* **2011**, *315*, 134.
- Heun, S.; Radha, B.; Ercolani, D.; Kulkarni, G. U.; Rossi, F.; Grillo, V.; Salviati, G.; Beltram, F.; Sorba, L. *Cryst. Growth Des.* **2010**, *10*, 4197.
- Xu, H. Y.; Wang, Y.; Guo, Y.; Liao, Z.; Gao, Q.; Tan, H. H.; Jagadish, C.; Zou, J. *Nano Lett.* **2012**, *12*, S744.
- Jabeen, F.; Piccin, M.; Felisari, L.; Grillo, V.; Bais, G.; Rubini, S.; Martelli, F.; d'Acapito, F.; Rovezzih, M.; Boscherini, F. *J. Vac. Sci. Technol., B: Microelectron. Nanometer Struct.—Process., Meas., Phenom.* **2010**, *28*, 478.
- Martelli, F.; Rubini, S.; Piccin, M.; Bais, G.; Jabeen, F.; De Franceschi, S.; Grillo, V.; Carlino, E.; D'Acapito, F.; Boscherini, F.; Cabrini, S.; Lazzarino, M.; Businaro, L.; Romanato, F.; Franciosi, A. *Nano Lett.* **2006**, *6*, 2130.
- Wen, C. Y.; Reuter, M. C.; Bruley, J.; Tersoff, J.; Kodambaka, S.; Stach, E. A.; Ross, F. M. *Science* **2009**, *326*, 1247.
- Wanghua Chen, W.; Yu, L.; Misra, S.; Fan, Z.; Pareige, P.; Patriarche, G.; Bouchoule, S.; Roca i Cabarrocas, P. *Nat. Commun.* **2014**, *5*, 4134.
- Yu, L.; O'Donnell, B.; Alet, P.-J.; Conesa-Boj, S.; Peiro, F.; Arbiol, J.; Roca i Cabarrocas, P. *Nanotechnology* **2009**, *20*, 225604.
- Chockla, A. M.; Klavetter, K. C.; Mullins, C. B.; Korgel, B. A. *Chem. Mater.* **2012**, *24*, 3738.
- Jeon, M.; Uchiyama, H.; Kamisako, K. *Mater. Lett.* **2009**, *63*, 246.
- Jeon, M.; Kamisako, K. *Mater. Lett.* **2009**, *63*, 777.
- Yu, L.; O'Donnell, B.; Maurice, J.-L.; Roca i Cabarrocas, P. *Appl. Phys. Lett.* **2010**, *97*, 023107.
- Rathi, S. J.; Jariwala, B. N.; Beach, J. D.; Stradins, P.; Craig Taylor, P.; Weng, X. J.; Ke, Y.; Redwing, J. M.; Agarwal, S.; Collins, R. T. *J. Phys. Chem. C* **2011**, *115*, 3833–3839.
- Regolin, I.; Gutsche, C.; Lysov, A.; Blekker, K.; Li, Z. A.; Spasova, M.; Prost, W.; Tegude, F.-J. *J. Cryst. Growth* **2011**, *315*, 143–147.
- Laznicka, M.; Trung Dung, P.; Oswald, J.; Vorlicek, V.; Gregora, I.; Simeckova, M.; Jurek, K.; Doubrava, P. *Czech. J. Phys. B* **1988**, *38*, 224–230.
- Jadczak, J.; Plochocka, P.; Mitiglu, A.; Breslavetz, I.; Royo, M.; Bertoni, A.; Goldoni, G.; Smolenski, T.; Kossacki, P.; Kretinin, A.; Shtrikman, H.; Maude, D. K. *Nano Lett.* **2014**, *14*, 2807–2814.
- Wallentin, J.; Borgström, M. T. *J. Mater. Res.* **2011**, *26*, 2143–2156.
- Gutsche, C.; Lysov, A.; Regolin, I.; Blekker, K.; Prost, W.; Tegude, F.-J. *Nanoscale Res. Lett.* **2011**, *6*, 65.
- Messing, M. E.; Hillerich, K.; Johansson, J.; Deppert, K.; Dick, K. A. *Gold Bull.* **2009**, *42*, 172.
- Krogstrup, P.; Jorgensen, H.; Heiss, M.; Demichel, O.; Holm, J.; Aagersen, M.; Nygard, J.; Fontcuberta i Morral, A. *Nat. Photonics* **2013**, *7*, 206.
- Joyce, H. J.; Gao, Q.; Tan, H. H.; Jagadish, C.; Kim, Y.; Zhang, X.; Guo, Y.; Zou, J. *Nano Lett.* **2007**, *7*, 921–926.
- Lehmann, S.; Jacobsson, D.; Deppert, K.; Dick, K. *Nano Res.* **2012**, *515*, 470–476.
- Joyce, H. J.; Gao, Q.; Tan, H. H.; Jagadish, C.; Kim, Y.; Fickenscher, M. A.; Perera, S.; Hoang, T. B.; Smith, L. M.; Jackson, H. E.; Yarrison-Rice, J. M.; Zhang, X.; Zou, J. *Adv. Funct. Mater.* **2008**, *18*, 3794–3800.
- Joyce, H. J.; Gao, Q.; Tan, H. H.; Jagadish, C.; Kim, Y.; Fickenscher, M. A.; Perera, S.; Hoang, T. B.; Smith, L. M.; Jackson, H. E.; Yarrison-Rice, J. M.; Zhang, X.; Zou, J. *Nano Lett.* **2009**, *9*, 695–701.
- Tosaporn, C. *Impurity Doping in Compound Semiconductors*. <https://dspace.wul.waseda.ac.jp/dspace/bitstream/2065/28498/3/Honbun-4475.pdf> (Accessed May 1, 2015).
- Calculations of cross-sectional area for tunneling based on the assumption of a shell around the base of the core.
- Thelander, C.; Dick, K. A.; Borgström, M. T.; Fröberg, L. E.; Caroff, P.; Nilsson, H. A.; Samuelson, L. *Nanotechnology* **2010**, *21*, 205703.
- Salehzadeh, O.; Watkins, S. P. *Nanotechnology* **2011**, *22*, 165603.
- Casadei, A.; Schwender, J.; Russo-Averchi, E.; Rüffer, D.; Heiss, M.; Alarcó-Lladó, E.; Jabeen, F.; Ramezani, M.; Nielsch, K.; Fontcuberta i Morral, A. *Phys. Status Solidi RRL* **2013**, *7*, 890–893.
- Jensen, K. F.; Fotiadis, D. I.; Mountziaris, T. J. *J. Cryst. Growth* **1991**, *107*, 1–11.
- van Deelen, J.; Bauhuis, G. J.; Schermer, J. J.; Larsen, P. K. J. *Cryst. Growth* **2004**, *271*, 376–384.

Sn-seeded GaAs nanowires as self-assembled radial p-n junctions

Rong Sun¹, Daniel Jacobsson¹, I-Ju Chen¹, Malin Nilsson¹, Claes Thelander¹, Sebastian

Lehmann¹, Kimberly. A. Dick^{1,2}

¹ *Solid State Physics, Lund University, Box 118, S-221 00 Lund, Sweden*

² *Center for Analysis and Synthesis, Lund University, Box 124, S-221 00 Lund, Sweden*

SUPPLEMENTARY INFORMATION

Table of Contents

S1. EDX spectra taken from different points along a nanowire	2
S2. Electrical characterization of a nanowire grown at low temperature	2
S3. Comparison of Sn atoms in particle to degenerate doping in nanowire	3

S1. EDX spectra taken from different points along a nanowire

EDX analysis has been performed on three different spots along a Sn seeded GaAs nanowire as shown in figure S1. Besides the strong As signal detected in the Sn seed particle, there is a weak trend that the Sn signal decreases towards the bottom of the nanowire. This is due to less radial overgrowth on the top part of the nanowire which is not doped by Sn. Note again that the Sn signal here is around the EDX measurement resolution limit.

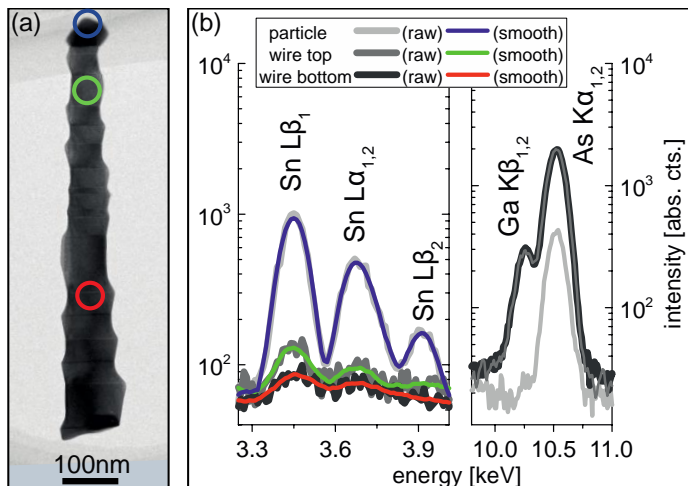


Figure S1. Positions of the EDX-analyzed areas in bright field overview of the nanowire in (a) (color-coded) and spectra given in (b). Nanowire top and bottom spectra are normalized to As K-line. Smooth by Savitzky-Golay 20 point averaging for nanowire top and bottom spots and 15 point averaging for particle spectrum raw data.

S2. Electrical characterization of a nanowire grown at low temperature

Electrical measurements for a sample grown at 455 °C, with a less tapered morphology, showed no Esaki diode electrical characteristics. However, the diode-like properties observed are still consistent with a p-doped region near the base, and an n-doped region near the tip of the nanowires. Electrical measurements for the tip-part, show values for $\rho \approx 1 \times 10^{-1} \Omega\text{cm}$, thus pointing to a lower n -carrier concentration at this growth temperature, likely due to reduced Sn incorporation.

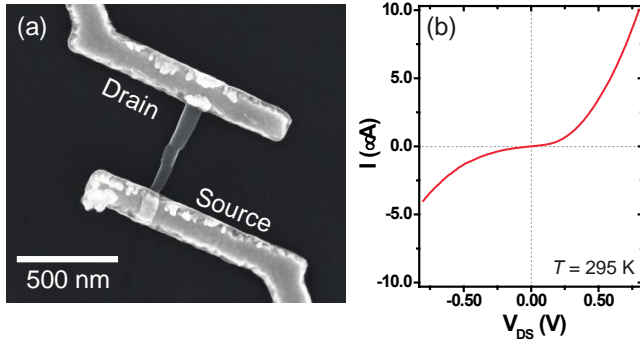


Figure S2. (a) SEM image of a contacted Sn-seeded GaAs nanowire grown at 455 °C. (b) Electrical measurements show no Esaki diode characteristics.

S3. Comparison of Sn atoms in particle to degenerate doping in nanowire

To demonstrate that the amount of Sn atoms present in a typical seed droplet is in principle sufficient to degenerately dope a nanowire of approximately 1 μm in length, a simple calculation can be performed. Assuming that a typical Sn droplet is a hemisphere of 60 nm diameter at the start of growth (consistent with the measurements described in the paper), while the droplet after growth is about 55 nm in diameter (estimated from TEM measurements), the total volume lost is about $1.3 \times 10^4 \text{ nm}^3$. Sn has a density of about 7 g/cm^3 (β -Sn at room temperature, or liquid Sn at its melting point) and a molar mass of 118.7 g, so a Sn particle/droplet will contain about 35 atoms per nm^3 . The number of atoms “lost” during growth can then be estimated as around 4.6×10^5 . We then compare this to the number of atoms in a degenerately doped nanowire. Using a maximum doping density of $1 \times 10^{20} \text{ cm}^{-3}$, a nanowire of 60 nm radius and 1 μm length can contain up to 2.8×10^5 Sn atoms. Comparing these two estimates indicates that the number of atoms lost during growth (4.6×10^5) is in fact more than enough to degenerately dope the nanowire (requiring up to 2.8×10^5). It is probable that not all lost Sn ends up on the nanowire; mostly likely some atoms diffuse along the nanowire surface and onto/into the GaAs substrate.

This calculation is very simple and not quantitatively accurate: for example, the Sn doping density is probably unrealistically high. This very high doping level is chosen to provide an upper limit of the number of atoms required to dope the nanowire. Conversely, the Sn droplets do not contain pure Sn but some As as well, so the number of atoms in the particle (both before and after growth) is probably overestimated. However, this calculation gives an order-of-magnitude indication that the number of atoms lost from the Sn droplet could indeed give the observed electrical properties.

Paper II



Sn-seeded GaAs nanowires grown by MOVPE

Rong Sun¹, Neimantas Vainorius¹, Daniel Jacobsson¹, Mats-Erik Pistol¹, Sebastian Lehmann¹ and Kimberly A Dick^{1,2}

¹ Solid State Physics and NanoLund, Lund University, PO Box 118, SE-221 00 Lund, Sweden

² Centre for Analysis and Synthesis, Lund University, PO Box 124, SE-221 00 Lund, Sweden

E-mail: Kimberly.Dick@ftf.lth.se

Received 14 January 2016, revised 19 March 2016

Accepted for publication 24 March 2016

Published 18 April 2016



Abstract

It has previously been reported that *in situ* formed Sn nanoparticles can successfully initiate GaAs nanowire growth with a self-assembled radial p–n junction composed of a Sn-doped n-type core and a C-doped p-type shell. In this paper, we investigate the effect of fundamental growth parameters on the morphology and crystal structure of Sn-seeded GaAs nanowires. We show that growth can be achieved in a broad temperature window by changing the TMGa precursor flow simultaneously with decreasing temperature to prevent nanowire kinking at low temperatures. We find that changes in the supply of both AsH₃ and TMGa can lead to nanowire kinking and that the formation of twin planes is closely related to a low V/III ratio. From PL results, we observe an increase of the average luminescence energy induced by heavy doping which shifts the Fermi level into the conduction band. Furthermore, the doping level of Sn and C is dependent on both the temperature and the V/III ratio. These results indicate that using Sn as the seed particle for nanowire growth is quite different from traditionally used Au in for example growth conditions and resulting nanowire properties. Thus, it is very interesting to explore alternative metal seed particles with controllable introduction of other impurities.

Online supplementary data available from stacks.iop.org/NANO/27/215603/mmedia

Keywords: MOVPE, nanowires, GaAs, alternative seed particle, TEM, tin

(Some figures may appear in colour only in the online journal)

1. Introduction

Epitaxial synthesis of III–V nanowires has almost exclusively used Au as a catalyst particle since III–V nanowires were demonstrated by Hiruma *et al* [1]. To implement this promising one-dimensional nanostructure with its outstanding properties like direct band gap and high carrier mobility into electronic and optical devices, it needs to be compatible with the existing semiconductor technology. However, gold severely limits the possibility to integrate these building blocks into, for example, conventional Si industry since gold

can easily diffuse into silicon creating mid-gap electronic states, which will degrade device performance drastically [2].

There has been much research of gold-free nanowire growth methods including selective area, self-seeded, and non-gold foreign metal seeded nanowire growth [3–7]. In the case of selective area nanowire growth, a pre-defined opening pattern is used to initiate the nanowire growth and no seed particle is required, but one-dimensional epitaxy strongly relies on the selected growth conditions to enable anisotropic growth rates. Thus, it usually has a rather narrow growth window [8]. For self-seeded nanowire growth, one of the elements that composes the nanowire acts as the seed material; usually Ga and In droplets are formed and used due to their low melting points. However, it is challenging to apply this method simultaneously in various nanowire material systems to achieve for example axial heterostructures where



Original content from this work may be used under the terms of the Creative Commons Attribution 3.0 licence. Any further distribution of this work must maintain attribution to the author(s) and the title of the work, journal citation and DOI.

the group III species is switched to induce the change in the material system.

So far reports on III–V nanowires seeded from metal particles different from gold are limited. Thus, exploring alternative foreign seed particle materials other than gold is of great interest. It may also be interesting for device applications to incorporate impurities from suitable seeding material to achieve for example self-doping without the use of extra dopants. By investigating the nanowire growth behavior from different seed particles, it may also give us some insights into why gold can be used to initiate the nanowire growth of any III–V material system in a wide growth parameter window and allows crystallographic manipulation of the nanowires. It is well documented that Sn seed particles have been used for group IV, Si and Ge nanowire synthesis by different growth techniques [9, 10]. We have previously demonstrated the use of *in situ* formed Sn particles for GaAs nanowire growth, resulting in nanowires with a self-assembled p–n junction having a Sn-doped n-type core and a C-doped p-type shell [11]. The n-doping of the core is due to the consumption and incorporation of the Sn seed particle into the nanowire during growth, while the p-doping of the shell is attributed to the incorporation of C into the radial overgrowth from decomposition of metal organic precursors. Our first investigation suggested that Sn-seeded GaAs nanowire growth was successful only in a quite narrow temperature window; straight nanowires were observed between 487 °C and 525 °C. At temperatures lower than 487 °C, nanowires were kinked and at temperatures higher than 525 °C we did not observe nanowire growth. Transmission electron microscopy (TEM) and x-ray energy dispersive spectroscopy analysis revealed a zinc blende crystal structure of the nanowires and primarily Sn in the seed particle of all investigated nanowires with a weak but detectable Sn signal also along the nanowire.

In order to further develop the growth, it is important to understand how morphology and crystal structure of the nanowires are related to both temperature and V/III precursor ratio. In this paper, we present a more detailed and systematic study on the aspects of fundamental growth parameters for Sn-seeded GaAs nanowires. We demonstrate how the V/III ratio, obtained by changing either group III or group V precursor flows, allows to control nanowire crystal structure and nanowire kinking. We find that a lower V/III ratio can lead to twin plane formation. In addition, it is interesting that we observe a high ratio of nanowire kinking at both high group V flow and high group III flow at identical growth temperature. The effect of temperature on nanowire growth is related to the actual amount of available group III material, which is not surprising as the latter is suggested to be temperature-dependent. Furthermore, photoluminescence measurements were carried out on selected nanowires to investigate the simultaneous ‘seed-doping’ from the Sn particles where we find that the doping level is very high. We also find that carbon is incorporated in a temperature-dependent way.

2. Experimental methods

GaAs nanowires were grown on (111)B GaAs substrates in a low-pressure horizontal metal organic vapor phase epitaxy reactor (Aixtron 200/4) at a pressure of 100 mbar, a total flow of 131 min^{-1} with H_2 as carrier gas as well as in an Aixtron $3 \times 2''$ close coupled showerhead (CCS) reactor at a pressure of 100 mbar and a total flow of 81 min^{-1} . Most of the experiments were carried out in the low-pressure horizontal reactor unless otherwise specified. Trimethylgallium (TMGa) was used as group III precursor and AsH_3 as group V precursor. The GaAs substrates were first heated to an annealing temperature of 630 °C in AsH_3 ambient with a molar fraction of 1.54×10^{-3} . After 10 min annealing the temperature was ramped down to a set value of 550 °C. Once the set temperature was reached, tetraethyltin (TESn) with a molar fraction of 1.17×10^{-5} was introduced into the reactor for a 15 min Sn particle formation step with an AsH_3 background of 7.68×10^{-5} . Then, TESn was turned off and the reactor temperature was set to the desired growth temperature. Once the temperature stabilized, TMGa was turned on and AsH_3 was set to the desired molar fraction for the nanowire growth. The particle deposition step was kept the same with an average diameter of $59 \pm 7 \text{ nm}$ and a density of $11 \pm 2 \mu\text{m}^{-2}$ which is identical to the conditions as reported in [11]. The growth temperature and the flows of group V and group III precursors were varied to determine the effect of these parameters on the resulting nanowire growth. The ranges of molar fractions that group V and group III precursors were varied are from 7.68×10^{-5} to 2.30×10^{-4} and from 2.01×10^{-5} to 1.04×10^{-4} , respectively. GaAs nanowires were grown for 10 min unless otherwise stated and cooled down in AsH_3 ambient. *Ex situ* characterization of nanowire morphology and crystal structure was performed by scanning electron microscopy (SEM: Hitachi SU8010 operated at 15 kV) and transmission electron microscopy (TEM: JEOL 3000F operated at 300 kV). Low temperature (7 K) photoluminescence spectroscopy (PL) measurements were performed on single nanowires which were broken off from the native growth substrate and transferred onto a gold-covered Si substrate which had markers for easy location of the nanowires. The gold cover also slightly enhanced the emission intensity. A frequency doubled yttrium–aluminum–garnet–laser was employed for excitation of the nanowires and an optical microscope to collect the luminescence, which was dispersed onto a thermoelectrically cooled charge-coupled device. Typically five single nanowires of each sample were characterized.

3. Results and discussion

3.1. Dependence of nanowire growth on V/III ratio changes: TMGa precursor flow variation

We have studied the effect of TMGa precursor flow on the GaAs nanowire morphology and crystal structure. We will start with discussing the impact of TMGa molar fraction

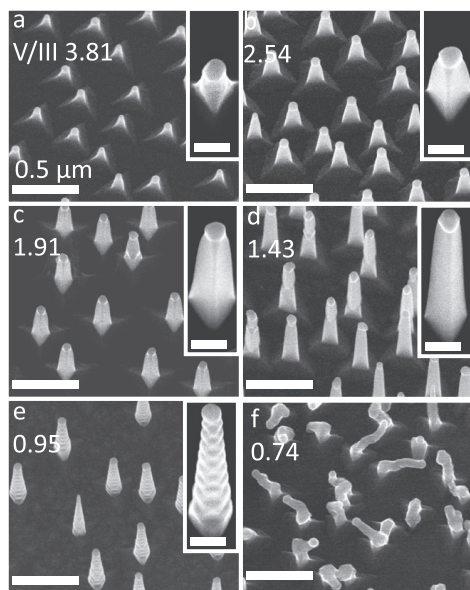


Figure 1. 30° tilted view SEM images of Sn-seeded GaAs nanowires grown at different V/III ratio with increasing TMGa precursor flow at a fixed AsH₃ molar fraction of 7.68×10^{-5} . Magnified views of single nanowires are given as insets in which scale bars are 100 nm.

variation from 2.01×10^{-5} to 1.04×10^{-4} while keeping the AsH₃ flow constant at a molar fraction of 7.68×10^{-5} resulting in V/III ratios ranging from 3.81 to 0.74. These experiments were carried out at 500 °C, which was found in our previous study to be the optimum growth temperature giving vertically aligned zinc blende GaAs nanowires with the most uniform morphology. A variation of the V/III ratio by changing the TMGa precursor flow has a strong effect on the nanowire morphology, especially the length and crystal structure are affected. Figure 1 shows SEM images of the nanowires grown with increasing TMGa flows, thus decreasing V/III ratio. As illustrated in figures 1(a)–(e), nanowires all grow vertically with increasing TMGa precursor flow, in other words decreasing the V/III ratio from 3.81 to 0.95. The length of the nanowires is strongly dependent on the TMGa precursor flow (see also supporting information S1) and higher V/III ratios result in shorter nanowires. This indicates that the length of the nanowire mainly depends on the flow of group III precursor. This is in agreement with what has been reported for gold-seeded GaAs nanowires in which the length of the nanowire is linearly or sublinearly dependent on the flow of TMGa precursor [12]. With a further increase of TMGa flow leading to a V/III ratio of 0.74, the nanowires start to kink instead of growing vertically from the substrate as illustrated in figure 1(f). This will be discussed more in detail later. It is interesting to note that the density of nucleated vertical nanowires is identical to the

density of pre-deposited Sn droplets (for all samples exhibiting predominantly vertical nanowire growth). However, it is quite difficult to tell the density for the kinked nanowires since they have very irregular and random morphology which makes it hard to determine whether they are successfully nucleated or not. To a first approximation, the density of identifiable crystallites seems consistent with the density of Sn droplets.

Another interesting phenomenon observed is that when a high flow of TMGa is supplied, the nanowire side facets appear rough which is noted from the alternating contrast at the side facet of the nanowire, as shown in the inset of figure 1(e), instead of rather smooth side facets as has been observed at lower TMGa flows (figures 1(a)–(d)). These microfacets are correlated with multiple twin planes along the nanowires growth axis [13, 14]. Note that in figure 1(d), one can also see that the side facets are not perfectly smooth in the nanowires; instead there are one or two facet rotations, associated with twin planes, in some of the nanowires. This clearly indicates that the twin formation in Sn-seeded GaAs nanowires is progressively interconnected with lowered V/III ratio [15]. Previously we reported that Sn-seeded nanowires mostly have a pure zinc blende crystal structure with $\{112\}_A$ side facets at optimized growth conditions [11]. Similarly to what has been demonstrated for Au-seeded GaAs nanowires, the $\{112\}$ -type sidewalls usually have anisotropic growth rates as a result of different polarities [16]. Here, the finally observed $\{112\}_A$ side facets imply that $\{\bar{1}\bar{1}2\}_B$ planes grow faster instead of the $\{112\}_A$ ones as for the Au-seeded case reported in [16]. $\{112\}$ -type planes are partially polar (being constructed of microfacets of the $\{111\}$ - and $\{100\}$ -type respectively), indicating that $\{112\}_A$ planes have more dangling bonds available on Ga atoms, while $\{\bar{1}\bar{1}2\}_B$ planes have more As atoms with non-saturated bonds. Considering our very low V/III ratio growth condition outlined here, relatively more Ga species should be available in this environment which will quickly bind to the accessible As spots. Consequently the As dominant $\{\bar{1}\bar{1}2\}_B$ planes would grow much faster causing them to outgrow and finally leaving nanowires with only $\{112\}_A$ side facets. Or in other words, the surface energy of $\{112\}_A$ facets is significantly lower compared to the $\{\bar{1}\bar{1}2\}_B$ counterparts under the applied low V/III ratio growth conditions which makes a fast over-respective outgrowth of the latter highly probable resulting in $\{112\}_A$ -terminated nanowires. A similar V/III-ratio dependence of surface energy of polar III–V surfaces in GaAs has been calculated and reported as a function of the chemical potential in [17].

However, in the case of frequently occurring rotational twinning along the nanowire growth axis the geometrical/morphological result of overgrowth processes is slightly different which will be discussed in the following. From TEM images in figure 2 (which represents the analysis of a single nanowire from the sample shown in figure 1(e)), we find a zinc blende crystal structure with a high number of semi-periodic rotational twins (figures 2(a)–(c)). The spacing of the twin planes, as shown by the conventional dark field images in figure 2(c), correlates to a good degree with the features

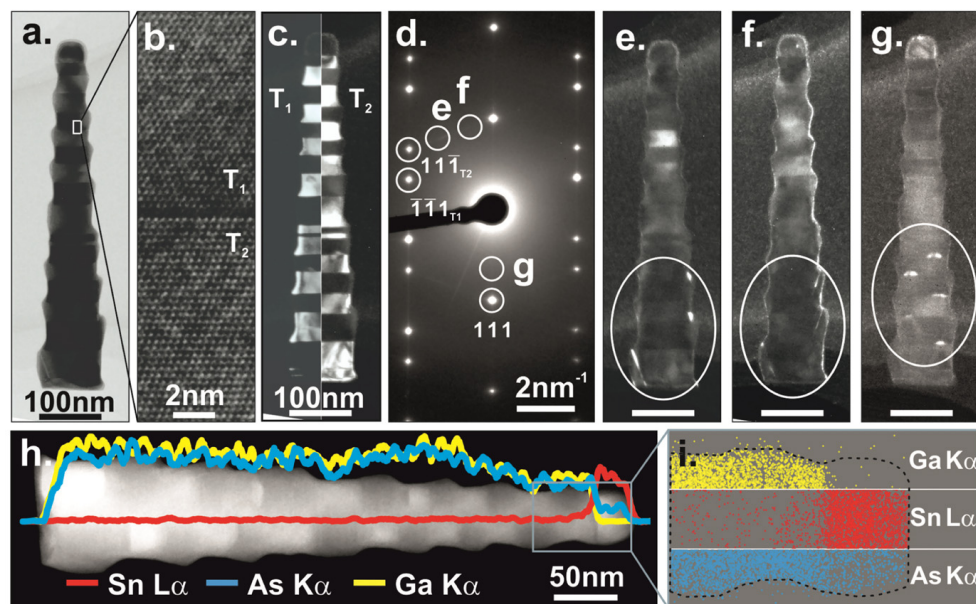


Figure 2. TEM images for a GaAs nanowire in figure 1(e) at a V/III ratio of 0.95 by using high TMGa flow viewed along the $\langle 110 \rangle$ zone axes. (a) Bright field overview image of a single nanowire with high resolution TEM at a twin plane in (b). (c) Merged conventional dark field images for twin 1 (T_1) and twin 2 (T_2) with (d) the characteristic selected area diffraction pattern indicating the twinned zinc blende character. (e–g) Conventional dark field images taken with the diffractions spots as highlighted in (d) indicating the twinning occurring for overgrowth on the $\{\bar{1}\bar{1}\bar{1}\}_B$ -type facets. (h) STEM-HAADF image with overlaid EDX line scans as well as (i) an EDX map of the particle area acquired in STEM-HAADF mode indicating the Sn-rich particle.

observed as rough facets in figure 1(e), meaning that the rough side facets in the SEM image are associated with the multiple twin planes here. Unlike Au-seeded GaAs nanowires which usually have short and dense twin segments [18–20], here we can see that the length of each twin segment can be up to 60 nm. There is also distinct radial overgrowth on the alternating, twinned zinc blende segments as highlighted by the conventional dark field images in figures 2(e)–(g). Here we see brighter contrast occurring at similar positions on every other zinc blende segment and alternated (60° rotated) on consecutive segments when using $\{111\}$ -related twin-characteristic diffractions spots which is especially visible in figure 2(g). A possible explanation for the overgrowth is that in the early stage of a twin formation, the nanowires primarily possess $\{111\}$ -type facets. Whenever a twin plane appears, the segments are rotated by 60° with respect to each other around the $\langle \bar{1}\bar{1}\bar{1} \rangle_B$ growth axis. Thus, the $\{111\}_A$ facets are meeting $\{\bar{1}\bar{1}\bar{1}\}_B$ facets at alternating twin planes in the axial direction with the global tendency to finally form $\{112\}$ -type facets as discussed above. However, as we also discussed above $\{\bar{1}\bar{1}\bar{2}\}_B$ facets preferably grow faster in order to attain $\{112\}_A$ side facets on both segments separated by a twin plane. From a purely geometrical perspective this overgrowth would result in triangular cross sectional segments stacked along the $\langle \bar{1}\bar{1}\bar{1} \rangle_B$ growth axis, terminated by 3 $\{112\}_A$ -type

facets, and with every other segment rotated by 60° with respect to each other. Although this situation is not realistic, we do still observe the alternating overgrowth on the zinc blende segments but not with the ultimate geometrical consequences as described in the previous sentence.

3.2. Dependence of nanowire growth on V/III ratio changes: AsH_3 precursor flow variation

We also investigated the effect of AsH_3 precursor flow on GaAs nanowire growth, in which the flow of TMGa precursor was set to a constant molar fraction of 4.03×10^{-5} at 500°C , while varying the AsH_3 molar fraction from 7.68×10^{-5} to 2.30×10^{-4} , corresponding to V/III ratios between 1.91 and 5.71. As illustrated in figure 3(a) and the inset, at a low V/III ratio the nanowires have rough side facets, which are associated with twin planes perpendicular to the growth direction. This correlates to what we have observed for the nanowires grown at high TMGa supply (figure 1(e)), also resulting in a low V/III ratio. It seems that the formation of twin planes can be associated with a low V/III ratio but not with absolute precursor flows within the investigated flow regime. There is no obvious relation between the lengths of the nanowires with AsH_3 flow (see also supporting information S1). Moreover, a distinct trend in the rate of kinking nanowires with increasing

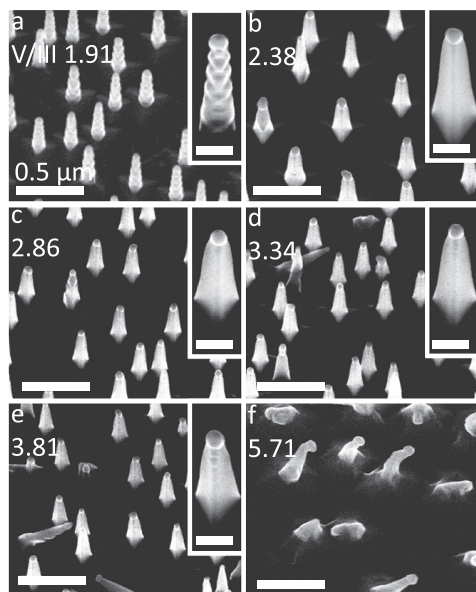


Figure 3. 30° tilted view SEM images of GaAs nanowires grown at 500 °C with increasing V/III ratio by increasing AsH₃ flow at a constant TMGa precursor molar fraction of 4.03×10^{-5} . The scale bars in insets of single nanowires are 100 nm.

AsH₃ flow is observed from figure 3. At a critical V/III ratio of 3.34, around 6% of the nanowires start to kink into a non-vertical growth direction (see supporting information S2). An even larger amount of kinked nanowires occurs with increasing AsH₃ flow and thus at higher V/III ratio until eventually at a V/III ratio of 5.71 no straight, vertically aligned nanowires are observed. And we expect with V/III ratios higher than 6, there will not be any successful growth of straight and vertically aligned nanowires at this temperature and instead all nanowires will be kinked. This kinking effect is consistent with what has been reported for Au-seeded GaAs nanowires grown at high V/III ratios [15]. One possible reason behind this is that high AsH₃ flows could lead to a surface reconstruction on GaAs substrate [21] which might assist another growth direction other than $\langle 111 \rangle_B$ causing nanowire kinking. On the other hand, it is surprising that kinking also occurs at high TMGa flows as shown in figure 1(f). It was demonstrated previously that in III–V/IV heterostructure system, the particle volume, the contact angle of the droplet particle, and the match between particle and nanowire growth interface are fundamental factors in determining the nanowire morphology, more specifically nanowire kinking [22]. We have previously reported that from EDX analysis on our Sn-seeded GaAs nanowires, there is a substantial fraction of As in the seed particle (see also figure 2(i) here) in contrast to the case of gold [11]. The composition of the Sn particle is very likely to be a dynamic state during

nanowire growth. Thus, excessive group V or group III precursor availability could lead to a volume change in the Sn seed particle and also changes of the contact angle. These two extreme cases could both lead to nanowire kinking, however, from different mechanisms. Indeed, in figure 1(f) (high TMGa), the shape and diameter of the nanowires change substantially, the nanowires lost its shape and become like a cluster, despite the fact that they are also kinking. However, in figure 3(f) (high AsH₃), it seems that the nanowires still grow straight after kinking happens in an early stage (see also supporting information S3). Thus, it is possible that the kinking of these Sn-seeded GaAs nanowires originates from two different mechanisms for the two regimes (high TMGa versus high AsH₃).

As discussed above, Sn-seeded GaAs has a quite low suitable V/III ratio for the growth compared to Au-seeded reference growth, and the nanowires have either pure zinc blende crystal structure or zinc blende with a few rotationally twinned segments. No wurtzite crystal structure nanowires, not even short segments of wurtzite have been observed so far in the growth range investigated. In the case of Au-seeded nanowire growth, the V/III ratio can be up to 240 and denser twin planes or even twin plane superlattices can be observed under certain growth conditions [23, 24]. Wurtzite structure can also be achieved at selected growth conditions. However, nanowires seeded from both Sn and Au nanoparticles follow the same trend with different V/III ratio, which is the density of twin defects is closely related to lower V/III ratio and the formation of twinning can be prevented by either increasing AsH₃ precursor flow or decreasing the TMGa precursor flow [15].

3.3. Broadening the growth temperature window

In our previous investigation of Sn-seeded GaAs nanowires, a temperature range from 475 °C to 535 °C was used for the GaAs nanowire growth at a V/III ratio of 1.9 where straight vertically aligned nanowires were only observed in a limited range, from 487 °C to 525 °C. This is narrower compared to Au-seeded GaAs nanowire growth, which usually occurs within the range from 380 °C to 540 °C [23, 25].

For Sn-seeded GaAs nanowires we previously found that there was barely any nanowire nucleation and the vapor-solid surface growth was dominant at a temperature of 535 °C and we expected the same for temperatures above that. Conversely most of the nanowires were still growing but just kinked when the temperature was lower than 487 °C. In addition it is well documented that for Au-seeded GaAs nanowire growth the radial overgrowth or tapering is substantially minimized at lower temperature [24, 25]. This makes it interesting to explore further the nanowire growth in the low temperature range to improve the yield of straight versus kinked nanowires. At low temperatures, the resulting nanowire kinking and growth along other directions different from $\langle 111 \rangle_B$ appeared similar to the case with a high AsH₃ supply as shown in figure 3(f) [11].

It was previously shown that Sn-seeded GaAs nanowire kinking could be prevented by a two-step approach consisting

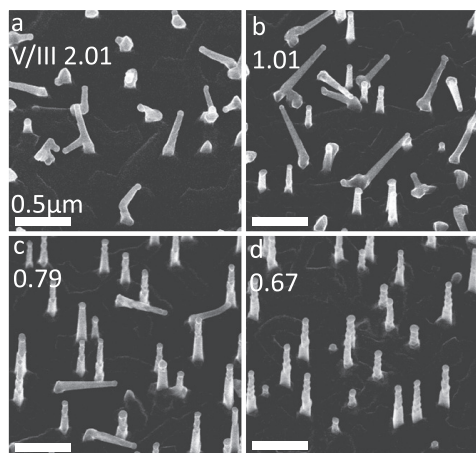


Figure 4. Broadening the growth temperature window of Sn-seeded GaAs nanowires down to 455 °C by increasing the TMGa precursor flow thus decreasing the V/III ratio at a fixed AsH₃ molar fraction of 7.31×10^{-5} . The proportion of vertically aligned GaAs nanowires increases with increasing TMGa flow (see also supporting information S4 (stacks.iop.org/27/215603/mmedia)).

of a nucleation step at high temperature and then cooling down to a lower temperature for the growth [11]. This implies that there could be a similar nucleation problem for Sn-seeded GaAs nanowires at low temperatures following the same trend as reported for Au-seeded nanowires [26]. Considering the fact that changes in temperature will affect the decomposition rate of precursors it is likely that the actual V/III ratio at the growth front will change with temperature even for constant precursor flows. To investigate whether the kinking of nanowires observed at low temperatures is associated to a relatively higher effective V/III ratio, another series of experiments was carried out at a temperature of 455 °C with increasing TMGa flow while holding the AsH₃ flow constant at 7.31×10^{-5} . As can be seen from SEM images in figure 4, there is less tapering of the resulting nanowires due to the lower growth temperature and the proportion of vertical nanowires increases from around 13% to almost 100% with increasing TMGa supply. From this we can conclude that AsH₃ is closely related to nanowire kinking and increasing the TMGa supply at low temperature can be used to counterbalance this effect of AsH₃ resulting in straight vertically aligned nanowires. One possible reason for this could be that As trimers form on the substrate surface at low temperature with a higher effective V/III ratio leading to an As-rich environment interfering with nanowire nucleation. We have also discussed previously that two extreme regimes could cause nanowire kinking with either excessive Ga or As in the Sn particle during growth. Hence, another possible reason could be that abundant As would accumulate in Sn seed particles at low temperature which would result in

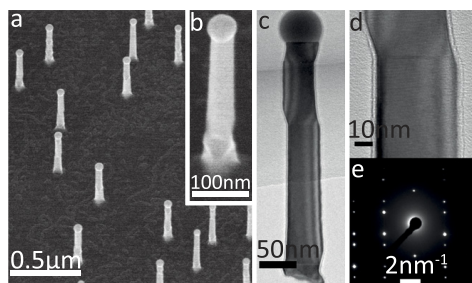


Figure 5. (a), (b) 30° tilted view SEM image of GaAs nanowires with a larger magnification inset grown in the CCS setup at 420 °C under 'optimized' conditions with reduced radial overgrowth. (c), (d) Overview and higher magnification TEM image of a representative nanowire indicating the reduced overgrowth, the triangular cross-sectional morphology (noticeable from the thickness fringes and SEM images (a) and (b)), and the few rotational twins. The latter is further supported by the SADP (e).

kinked nanowires, but adding more TMGa could again balance the composition in the Sn particle and prevent nanowire kinking.

Based on this observation and to further optimize the growth result, the experiments were transferred to an Aixtron CCS $3 \times 2''$ reactor in which higher TMGa flows could be attained technically. We find that the temperature window can be broadened to as low as 400 °C by stepwise increasing the TMGa with decreasing temperature. As shown in figure 5, at 'optimized' conditions of 420 °C with a V/III ratio of 0.86, the radial shell overgrowth can be significantly reduced due to the lower growth temperature used. Also worth noting is that the axial nanowire growth rate decreases remarkably with decreasing temperature and here the nanowire growth time is 30 min. From SEM and TEM studies presented in figure 5, we find that the nanowires exhibit zinc blende crystal structure with few rotational twins. From EDX spectra we further find detectable signals from both As and Ga in the Sn seed particle. A weak but detectable Sn signal can also be measured at the GaAs nanowire body which is consistent with what we previously reported for nanowires grown at higher temperatures [11]. Since the shell growth was previously found to be highly p-doped by C incorporation, the possibility to tune the growth to either include or eliminate radial overgrowth makes it potentially very interesting for device applications.

3.4. Optical properties

We have investigated selected nanowire samples to represent characteristic points in a growth series by photoluminescence (PL) spectroscopy to study the effect of for example temperature. Figure 6 shows the low temperature PL spectra of the nanowires grown at different V/III ratios at a constant growth temperature (figure 6(a)) and at different temperatures, but constant V/III ratio (figure 6(b)). The spectra are normalized and plotted with an offset for clarity. We observed a strong Burstein–Moss shift, which we attribute to the highly n-type

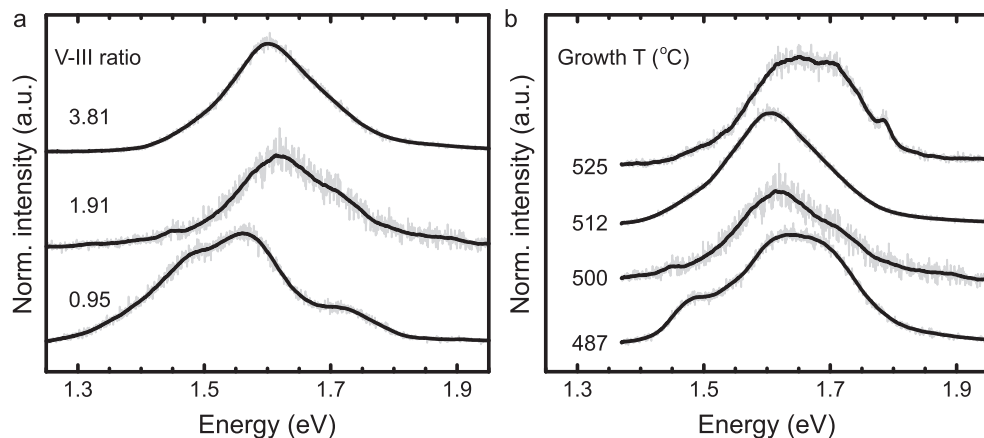


Figure 6. Low temperature PL results of GaAs nanowires as well as free carrier concentrations on the order of 10^{19} extracted from the Fermi-tail fitting. (a) Spectra taken from nanowires grown at 500 °C but different V/III ratio. (b) PL spectra of nanowires grown at constant V/III ratio at 1.91 but different temperatures. Broad spectra as well as blue-shifting with respect to the bandgap energy of GaAs indicates a high doping level as well as a high concentration of defects. Black spectra is smoothed and grey is raw data.

doped core. The heavy doping shifts the Fermi level into the conduction band, which increases the average recombination energy and broadens the spectra. It should be noted that the PL did not show any noticeable changes with excitation power density apart from the intensity. In order to acquire a rough estimate of the free carrier concentration we used the Fermi-tail fitting method [27], taking into consideration changes in the effective carrier mass and the bandgap renormalization. The carrier concentration is on the order of 10^{19} cm^{-3} for all the samples (figure 6(a)), which is consistent with our estimation in the previous study that according to the consumption of Sn nanoparticle during growth, the doping density can be up to 10^{20} cm^{-3} [11]. Calculations of carrier concentration for nanowires grown at different V/III ratios show a trend of Sn incorporation which is more favorable on the As sites with decreasing V/III ratio.

Our previous studies of GaAs nanowires grown at 500 °C with a V/III ratio of 1.91 showed strong Esaki diode behavior, with the C-doped p-type overgrowth (the shell) and the heavily Sn-doped n-type core [11]. This complicates the analysis further making an interpretation of the spectra not trivial. The low energy shoulder at 1.48 eV can be caused by crystal defects, such as rotational twins, where spatially indirect recombination takes place [20]. However, PL measurements show decreased intensity of the low energy shoulder with increasing temperature (figure 6(b)), despite the higher density of rotational twins. This makes the crystal defects very unlikely to be the origin of the low energy emission in our nanowires. As an alternative explanation we speculate that it is related to carbon impurities in the p-doped shell. This suggests that carbon incorporation decreases with increasing V/III ratio as well as with increasing growth temperature, both of which are consistent with layer growth studies [28, 29]. It can also be related to other point defects

incorporated during the growth. The high energy peak cannot be assigned to any optical transitions involving band-to-band transitions. We speculate, that it may be related to states created by Sn below the conduction band at the L point. The L point has energy of 1.815 eV where the valence band maximum is at 0 eV.

4. Summary and conclusion

In summary, we have investigated the growth of Sn-seeded GaAs nanowires in detail by varying the temperature as well as group III and group V precursor flows to further understand the nanowire growth mechanism. The growth rate of nanowires is strongly dependent on group III precursor supply (TMGa). High amounts of either TMGa or AsH₃ flows result in nanowire kinking, suggested to be caused by different mechanisms due to the composition change in the Sn seed droplet during nanowire growth. Moreover the twin plane formation in nanowires is found to be closely related to V/III ratio and happens at low V/III ratio regardless of whether group V or group III precursor is changed. We demonstrate that vertical GaAs nanowires with reduced shell growth can be obtained in a broadened temperature range by adjusting the TMGa precursor flow together with decreasing temperature, which could be attributed to a different effective V/III ratio involved in the nanowire growth at lower temperature. Furthermore, PL results reveal the temperature and V/III dependence of carbon incorporation related doping and confirm the high level of Sn-doping in the nanowires. Our results could be used in order to grow highly n-type GaAs nanowires without the use of Au seed particles or addition of extra dopants for future device applications.

Acknowledgments

The authors acknowledge financial support from the European Research Council under the European Union's Seventh Framework Programme (FP/2007-2013)/ERC Grant Agreement No. 336126. We further acknowledge financial support by the Swedish Research Council (VR), the Knut and Alice Wallenberg Foundation (KAW), and NanoLund.

References

- [1] Hiruma K, Yazawa M, Katsuyama T, Ogawa K, Haraguchi K, Koguchi M and Kakibayashi H 1995 Growth and optical properties of nanometer-scale GaAs and InAs whiskers *J. Appl. Phys.* **77** 447
- [2] Lang D V, Grimmeiss H G, Meijer E and Jaros M 1980 Complex nature of gold-related deep levels in silicon *Phys. Rev. B* **22** 3917–34
- [3] Motohisa J, Noborisaka J, Takeda J, Inari M and Fukui T 2004 Catalyst-free selective-area MOVPE of semiconductor nanowires on (111)B oriented substrates *J. Cryst. Growth* **272** 180–5
- [4] Gao L et al 2009 Self-catalyzed epitaxial growth of vertical indium phosphide nanowires on silicon *Nano Lett.* **9** 2223–8
- [5] Ambrosini S, Fanetti M, Grillo V, Franciosi A and Rubini S 2011 Self-catalyzed GaAs nanowire growth on Si-treated GaAs(100) substrates *J. Appl. Phys.* **109** 094306
- [6] Han N, Wang F, Hui A T, Hou J J, Shan G, Xiu F, Hung T and Ho J C 2011 Facile synthesis and growth mechanism of Ni-catalyzed GaAs nanowires on non-crystalline substrates *Nanotechnology* **22** 285607
- [7] Hillerich K, Dick K A, Messing M E, Deppert K and Johansson J 2012 Simultaneous growth mechanisms for Cu-seeded InP nanowires *Nano Res.* **5** 297–306
- [8] Ikejiri K, Noborisaka J, Hara S, Motohisa J and Fukui T 2007 Mechanism of catalyst-free growth of GaAs nanowires by selective area MOVPE *J. Cryst. Growth* **298** 616–9
- [9] Yu L, O'Donnell B, Alet P-J, Conesa-Boj S, Peiró F, Arbiol J and Cabarrocas P R I 2009 Plasma-enhanced low temperature growth of silicon nanowires and hierarchical structures by using tin and indium catalysts *Nanotechnology* **20** 225604
- [10] Mullane E, Kennedy T, Geaney H, Dickinson C and Ryan K M 2013 Synthesis of tin catalyzed silicon and germanium nanowires in a solvent-vapor system and optimization of the seed/nanowire interface for dual lithium cycling *Chem. Mater.* **25** 1816–22
- [11] Sun R, Jacobsson D, Chen I-J, Nilsson M, Thelander C, Lehmann S and Dick K A 2015 Sn-seeded GaAs nanowires as self-assembled radial p–n junctions *Nano Lett.* **15** 3757–62
- [12] Soci C, Bao X-Y, Aplin D P R and Wang D 2008 A systematic study on the growth of GaAs nanowires by metal-organic chemical vapor deposition. *Nano Lett.* **8** 4275–82
- [13] Johansson J, Karlsson L S, Patrik T, Svensson C, Mårtensson T, Wacaser B A, Deppert K, Samuelson L and Seifert W 2006 Structural properties of (111) B-oriented III–V nanowires *Nat. Mater.* **5** 574–80
- [14] Caroff P, Dick K A, Johansson J, Messing M E, Deppert K and Samuelson L 2009 Controlled polytypic and twin-plane superlattices in iii–v nanowires *Nat. Nanotechnol.* **4** 50–5
- [15] Joyce H J et al 2008 High purity GaAs nanowires free of planar defects: growth and characterization *Adv. Funct. Mater.* **18** 3794–800
- [16] Zou J, Paladugu M, Wang H, Auchterlonie G J, Guo Y-N, Kim Y, Gao Q, Joyce H J, Tan H H and Jagadish C 2007 Growth mechanism of truncated triangular III–V nanowires *Small* **3** 389–93
- [17] Moll N, Kley A, Pehlke E and Scheffler M 1996 GaAs equilibrium crystal shape from first principles *Phys. Rev. B* **54** 8844–55
- [18] Koguchi M, Kakibayashi H, Yazawa M, Hiruma K and Katsuyama T 1992 Crystal structure change of GaAs and InAs whiskers from ZB to WZ *Japan. J. Appl. Phys.* **31** 2061–5
- [19] Bussone G, Schott R, Biermanns A, Davydok A, Reuter D, Carbone G, Schülli T U, Wieck A D and Pietsch U 2013 Grazing-incidence x-ray diffraction of single GaAs nanowires at locations defined by focused ion beams *J. Appl. Crystallogr.* **46** 887–92
- [20] Bolinsson J, Ek M, Trägårdh J, Mergenthaler K, Jacobsson D, Pistol M E, Samuelson L and Gustafsson A 2014 GaAs/AlGaAs heterostructure nanowires studied by cathodoluminescence *Nano Res.* **7** 473–90
- [21] Biegelsen D, Bringans R, Northrup J and Swartz L-E 1990 Reconstructions of GaAs(1 \times 1 \times 1) surfaces observed by scanning tunneling microscopy *Phys. Rev. Lett.* **65** 452–5
- [22] Hillerich K, Dick K A, Wen C Y, Reuter M C, Kodambaka S and Ross F M 2013 Strategies to control morphology in hybrid group III–V/group IV heterostructure nanowires *Nano Lett.* **13** 903–8
- [23] Lehmann S, Jacobsson D and Dick K A 2015 Crystal phase control in GaAs nanowires: opposing trends in the Ga- and As-limited growth regimes *Nanotechnology* **26** 301001
- [24] Burgess T, Breuer S, Caroff P, Wong-Leung J, Gao Q, Hoe Tan H and Jagadish C 2013 Twinning superlattice formation in GaAs nanowires *ACS Nano* **7** 8105–14
- [25] Borgström M, Deppert K, Samuelson L and Seifert W 2004 Size- and shape-controlled GaAs nano-whiskers grown by MOVPE: a growth study *J. Cryst. Growth* **260** 18–22
- [26] Joyce H J, Gao Q, Tan H H, Jagadish C, Kim Y, Zhang X, Guo Y and Zou J 2007 Twin-free uniform epitaxial GaAs nanowires grown by a two-temperature process *Nano Lett.* **7** 921–6
- [27] Lindgren D, Hultin O, Heurlin M, Storm K, Borgström M T, Samuelson L and Gustafsson A 2015 Study of carrier concentration in single InP nanowires by luminescence and Hall measurements *Nanotechnology* **26** 045705
- [28] Jensen K F, Fotiadis D I and Mountziaris T J 1991 Detailed models of the MOVPE process *J. Cryst. Growth* **107** 1–11
- [29] Van Deelen J, Bauhuis G J, Schermer J J and Larsen P K 2004 Parameter study of intrinsic carbon doping of Al_xGa_{1-x}As by MOCVD *J. Cryst. Growth* **271** 376–84

Supplementary information to:

Sn-seeded GaAs nanowires grown by MOVPE

Rong Sun¹, Neimantas Vainorius¹, Daniel Jacobsson¹, Mats-Erik Pistol¹, Sebastian Lehmann¹, and
Kimberly A. Dick^{1,2}

¹Solid State Physics and NanoLund, Lund University, P.O. Box 118, SE-221 00 Lund, Sweden

²Also at Centre for Analysis and Synthesis, Lund University, P.O. Box 124, SE-221 00 Lund, Sweden

Electronic mail: Kimberly.Dick_Thelander@ftf.lth.se

Table of contents

S1. GaAs nanowire length dependence on V/III ratio by varying TMGa flow	2
S2. Proportion of vertical nanowires on V/III ratio by varying AsH ₃ flow	3
S3. Top view of kinked nanowires with high AsH ₃ flow	4
S4. Improved yielding of vertical nanowires at 455°C	5

S1. GaAs nanowire length dependence on V/III ratio by varying TMGa flow

Since the length of Sn-seeded GaAs nanowire is very sensitive to the TMGa precursor flow at 500°C, we carried out measurements on over 90 nanowires for each sample at different spots on substrate to acquire statistically representative data. As shown in figure S1.1, the length of nanowires is strongly dependent on the TMGa flow or inversely dependent on the V/III ratio. We did the same analysis for nanowires grown with increasing AsH₃ flow as shown in figure S1.2, the length of nanowires first increases substantially, after a critical V/III ratio of 2.38 it starts to decrease with increasing AsH₃ flow.

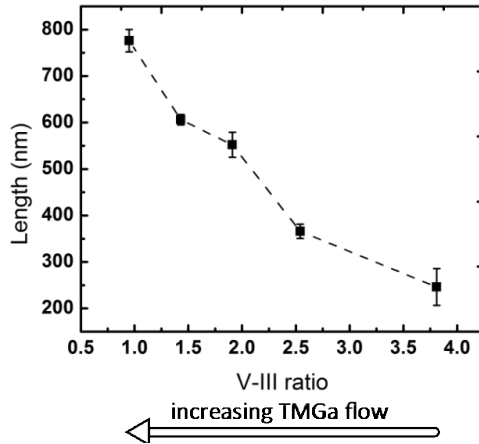


Figure S1.1. The lengths of the nanowires are plotted against V/III ratio by increasing TMGa precursor flow while AsH₃ is holding at a fixed molar fraction of 7.68×10^{-5} . (Dotted line is inserted as a guide to the eye only.)

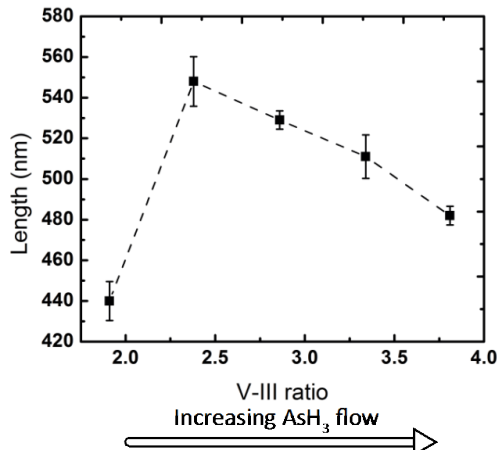


Figure S1.2. The lengths of the nanowires are plotted against V/III ratio by increasing AsH₃ precursor flow while TMGa is holding at a fixed molar fraction of 4.03×10^{-5} . (Dotted line is inserted as a guide to the eye only.)

S2. Proportion of vertical nanowires on V/III ratio by varying AsH₃ flow

It is very interesting to note from the study of AsH₃ precursor flow variation at 500°C that nanowire kinking is very closely related to the AsH₃ flow when the TMGa precursor flow is fixed at 4.03×10^{-5} . From figure S2, one can easily identify straight vertically aligned nanowire as a dot (more round appearance) if it has multiple twin planes or triangle if it possesses pure zinc blende crystal structure or only with very few twin planes. The yield of vertical nanowires is counted for different samples as can be seen from Table S1.

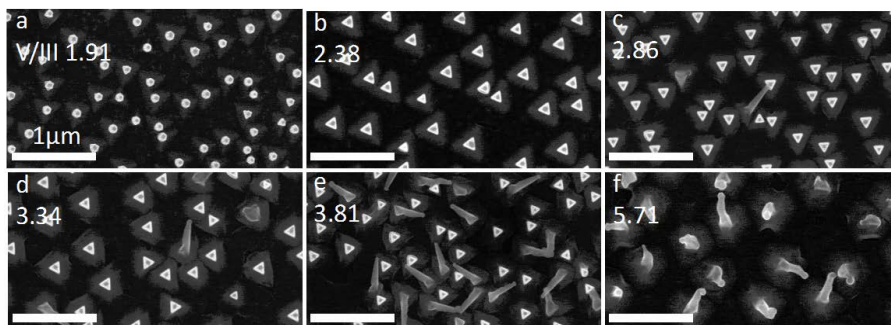


Figure S2. Top view SEM images of nanowires grown with increasing AsH₃ flow corresponding to figure 3 shown in the paper.

Table S1. Proportion of vertical nanowires on V/III ratio by varying AsH₃ flow

V/III ratio	1.91	2.38	2.86	3.34	3.81	5.71
Proportion of vertical nanowires(%)	100	100	97	94	75	0

S3. Top view of kinked nanowires with high AsH₃ flow

As can be seen from the top view image below for kinked nanowires grown at high AsH₃ flow, most of the nanowires still remain the one-dimensional nanowire shape instead of forming clusters and growing straight after kinking happens in the beginning.

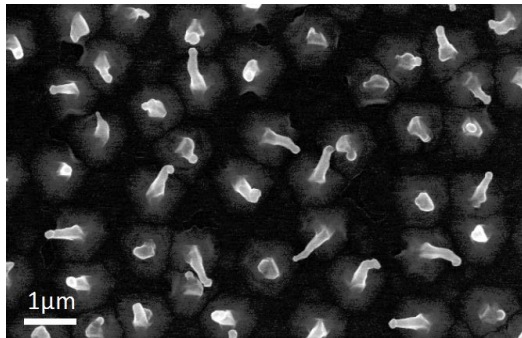


Figure S3. Top view image of figure 3f, Sn seeded GaAs nanowires grown with high AsH₃ flow and a V/III ratio of 5.71

S4. Improved yield of vertical nanowires at 455°C

By increasing the TMGa precursor flow stepwise at 455°C while holding the AsH₃ flow constant at 7.31×10^{-5} , the yield of straight vertical nanowires is improved. From figure S3, it is clear that the increment proportion of dots or triangles, which correspond to vertical nanowires, follows the increasing TMGa precursor flow. From this result, the temperature window for nanowire growth could be further broadened by simultaneous variation of the TMGa flow and a decrease of the growth temperature.

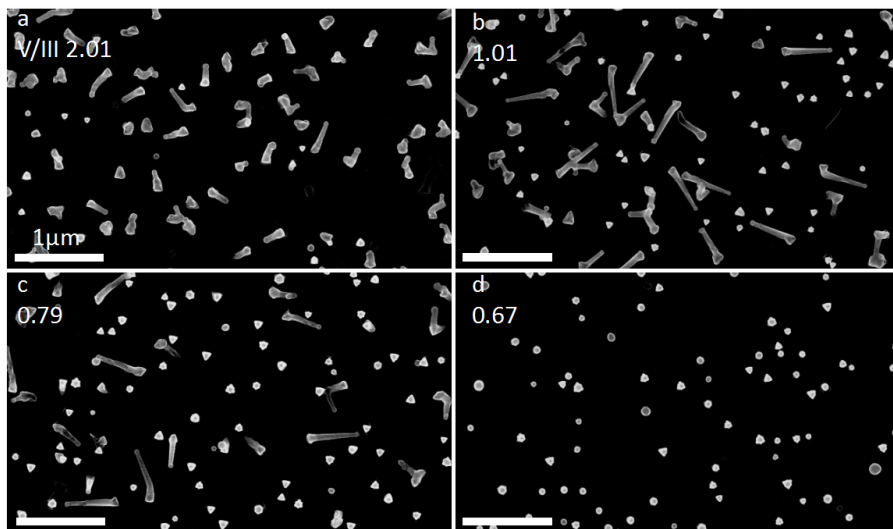


Figure S3. Top view SEM images of Sn seeded GaAs nanowires grown at 455°C with increasing TMGa flow thus decreasing V/III ratio.

Paper III



Sn seeded defect-free zincblende InAs nanowires

Rong Sun¹, Karl Winkler¹, Sarah McKibbin², Jonas Johansson¹, Rainer Timm²,
Sebastian Lehmann¹ and Kimberly A. Dick^{1,3}

¹ Solid State Physics, Lund University, Box 118, S-22100 Lund, Sweden

² Department of Physics, Lund University, Box 118, S-22 100 Lund, Sweden

³ Center for Analysis and Synthesis, Lund University, Box 124, S-22100 Lund,
Sweden

Abstract

In this paper, we report the epitaxial growth of defect-free zincblende structure InAs nanowires vertically aligned on (111)A substrate using in-situ formed Sn catalysts. The formation of the in-situ Sn particles has been investigated and the optimum condition has been used for InAs nanowire growth. Transmission electron microscopy study reveals pure zincblende InAs (111)A nanowires free from stacking defects and twin planes. Electrical measurement confirms that the resulting InAs nanowire exhibits high n-doping profile which is due to the incorporation of Sn particles into the nanowire. Moreover, scanning tunneling microscopy excludes the possibility of thick Sn layer segregation on the nanowire surface. This work provides an effective approach to achieve high n-doped InAs nanowire while simultaneously controlling the nanowire crystal structure.

1. Introduction

The epitaxial growth of III-V nanowires has been investigated over the past decades as they have great potentials of being used as building blocks for future electronic and optoelectronic devices. Au has almost been exclusively used for the growth of III-V nanowires since it has been the most successful and applicable seed material for all the III-V material system including InAs.[1] InAs is a versatile material since it has relatively narrow band gap (0.36 eV) and high electron mobility ($20000 \text{ cm}^2\text{V}^{-1} \text{ s}^{-1}$) compared to most other III-V materials. InAs nanowires have been used for the study of Majorana fermions, field effect transistors, quantum dots and photodetectors. [2–5] However, high doping of InAs nanowires remains difficult to achieve since usually highly-doped InAs nanowires come with significant change in the nanowire

morphology like diameter and length [6][7]. Intentional doping for InAs nanowires can also have significant radial growth leading to a highly doped shell [8]. The crystal structure of the InAs nanowire could also become more defected with the simultaneous doping [8]. Au-seeded InAs nanowires are usually wurtzite or mixed structure, or in some cases zinc blende with frequent twins. [9] The random mixtures of wurtzite/zincblende segment also drastically degrade the electrical properties of InAs nanowires [10]. Moreover it is very difficult to grow pure zinc blende InAs nanowires using Au particles especially if narrow diameter or high aspect ratio nanowires are desired [11][12]. It has been reported that by using alternative seed particle like palladium, defect-free InAs nanowires can be achieved [13]. Previously we have reported Sn seeded pure zinc-blende GaAs nanowires at selected growth conditions with simultaneous self-doping from the catalyst Sn during the growth.[14] It would be interesting to see if this high purity zinc blende crystal structure observed for Sn-seeded GaAs would also apply to the InAs system and if the Sn particles can be incorporated into the nanowire and simultaneously achieve high doping level without changing nanowire morphology and crystal structure.

In this paper, we have investigated in-situ formed Sn particles in the metal organic vapor phase epitaxy (MOVPE) reactor and InAs nanowire growth from these Sn particles. We have compared the Sn particles and InAs nanowires formed on InAs (111) substrates with different polarities namely (111)A and (111)B. The morphological, structural and compositional characterizations have been performed on the resulting (111)A nanowires. We have found that substrate polarity affects the formation of Sn particles resulting in different size, density as well as contact angle. Vertically aligned InAs nanowires with high-quality zincblende crystal structure can be grown on (111)A substrate. In addition, electrical characterization and scanning tunneling microscopy have been performed which indicate that the (111)A InAs nanowires are highly n-doped along the nanowire and there is no thick layer of segregated Sn or Sn oxide on the nanowire surface.

2. Experimental details

The epitaxial growth was performed with an Aixtron 3x2" close coupled showerhead (CCS) MOVPE reactor at a pressure of 100 mbar. Hydrogen was used as the carrier gas with a total flow of 8 l/min. Tetraethyltin (TESn) was used as the precursor for Sn

particle deposition. For InAs nanowire synthesis, trimethylindium (TMIn) and arsine (AsH_3) were used as the precursors.

InAs (111)A and (111)B substrates were first heated to an annealing temperature of 560 °C in arsine (AsH_3) background with a molar fraction of $2.5\text{E-}05$. After 10 min annealing, samples were cooled to the desired particle deposition temperature (in the range of 490 °C – 550 °C) in arsine. Once the temperature had stabilized the molar fraction of AsH_3 was changed to $2.8\text{E-}05$ and a TESn flow with a molar fraction of $4.3\text{E-}05$ was introduced. Following 15 min Sn deposition, TESn was turned off and the temperature was ramped down to the desired growth temperature (in the range of 455 °C – 510 °C) in arsine ambient. For Sn particle study, the sample was cooled down directly to room temperature in AsH_3 ambient. Once the growth temperature was reached, trimethylindium (TMIn) was turned on with a desired molar fraction. InAs nanowires were grown for 40 min unless otherwise stated and then cooled down in AsH_3 ambient.

The InAs nanowire morphology was characterized by scanning electron microscopy (SEM; Hitachi SU8010 at 15 kV), crystal structure was characterized with transmission electron microscopy (TEM; JEOL 3000 at 300 kV), and composition was characterized by X-ray energy dispersive spectroscopy (EDX) in high-angle annular dark field scanning TEM (HAADF-STEM) mode. Samples were prepared for TEM analysis by mechanically breaking the nanowires near the base onto carbon film-coated Cu grids.

For electrical characterization, nanowires were broken off from the growth substrate and transferred to a measurement chip with a micromanipulator under an optical microscope. The chip consists of a highly n-doped (P) Si covered with a 130nm thick thermally grown SiO_2 insulation layer with predefined outer contacts. Low magnification SEM images were taken to select individual nanowires and a standard EBL lithography step was used to define two- and four- contact geometries on individual nanowires. The native oxide on the nanowires was removed at the contact areas through a wet etching step in a $(\text{NH}_4)_2\text{Sx} : \text{H}_2\text{O} - 1:9$ solution at room temperature for 1min directly prior to metal contact evaporation. A metal stack of 25nm Ni and 100nm Au was evaporated onto the chip followed by a lift off in acetone. The chip was glued and wire-bonded to a carrier chip to enable electrical measurements. The measurements were performed under vacuum conditions without illumination.

In addition to that, Scanning tunneling microscopy (STM) and scanning tunneling spectroscopy (STS) was also performed on these nanowires to investigate whether Sn atoms segregate during growth to the outer surface of the nanowire. Nanowires were placed on a InAs(111)B substrate and cleaned by annealing in a flow of atomic H to 390-410°C to remove native oxides [15].

3. Results and discussion

In the following, we will discuss and compare the in-situ deposition of Sn particles on InAs (111)A and (111)B substrates, Sn seeded InAs nanowires growth on (111)A and (111)B substrates. The characterization and measurement are focused on the straight and vertically-aligned InAs nanowires on (111)A substrate.

3.1 Study on the in-situ Sn particle formation

To investigate the effect of temperature on Sn particle formation, we have performed the experiment by introducing AsH₃ and TESn for 15min at 490 °C, 510 °C, 530 °C and 550°C respectively on the InAs (111)A and (111)B substrate. Figure 1 shows 85 degree tilted view of Sn particles formed on InAs (111)A surface in a, c, e and g as well as on InAs (111)B surface in b, d, f, h.

The density and diameter of in-situ formed Sn particle distribution on InAs (111)A and (111)B substrates are shown in figure SI 1. Each sample was measured at 3 to 5 different spots corresponding to 60 to 100 nanoparticles and the error bar represents standard deviation from the mean value. As can be seen from SIa, the diameter of Sn particles increases with temperature on both (111)A and (111)B substrates which is consistent with what has been observed for Sn nanoparticles formed on GaAs (111)B substrate [16]. The density measurements in figure SI 1b shows that the density of Sn particles formed on (111)B substrate is much larger than that on (111)A substrate no matter at which temperature they have been deposited. This could be due to the combined effect from multiple factor, for example, the sticking coefficient of Sn atoms and the nucleation barrier for the nuclei.

In figure 1, the contact angle of Sn particles is measured from a newly proposed geometric model which is described in SI 2. In general the contact angle for particles on (111)B is larger than on (111)A substrate. It is not surprising considering the fact that (111)A surface has higher surface energy than (111)B, and the Sn particle prefers

to wet the higher energy surface more which leads to a smaller contact angle on (111)A substrates.

Furthermore, the density of Sn droplets formed on (111)A substrate is steady with increasing temperature which is about 1.1 ± 0.2 / μm^2 . The contact angle of the droplets increases from $49.7^\circ \pm 3$ at 490°C to $59.7^\circ \pm 2$ at 550°C . Contrarily, the density of Sn droplets on the (111)B substrate drops with increasing temperature which might be due to the Ostwald ripening and coalescence effect that the small droplets dissolve and incorporate into larger droplets. The contact angle of Sn droplets on (111)B substrate decreases from $73.9^\circ \pm 1$ at 490°C to $60.6^\circ \pm 2$ at 550°C . It is interesting that the contact angle of Sn droplets on (111)A and (111)B substrates becomes consistent at a temperature of 550°C no matter the opposite trend observed with increasing temperature. Taking into account the Young's equation at the particle-substrate interface, $\cos\beta \cdot \gamma_{lv} + \gamma_{sl} = \gamma_{sv}$, where β denotes the contact angle of a droplet at the substrate and γ_{lv} , γ_{sl} and γ_{sv} represent the surface energy between liquid-vapor, solid-liquid and solid-vapor interface respectively. Since γ_{lv} , which is the surface energy of liquid Sn droplet in our case, usually decreases with increasing temperature [19], the contact angle of the droplet should decrease, when the other two factors do not have temperature dependency, to meet the Young's equation at the particle substrate interface. However, the reason for the opposite trend observed here on (111)A and (111)B substrate is not clear yet. According to Nebo'sin criterion, the contact angle should be larger than 90° for stable nanowire growth [20]. In the particle-substrate geometry, the contact angle of the particle could be smaller but still it should be larger or close to 90° to initiate nanowire growth. Hence we decide that the optimum condition for Sn droplets formation happens at 550°C where a moderate contact angle and uniform particle diameter can be obtained.

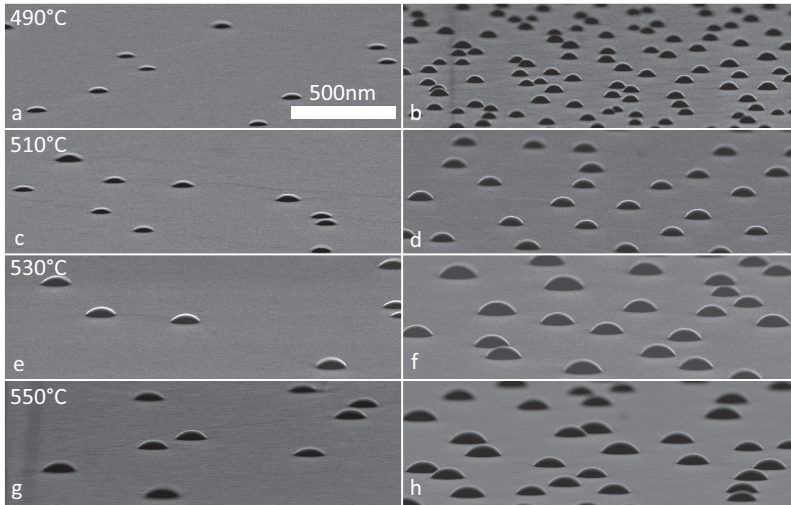


Figure 1. Sn particles deposited on InAs (111)A (left column) and (111)B (right column) substrates with increasing temperature from 490°C to 550°C respectively. Figures are taken at 85° tilt.

3.2 Study on InAs nanowire growth

We next studied the epitaxial growth of InAs nanowires with Sn droplets deposited at 550°C on InAs (111)A and (111)B substrate. Figure 2 shows InAs nanowires grown with a V/III ratio of 91.6 at 455°C, 490°C and 500°C respectively. In general, the growth rate of InAs nanowires are much higher on (111)B substrate than on (111)A. However, straight and vertically aligned InAs nanowire can only be observed on InAs (111)A substrate at selected temperatures and conversely on InAs (111)B substrate, the nucleated nanowires are non-vertical and inclined together with substantial parasitic surface growth at the base of the nanowires. Hence, we will focus the study on the growth of straight and vertical InAs nanowires on InAs (111)A substrate.

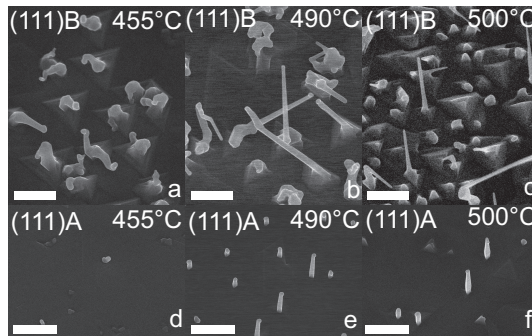


Figure 2. Sn seeded InAs nanowires grow on InAs (111)A and (111)B substrate with a constant V/III ratio of 91.6 at various temperatures. Straight and vertically-aligned InAs nanowires can be obtained at selected temperatures on InAs (111)A surface.

The effect from substrate temperature on the growth of InAs nanowires on (111)A substrate has been investigated where the V/III ratio is fixed constantly at 91.6. As shown in figure 3, the nanowire has been grown at a temperature from 455°C to 510°C in 3a-e, successful nanowire growth can be observed only within 473°C to 500°C in 3b-d. The suitable temperature range for Sn seeded InAs nanowire growth is much narrower compared to Au seeded InAs nanowires which can be from 380°C to 500°C.[12][21] The nanowire axial growth rate slightly increases from 473°C to 490°C, however at 490°C the nanowire growth rate is not uniform over the substrate. From 490°C to 500°C the axial growth rate drops with increasing radial growth on the nanowire sidewall. No obvious nanowire growth is observed at lower temperature of 455°C and higher temperature of 510°C.

There is also a strong edge effect observed for the sample in figure 3c as shown in SI 3, where uniform InAs nanowire growth can be observed at the edge of the substrate where we expect more decomposition of the precursor can occur. This indicates the nanowire growth in substrate center could be limited by the total precursor flow, Based on this observation, InAs nanowires are optimized with double total flow at a temperature of 490°C with a V/III ratio of 91.6 as shown in figure 3f. Close to the base of the nanowire, it exhibits a hexagonal cross section for a length of about 400nm, which is attributed to the radial overgrowth of the nanowire. Towards the top of the nanowire, the number of side facets changes from 6 to 3 resulting in a triangular cross section. This indicates that In diffusion length on InAs nanowire side facet is around 400nm. At the top part of the InAs nanowire where it has a triangular cross section, the side facets are proved to be (112)A which is identical to Sn seeded GaAs nanowires.

Transmission electron microscopy was used to characterize the nanowire grown at optimized condition as in figure 3f. From HRTEM and diffraction pattern in figure 4c, one can see that the nanowire is pure zincblende without any defects along the nanowire. The contrast in the Sn particle indicates phase segregation in the particle. XEDS results reveal that the particle at the tip consists mainly of Sn but also strong As signal. The bottom part of the nanowire which has more surface over-growth has unrelaxed strain as can be seen from the contrast in the dark field image. For Sn-seeded GaAs nanowire growth, Sn particle remains at the tip with a flat interface, which is normal to the growth direction. However, in this case Sn particle seems to slide off from the tip of the nanowire and the interface between the seed particle and

growth front seems to be tilted as shown in figure 4b. This has been observed by Wang et al [22], by manipulating the In composition in Au particle, the growth direction of InP nanowires can be switched between (100) and (111). After switching the growth direction back to (100), the Au particle sits at a tilted interface which is not perpendicular to the nanowire growth direction. In our case, the particle sliding is very likely coming from the cooling process after the nanowire growth when the TMIn precursor is turned off and the particle composition drifts from the growth composition. Within the investigated growth temperature window, TEM is used to investigate the crystal structure of representative nanowire. Interestingly, all of them show zinc blende crystal structure and no stacking defects can be observed. However, for Au seeded (111)B InAs nanowires, the growth in this temperature range usually leads to mixed crystal structure between zinc blende and wurzite. It has been observed that palladium seeded (110) InAs nanowires are also defect free zinc blende [13]. It has also been reported that defect-free Au-seeded GaAs nanowires can be achieved in (111)A direction [23]. It is very likely that the crystal structure of the nanowires is closely related to the nanowire growth direction.

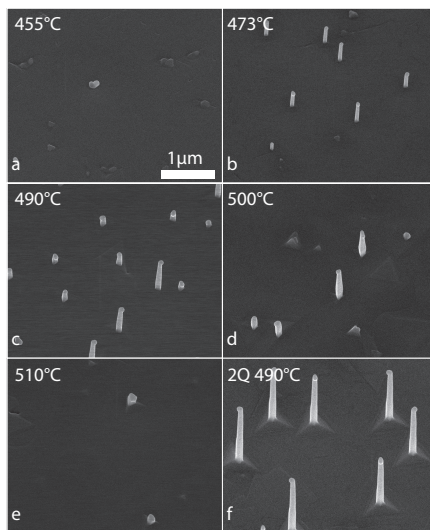


Figure 3. Growth of Sn seeded InAs nanowires on InAs (111)A substrate at constant V/III ratio of 91.6 with different temperatures (a) to (e). Suitable growth window is within 473°C to 500°C. Optimum InAs nanowire growth is achieved with double precursor flow for the growth of InAs nanowires at 490°C with V/III ratio of 91.6 (f).

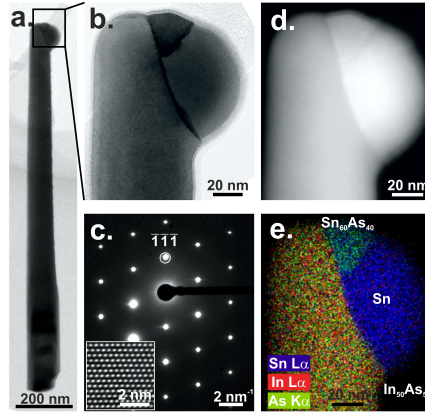


Figure 4. Bright field overview TEM image of a single nanowire grown at 490 °C viewed along the $\langle 110 \rangle$ zone axes in a, with a higher magnification of the top part from the same nanowire shown in b. A pure ZB crystal structure can be recognized from characteristic diffraction pattern as well as high-resolution image in c. Dark-field image and elemental mapping of the same nanowire in d and e.

3.3 Electrical Characterization

IV characteristics were taken from more than 20 nanowires in a voltage range of $V_D = \pm 10 \text{ mV}$ and a back gate voltage V_G of $\pm 15 \text{ V}$. The IV- characteristics of a Sn seeded InAs nanowires reveal linear ohmic behavior as can be seen in figure X a). The contact resistance was determined to be lower than 100Ω . The nanowire geometry was approximated by a cylindrical model with an average diameter of the nanowire D_{NW} and the nanowire length L_{NW} between the contacts. The resistivity of the nanowire was calculated according to $\rho = R \cdot D_{NW} / 2\pi \cdot L_{NW}$. The resistance R of the nanowires was determined through a linear fit of the IV- characteristic at a back-gate voltage of $V_G = 0 \text{ V}$. A resistivity in the range of $0.04 - 0.27 \times 10^{-3} \Omega \text{ cm}$ was calculated which is plotted in figure X b). The low resistivity of the nanowires proves the growth with Sn seed particle as a very efficient way to achieve high doping levels in InAs nanowires in comparison to other dopant sources [8][24]. Measurements of different segments of a single nanowire further show a uniform resistivity along the growth direction of the nanowire which confirms a uniform doping incorporation during growth. Back gated measurements show an n-type behavior of the nanowires however the influence of the gate voltage is very low which also confirms the high doping level. The highly n-doped Sn seeded InAs nanowires show beside their low resistivity also the capability to withstand high current densities J [8]. As shown in the

inset in Figure X a) a nanowire with an average diameter of 75nm is able carry a current of $I_D=1.3\text{mA}$ which corresponds to a current density of $J_{NW}=2.9\text{A/cm}^2$.

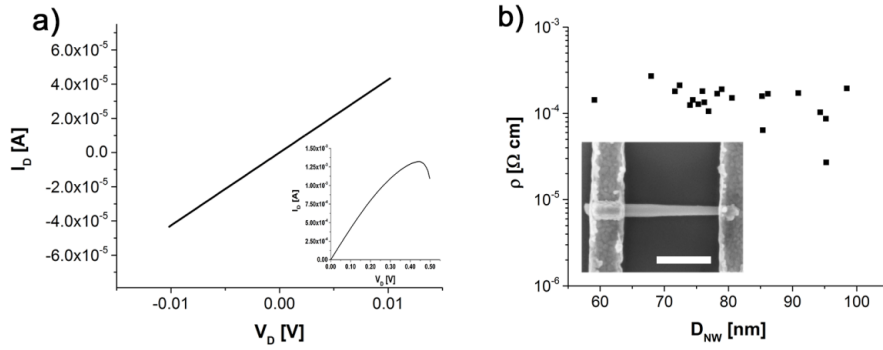


Figure 5: a. ID-VD sweep of a Sn seeded InAs nanowire at a back gate voltage $V_G = 0\text{V}$. The IV-characteristic shows linear contact behavior and very low resistance of the measured wire. The inset shows the IV-characteristic of a Sn seeded InAs nanowire with a diameter of 75nm measured up to a very high breakdown current of 1.3mA. b. Nanowire resistivity plotted against nanowire diameter. The resistivity is in the range of $0.04 - 0.27 \times 10^{-3} \Omega \text{ cm}$ and shows no significant dependence on the diameter. Inset: Sb seeded InAs nanowire in a two point back gate geometry with Ni-Au contacts (scale bar = 200nm)

3.4 Surface Characterization by STM

STM images in Figure 6 show that this procedure has been effective for both the oxide-free (a) InAs(111)B substrate and (b) (110) side facet of a Sn-seeded InAs NW. STS was then performed at various locations on these flat terraces by turning off the feedback loop of the STM and measuring the tunneling current between the tip and the sample while ramping the voltage. I-V curves for both the substrate (green triangles) and NW side facet (blue triangles) are shown in Fig 6 (c). The logarithmic of the current (absolute magnitude) as a function of tip bias is sensitive also to very small tunneling currents, which are obtained at small voltages close to the valence and conduction band (VB and CB) edges.

For the InAs(111)B substrate the I-V curve shows a very small, but clearly detectable current even at small voltages, resulting in an apparent band gap of significantly less than 0.36 eV, the literature value for bulk InAs. This behavior can be attributed to the presence of surface states, which are expected for the polar (111)B surface. The I-V spectra from the (110) nanowire side facet, on the other hand, show a clear decrease of the current towards the VB (negative sample bias) and the CB (positive sample bias) onset, with an apparent band gap (area with no measurable current) amounting to 0.4 eV, which agrees well both with the InAs bulk band gap and with previous STS

results from InAs(110) nanowire side facets [25]. The surface Fermi level is found to be located within the band gap, but closer towards the CB edge, corresponding to a weakly n-type behavior of the nanowire surface. This result is surprising insofar as electrical measurements showed n-type behavior of the NWs with high doping levels, and it indicates Fermi-level pinning at the NW surface.

We performed additional STS on the topmost area of an InAs NW where the Sn seed particle should be and obtained much larger apparent band gaps. An STM overview of the NW indicating the position of the Sn particle is shown in Fig. 6(d). The resulting I-V curves taken at two different locations on or near this particle are shown in Fig. 6(e). The first trace (red crosses) shows an estimated E_g of 0.9 eV and the second (pink diamonds) a larger E_g approximated between 2-3eV. These STS traces are the result of single measurements unlike those in Fig. 6(c), so there is a larger uncertainty in these estimates. We do not know exactly the chemical composition of the surface of the Sn particle or the nearby particle-NW interface, but the observed band gaps may be representative of both SnO₂ which has an $E_g \approx 3.6$ eV and SnO that has an indirect band gap of 0.7eV [26]. This larger band gap behavior was only observed at the location of the Sn particle and not elsewhere on the NW sidewalls.

Let us now come back to possible Sn segregation to the NW surface: In the case of extensive Sn clustering or the presence of a metallic Sn shell on the surface of the NW formed by extensive Sn segregation during growth, we would expect to see metallic behavior in the STS spectra, which we do not observe at all. We can also exclude the presence of a thick Sn oxide shell on the NW sidewall, which would result in larger band gap values than those obtained here. It should also be noted that any Sn oxides are stable until temperatures in excess of 1000°C and would thus be unaffected by the H cleaning process. We can also rule out substantial alloying of Sn with In since a thick shell of indium tin oxide (ITO), (74% In, 8% Sn, and 18% O₂), would present a large $E_g \approx 4$ eV [27]. Instead, our STM measurements on flat NW sidewalls result in E_g values that are typical for InAs (110) facets. However, we cannot rule out the presence of a very thin layer (<1nm) of insulating Sn oxide, that would be transparent to the STS/STM investigation as electrons would tunnel through to probe/image the underlying InAs surface. In fact, such an ultrathin amorphous oxide layer could be the reason for the Fermi-level pinning within the band gap of the NW surface as observed by STS. It might further explain the absence of atomic ordering in the STM images (which, however, could also be due to the state of the

STM tip). On the other hand, it cannot be thicker than one or two InAs atomic layers, as the nanowire sidewall imaged in Fig. 6(b) is still atomically flat with clear atomic-scale surface steps.

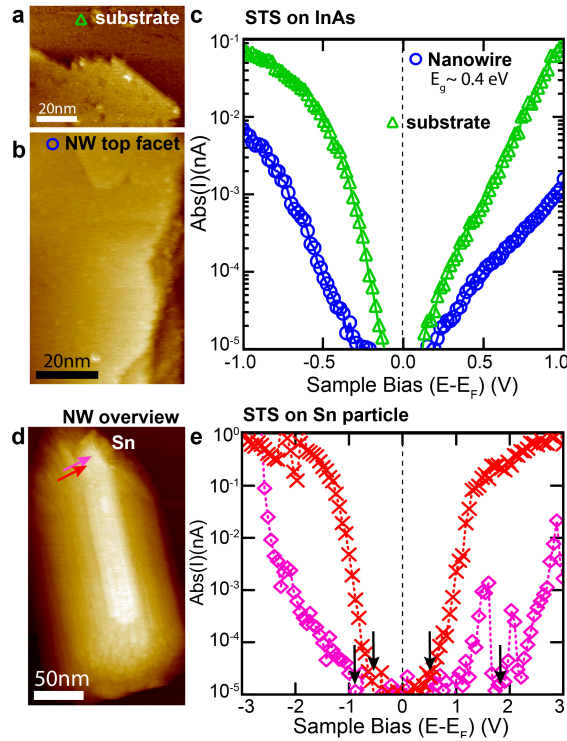


Figure 6. (a) InAs(111)B substrate and (b) side wall facet of an Sn-seeded InAs NW showing the clean (110) surface where STS measurements were taken from. (c) STS of a clean (110) top facet of a Sn-seeded InAs NW (blue) and of the InAs(111)B substrate (green). Seven (four) individual spectra from the same area were averaged to generate the shown NW (substrate) spectrum. (d) STM overview of the NW including the Sn particle. (e) STS of the Sn particle at the top of the NW show a larger 1-3 eV band gap.

4. Conclusion

We have investigated the growth of InAs nanowires seeded by in-situ formed Sn particles in MOVPE. We have found that the diameter, density and contact angle of the Sn particles formed on InAs (111)A and (111)B substrates are dependent on the deposition temperature. Sn seeded InAs nanowire growth has been performed and straight and vertical-aligned nanowires are found on (111)A substrate. TEM reveal that all the (111)A InAs nanowires have pure zincblende crystal structure without any stacking defects or twin planes. Electrical measurement confirms that the (111)A InAs nanowires are highly-doped. STM results exclude thick Sn and SnO layer on the

nanowire side facet which indicates that Sn is uniformly incorporated into the nanowire which contributes to the high n-doping profile.

References:

- [1] Dick K a and Caroff P 2014 Metal-seeded growth of III-V semiconductor nanowires: towards gold-free synthesis. *Nanoscale* **6** 3006–21
- [2] Das A, Ronen Y, Most Y, Oreg Y, Heiblum M and Shtrikman H 2012 Zero-bias peaks and splitting in an Al-InAs nanowire topological superconductor as a signature of Majorana fermions *Nat. Phys.* **8** 887–95
- [3] Egard M, Johansson S, Johansson A C, Persson K M, Dey A W, Borg B M, Thelander C, Wernersson L E and Lind E 2010 Vertical InAs nanowire wrap gate transistors with $f_t > 7$ GHz and $f_{max} > 20$ GHz *Nano Lett.* **10** 809–12
- [4] Nilsson M, Namazi L, Lehmann S, Leijnse M, Dick K A and Thelander C 2015 Single-electron transport in InAs nanowire quantum dots formed by crystal phase engineering
- [5] Miao J, Hu W, Guo N, Lu Z, Zou X, Liao L, Shi S, Chen P, Fan Z, Ho J C, Li T X, Chen X S and Lu W 2014 Single InAs nanowire room-temperature near-infrared photodetectors *ACS Nano* **8** 3628–35
- [6] Wirths S, Weis K, Winden A, Sladek K, Volk C, Alagha S, Weirich T E, Ahe M Von Der, Hardtdegen H, Demarina N, Grützmacher D, Schäpers T, Wirths S, Weis K, Winden A, Sladek K, Volk C, Alagha S and Weirich T E 2017 Effect of Si-doping on InAs nanowire transport and morphology **53709**
- [7] Ghoneim H, Mensch P, Schmid H, Bessire C D, Rhyner R, Schenk A, Rettner C, Karg S, Moselund K E, Riel H and Björk M T 2012 In situ doping of catalyst-free InAs nanowires. *Nanotechnology* **23** 505708
- [8] Thelander C, Dick K a, Borgström M T, Fröberg L E, Caroff P, Nilsson H a and Samuelson L 2010 The electrical and structural properties of n-type InAs nanowires grown from metal-organic precursors. *Nanotechnology* **21** 205703
- [9] Caroff P, Dick K a, Johansson J, Messing M E, Deppert K and Samuelson L 2009 Controlled polytypic and twin-plane superlattices in iii-v nanowires. *Nat. Nanotechnol.* **4** 50–5
- [10] Nanowires I, Thelander C, Caro P, Dey A W and Dick K A 2011 Effects of Crystal Phase Mixing on the Electrical Properties of InAs Nanowires 2424–9
- [11] Johansson J, Dick K a., Caroff P, Messing M E, Bolinsson J, Deppert K and Samuelson L 2010 Diameter dependence of the wurtzite-zinc blende transition in inas nanowires *J. Phys. Chem. C* **114** 3837–42
- [12] Dick K a., Bolinsson J, Messing M E, Lehmann S, Johansson J and Caroff P

- 2011 Parameter space mapping of InAs nanowire crystal structure *J. Vac. Sci. Technol. B Microelectron. Nanom. Struct.* **29**04D103
- [13] Xu H, Wang Y, Guo Y, Liao Z, Gao Q, Tan H H, Jagadish C and Zou J 2012 by Palladium
- [14] Sun R, Jacobsson D, Chen I-J, Nilsson M, Thelander C, Lehmann S and Dick K a. 2015 Sn-seeded GaAs nanowires as self-assembled radial p-n junctions *Nano Lett.* 150519161550005
- [15] Hilner E, Ha U, Fro L E, Karlsson M, Kratzer P, Lundgren E, Samuelson L and Mikkelsen A 2008 Direct Atomic Scale Imaging of III - V Nanowire Surfaces
- [16] Tornberg M, Mårtensson E K and Zamani R R 2016 Demonstration of Sn-seeded GaSb homo- and GaAs – GaSb heterostructural nanowires
- [17] Moll N, Scheffler M and Pehlke E 1998 Influence of surface stress on the equilibrium shape of strained quantum dots *Phys. Rev. B* **58** 4566–71
- [18] Björk M T, Schmid H, Breslin C M, Gignac L and Riel H 2012 InAs nanowire growth on oxide-masked $\langle 111 \rangle$ silicon *J. Cryst. Growth* **344** 31–7
- [19] Lee J, Shimoda W and Tanaka T 2004 Surface Tension and its Temperature Coefficient of Liquid Sn-X (X = Ag , Cu) Alloys **45** 2864–70
- [20] Nebol V A and Shchetinin A A 2003 Role of Surface Energy in the Vapor – Liquid – Solid Growth of Silicon **39** 899–903
- [21] Joyce H J, Wong-leung J, Gao Q, Tan H H and Jagadish C 2010 Phase Perfection in Zinc Blende and Wurtzite III - V Nanowires Using Basic Growth Parameters 908–15
- [22] Wang J, Plissard R, Verheijen M A, Feiner L, Cavalli A and Bakkers E P A M 2013 Reversible Switching of InP Nanowire Growth Direction by Catalyst Engineering
- [23] Wacaser B A, Deppert K, Karlsson L S, Samuelson L and Seifert W 2006 Growth and characterization of defect free GaAs nanowires **287** 504–8
- [24] Park D W, Jeon S G, Lee C, Lee S J, Song J Y, Oh J, Noh S K, Leem J and Kim J S Structural and electrical properties of catalyst-free Si-doped InAs nanowires formed on Si (111) *Nat. Publ. Gr.* 1–8
- [25] Hjort M, Lehmann S, Knutsson J, Zakharov A A, Du Y A, Sakong S, Timm R, Nylund G, Lundgren E, Kratzer P, Dick K A and Mikkelsen A 2014 Electronic

and Structural Differences between Wurtzite and Zinc Blende InAs Nanowire Surfaces : Experiment and Theory 12346–55

- [26] Ogo Y, Hiramatsu H, Nomura K, Yanagi H, Kamiya T, Hirano M, Ogo Y, Hiramatsu H, Nomura K, Yanagi H and Kamiya T 2016 -channel thin-film transistor using -type oxide semiconductor , SnO p -channel thin-film transistor using p -type oxide semiconductor , SnO **32113** 1–4
- [27] Kim H, Gilmore C M, Piqué A, Horwitz J S, Mattoussi H, Murata H, Kafafi Z H and Chrisey D B 2000 Electrical , optical , and structural properties of indium – tin – oxide thin films for organic light-emitting devices Electrical , optical , and structural properties of indium – tin – oxide thin films for organic light-emitting devices **6451**

Supplementary information

Rong Sun¹, Karl Winkler¹, Sarah McKibbin², Jonas Johansson¹, Rainer Timm², Sebastian Lehmann¹
and Kimberly A. Dick^{1,3}

¹ Solid State Physics, Lund University, Box 118, S-22100 Lund, Sweden

² Department of Physics, Lund University, Box 118, S-22 100 Lund, Sweden

³ Center for Analysis and Synthesis, Lund University, Box 124, S-22100 Lund, Sweden

S1. Diameter and density distribution of Sn particles formed on InAs (111)A and (111)B substrate

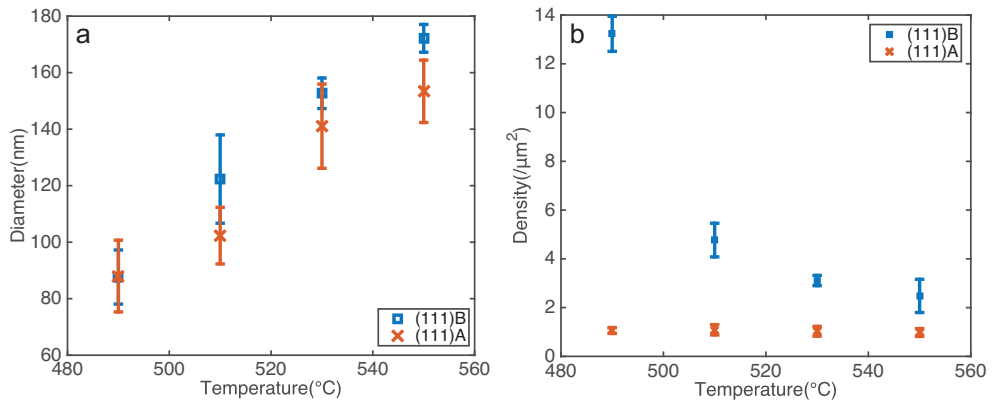


Figure S1: The diameter (a) and density (b) distribution of the in situ-formed Sn nanoparticles with respect to the growth temperature. The blue squares represent (111)B substrates and red crosses represent (111)A substrates.

S2. Wetting angle extraction from tilted view images

Here we explain how to measure the wetting angle of a spherical cap-shaped drop, thinner than a hemisphere, resting on a flat surface when the drop is viewed from an angle β ($0 \leq \beta < 90^\circ$), where $\beta = 0$ corresponds to side view and $\beta = 90^\circ$ corresponds to top view.

The system is illustrated in Fig. S2

, where all distances, vectors, and angles are indicated. The angle θ is the sought wetting angle and the angle θ' is the projected contact angle, as directly observed in the view tilted by an angle β .

Now we construct the plane P with the normal $\vec{n} = (0, \sin \theta, \cos \theta)$, given by the equation $y \sin \theta + z \cos \theta = R$. The wetting angle θ is the angle between the vectors $\vec{b} = (0, -1, 0)$ and $\vec{v}_0 = (0, -\cos \theta, \sin \theta)$ and the angle θ' is the angle between \vec{b} and \vec{v}_β . The key point in this analysis is that the vectors \vec{v}_0 and \vec{v}_β both are orthogonal to \vec{n} . The vector \vec{v}_β is given by the equations $\vec{v}_\beta \cdot \vec{v}_0 = \cos \beta$, $\vec{v}_\beta \cdot \vec{n} = 0$, and a normalization condition $|\vec{v}_\beta| = 1$.

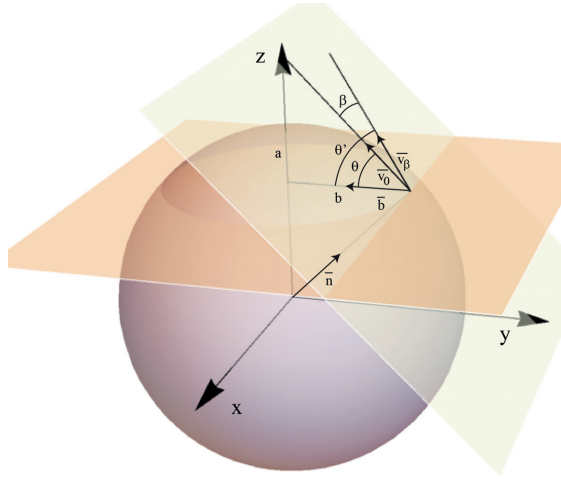


Fig. S2 Schematic image of a spherical cap resting on a surface. The height of the cap is a and the radius of its bottom area is b .

As $\cos \theta' = \vec{b} \cdot \vec{v}_\beta$ we have established a relation for the three angles,

$$\cos \theta' = \cos \beta \cos \theta. \quad (\text{S1})$$

In principle we are done here. However, using a protractor to directly measure the angle θ' in e.g. a scanning electron micrograph is not very accurate. It is better to measure the distances.

So what remains is to express θ' in a , b , and β . The standard equations for the geometry of a spherical cap give

$$\cos \theta = \frac{b^2 - a^2}{b^2 + a^2}, \quad (\text{S2})$$

and correspondingly

$$\cos \theta' = \frac{b^2 - a'^2}{b^2 + a'^2}, \quad (\text{S3})$$

where a' is defined in Fig. S3. It is, however, easiest to measure the total projected thickness, $h = a' + b'$, just as the total width $2b$ is measured, see Fig. S3. As $b' = b \sin \beta$, we have that

$$a' = h - b \sin \beta. \quad (\text{S4})$$

Combining Eqs. S1, S3, and S4 yields a final expression for the wetting angle in terms of distances directly measured in a tilted view image where the tilt angle is β ,

$$\cos \theta = \frac{1}{\cos \beta} \frac{b^2 - (h - b \sin \beta)^2}{b^2 + (h - b \sin \beta)^2}. \quad (\text{S5})$$

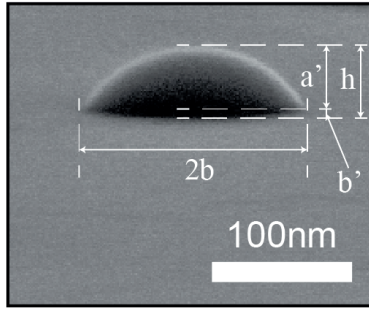


Fig. S3 Scanning electron micrograph of an Sn drop on an InAs (111)B surface. The tilt angle is $\beta = 85^\circ$.

S3. Difference between the center and edge of growth substrate

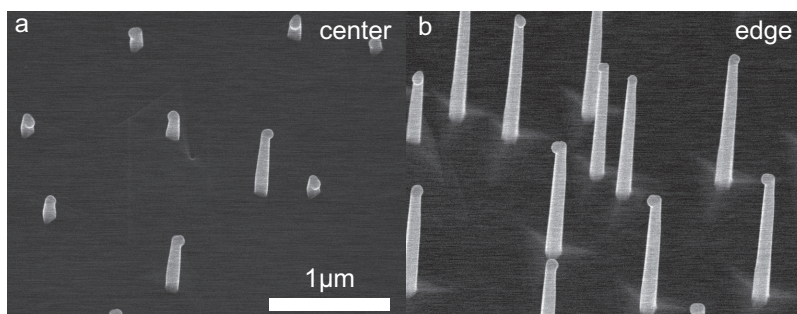


Figure S4. Sn-seeded InAs nanowire growth at 490C with a V/III ratio of 91.6 in the center of the (111)A substrate as in a and at the edge as in b.

S4. STM overview image showing InAs nanowire side facets

An STM overview image of an H-cleaned Sn-seeded InAs NW lying on an InAs(111)B substrate is shown in Fig. S5 (a). The observed broadening is a tip artifact often observed for STM imaging of nanowires. Observations of flat facets were rare though in some instances we observed highly vicinal (110) surfaces, shown by the close up STM image in (b). The NW sidewalls were more frequently observed to contain substantial roughness and in some cases as shown in (c) islanding typical for (111) surfaces. This supports the observation that the NWs contain (112) sidewalls which may be made up of small alternating (111)A/B surfaces.[1] These NWs required several rounds of atomic H cleaning for successful STM imaging, likely due to the highly faceted and rough nature of the (112) side walls which contain complex reconstructions difficult to image with STM.

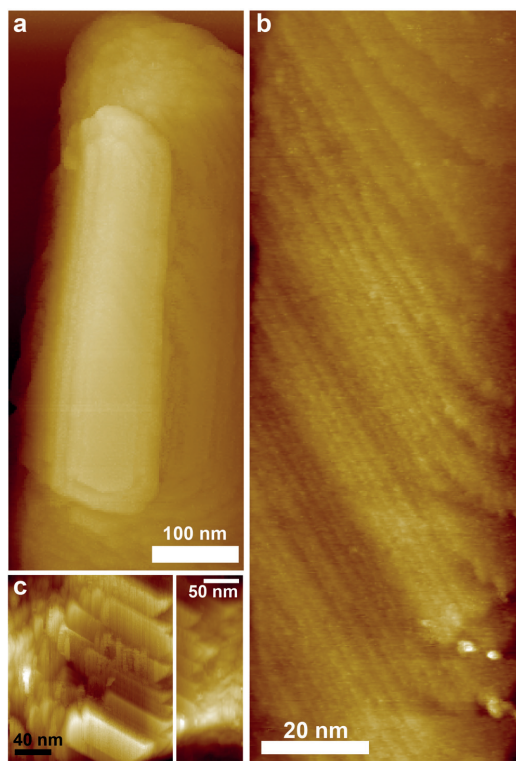


Figure S5. STM images of the Sn seeded NW after H cleaning that exhibited a triangular shape (a) NW overview, (b) a highly stepped surface showing extremely small (110) terraces (c) islanding and rough surfaces of a NW. $V=-2.3\text{V}$, $I=60\text{pA}$.

Paper IV



Thermodynamic understanding on the effect of V/III ratio for the growth of Sn seeded InAs nanowires

Rong Sun¹, Jonas Johansson¹, Kimberly A. Dick^{1,2}

¹ Solid State Physics, Lund University, Box 118, S-22100 Lund, Sweden

² Center for Analysis and Synthesis, Lund University, Box 124, S-22100 Lund, Sweden

Abstract

It has been previously reported that the epitaxial growth of InAs nanowires can be initiated with Sn seed particle in Metal Organic Vapor Phase Epitaxy(MOVPE). In this paper, we investigate the effect of precursor flows on the growth mechanism of Sn seeded InAs nanowire. We find that the nucleation of InAs nanowires from the growth substrate is a critical step for vertical nanowire growth. The nanowire nucleation rate decreases with increasing TMIn flow and increases with AsH₃ flow. To understand this we have calculated an isothermal section of the ternary phase diagram for the Sn-In-As system. We find that the nucleation of InAs nanowires from Sn catalytic particles requires enough As content in the Sn particle to reach supersaturation.

Introduction

Previously, we have shown that with in-situ formed Sn droplets, it is possible to achieve highly doped pure zincblende GaAs nanowires with a C-doped p-type shell and a Sn-doped n-type core in the MOVPE system without the addition of extra doping precursors during nanowire growth [1]. It has been observed that the Sn droplet is gradually consumed and also incorporated into the GaAs nanowires during growth. Defect free zincblende GaAs nanowires can be achieved at selected growth conditions. Unlike Au seeded GaAs nanowires, in which usually a Ga rich Au particle is found during and after growth [2], an As rich Sn particle is identified after growth in this system which also indicates that Sn is more likely to alloy with As. Recently, we have managed to extend the use of Sn particle to the InAs system, which is of interest due to its high n-doped properties for electrical devices. However, the understanding of how Sn particle behaves in this system is still lacking.

It is commonly accepted that for the growth of Au seeded GaAs or InAs nanowires, a

Au-Ga or Au-In alloy is active in initiating the nanowire growth. And it has been proven that the solubility of As in Au nanoparticle is extremely low compared to the group III element. From binary phase diagrams of Au-Ga and Au-In, one can see that there are several intermetallic compounds including Au_2Ga , AuGa , and AuGa_2 in the former case [3] and in the latter case Au_4In , $\text{Au}_{10}\text{In}_3$, Au_3In , Au_7In_3 , AuIn and AuIn_2 [4]. In both cases the terminal phases are the solid group III solution (Ga or In) and the pure (Au). While for binary phase diagram of Au-As, there are no intermetallic compounds available at room temperature and above the eutectic point at 636C, everything becomes liquid.

In the binary phase diagram of Sn-Ga, the eutectic point is at 30C and no compound form exists [5] which is very similar to the Au-As binary phase diagram. But in the Sn-In system, there are two compounds available, namely $\text{In}_{0.75}\text{Sn}_{0.25}$ and $\text{In}_{0.2}\text{Sn}_{0.8}$ with pure (In) and pure (Sn) as terminating phases [6]. The Sn-As system consists of two intermetallic compounds, AsSn and As_3Sn_4 . The terminal phases are the solid solution (As) and the pure (Sn) [7]. The Sn-As phase diagram is comparable to the Au-Ga/In phase diagram. In the case of Sn seeded GaAs nanowires, it is assumed that an effective Sn-As liquid alloy facilitates the nanowire growth and from the perspective of phase diagram there are also intermetallic compounds of Sn-As existing. Considering the fact that there also exist intermetallic compounds of Sn-In in the phase diagram, thus it would be interesting to see in the growth of InAs nanowires, if Sn behaves more like Au which would alloy with In or it's identical in the case of Sn seeded GaAs nanowires where Sn is more likely to alloy with As.

Experimental methods:

Nanowire growth is performed using InAs (111)A substrates placed in an Aixtron 3x2" close coupled showerhead (CCS) reactor at a pressure of 100 mbar, a total flow of 8 l/min. Substrates are first heated to an annealing temperature of 560 °C in arsine (AsH_3) background with molar fraction $2.5\text{E-}05$. After 10 min annealing, samples are cooled to 525 °C in arsine. Once the temperature has stabilized AsH_3 is changed to $2.8\text{E-}05$ and a TESn flow with molar fraction $4.3\text{E-}05$ is introduced. Following a 15 min deposition unless specified otherwise, TESn is turned off and the samples cooled to the desired growth temperature (in the range 455 – 510 °C) in arsine ambient. Once growth temperature is reached, trimethylindium (TmIn) is turned on with a desired molar fraction. Nanowires are grown for 40 min unless otherwise stated.

Morphology is characterized by scanning electron microscopy (SEM; Hitachi SU8010 at 15 kV).

Results and discussion

The formation of Sn particles on InAs substrates has been studied and discussed elsewhere. It has been decided that the optimized condition for Sn particle formation is at 560C and the density of formed Sn droplets is $1.2 \pm 0.2 / \mu\text{m}^2$. In the section, we focus on the effect of V/III ratio on InAs nanowire nucleation and growth.

Growth of InAs nanowires

The growth of InAs nanowires has been performed from Sn droplets with Trimethylindium and AsH₃ as precursors. The growth of InAs nanowires behave very differently on InAs (111)A and (111)B substrate, which will be discussed in details elsewhere. Here, we will focus the discussion on InAs nanowire growth on (111)A substrate. It has been studied that the suitable temperature range for Sn seeded InAs nanowire growth is between 473C to 500C. Here the effects from vapor V/III ratio on the growth of InAs nanowires at 473C are investigated. The V/III ratio is varied by both altering TMIn flow rate at a fixed AsH₃ flow rate and vice versa.

For Sn seeded InAs nanowires, the V/III ratio can be tuned within a wide range from 61.1 to 366.5, which interestingly is much higher than the V/III window for Sn-seeded GaAs and in fact very comparable to Au-seeded InAs [8].

The effect of TMIn on the growth of InAs nanowire is investigated by varying the molar fraction of TMIn from $7.3\text{E-}6$ to $1.2\text{E-}6$ at a constant AsH₃ flow of $4.4\text{E-}4$ at 470C. The equivalent V/III ratio is from 61.1 to 366.5. As shown in figure 1, the density of nucleated InAs nanowires increases dramatically with decreasing TMI flow thus increasing V/III ratio. At a V/III ratio of 183.2 and higher up to 366.5, the nucleation rate from Sn particles is close to 100% which resulting in a nanowire density of $1.2 \pm 0.2 / \mu\text{m}^2$. When increasing TMIn flow resulting a V/III ratio in the range of 91.6 to 122.2, the nucleation rate drops about 20%. With further addition of TMIn flow into the reactor, only 40% to 50% of the Sn droplets lead to successful nucleation of InAs nanowires. It could be that for successful nanowire nucleation from Sn droplets, only a limited amount of In content in the particle is required. When In reaches its threshold condition in the Sn droplets, the particle will become an In

rich droplet which can change the contact angle between the droplet and the substrate which might hinder the nucleation of the nanowires.

Moreover, it seems that the growth rate of the InAs nanowires is also closely associated with TMIn flow. At high TMIn flow figure 1a, the length of nanowires is more uniform compared to the nanowires at low TMIn flow figure 1f where there is a big variation in the length of the nucleated nanowires.

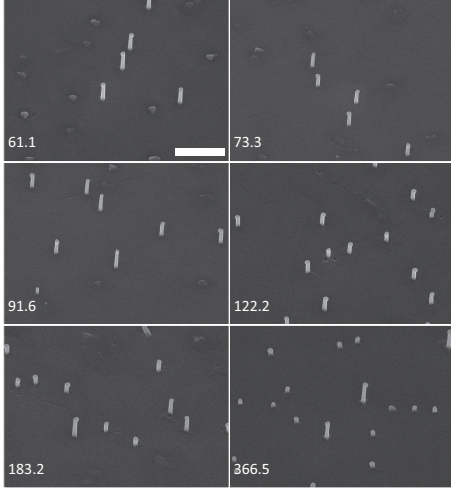


Figure 1. Sn seeded InAs nanowire growth with varied TMIn flow at constant AsH₃ flow corresponding to V/III ratio from 61.1 to 366.5.

In order to understand the nucleation and growth of the nanowires in figure 1f, a series of experiments are conducted by shortening the growth time stepwise from 40min to 5min while keeping the other growth parameters constant as shown in figure 2. As can be seen from figure 2, the critical nucleation time is around 5min. From 10min to 40min, the length of the longer nanowires increases while the length of short nanowires does not seem to change with growth time. It might be that after the critical nucleation time, the nanowire growth rate is limited by TMIn precursor flow.

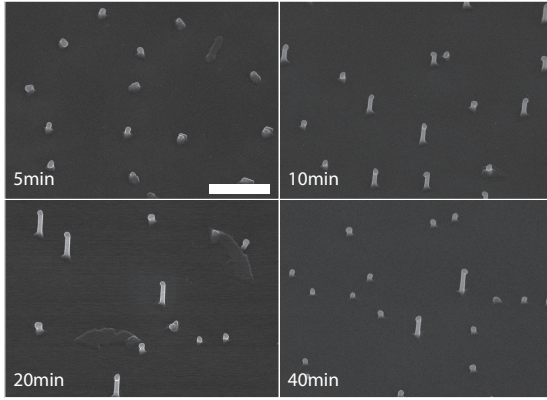


Figure 2. Time series for Sn seeded InAs NW growth at V/III ratio of 366.5.

In order to study the effect of AsH₃ flow, InAs nanowire growth is performed with varied AsH₃ flow from 3.3E-4 to 6.7E-4 while keeping TMI flow constant at 4.9E-6 at 470C. As can be seen from figure 3, the V/III ratio is changed in the range of 31.4 to 137.4. Within the V/III range between 68.7 and 137.4, InAs nanowires have identical nucleation rates and growth rate. It seems that AsH₃ has very little effect on nanowire nucleation and growth. However, with lower AsH₃ flow rate which corresponding to lower V/III ratio, the nucleation rate of the nanowires drops drastically and eventually at a V/III ratio of 31.4, there is no vertical nanowires can be observed. At lower V/III ratio, there is more parasitic surface growth instead. This phenomenon is consistent with the trend that has been observed when varying the TMI flow. At lower AsH₃ flow, which means lower V/III ratio, there might be more TMI precursor available in the vapor and more In adatoms diffusing on the substrate and also incorporated into Sn droplets. However, the excess accumulation of In in Sn droplets destroys the balance between the group III and group V elements in the particle. This can be explained by the ternary phase diagram of the Sn-In-As system. In figure 4, we show an isothermal section calculated at 473C with the data in ref [7]. Here it can be seen that for In concentration higher than approximate 4%, the As solubility rapidly decreases from around 15% to approximately 2% for pure In. This decrease in solubility is most pronounced for low value of In component, that is when In is increases from 4% up to 20%. Thus, an increased amount of In can make it more difficult to supersaturate the particle. Since the contact angle and surface energy are

associated with the particle composition, the abundant In in the droplet eventually kills the nanowire nucleation.

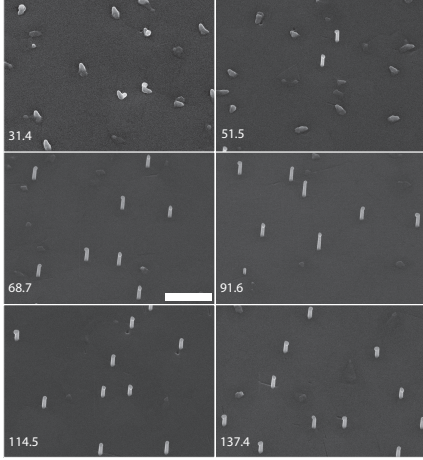


Figure 3. Sn seeded InAs nanowire growth with varied AsH₃ flow resulting in V/III ratio from 31.4 to 137.4.

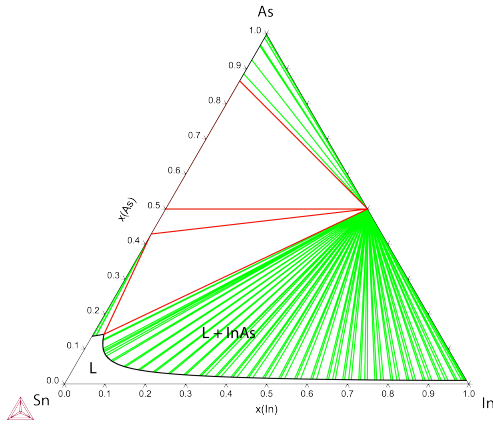


Figure 4. Calculated ternary phase diagram of Sn-As-In system at 473°C which is the growth temperature.

Based on what has been observed, it seems that in Sn seeded InAs nanowire growth the flow of TMIn precursor plays a very crucial role. In the nucleation step of the nanowire, TMIn has a poisoning effect on it. However, after successful nucleation from the Sn droplets, TMIn flow has an impact on the growth rate of the nanowire. To prove this, InAs nanowires are grown with a two-step growth approach, 5min nucleation at V/III ratio of 366.5 followed by 35min growth at V/III ratio of 61.1. As seen in figure 4, the nucleation rate of the nanowire is around 50% compared to Sn

droplets formed on bare InAs substrate. Moreover the length of the nanowires is about twice of that grown at a V/III ratio of 61.1. This indicates that the nucleation step at a higher TMIn flow which means a lower V/III ratio is more difficult and takes longer time compared to the nanowires which nucleate at lower TMIn flow.

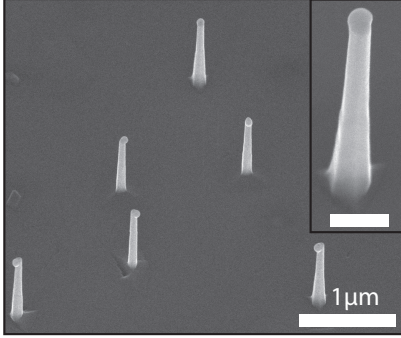
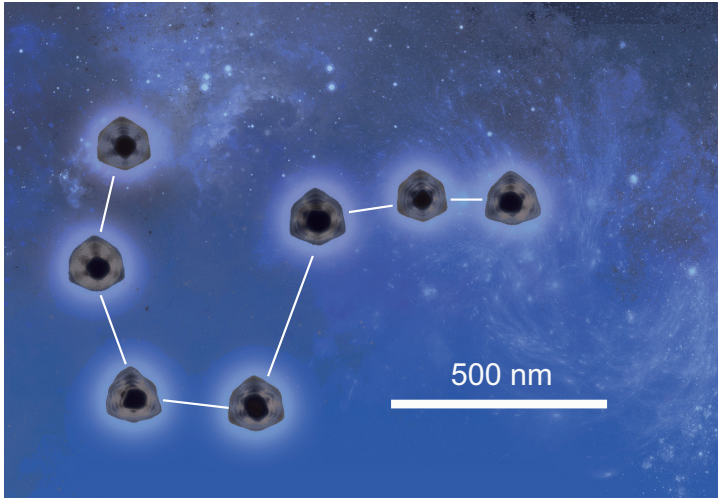


Figure 5. Sn seeded InAs nanowires nucleate for 5min at V/III ratio of 366.5 and grow for 35min at V/III ratio of 61.1. The scale bar in the magnified view is 200nm.

In summary, Sn seeded InAs nanowire growth on InAs 111A substrate has been demonstrated. The In content in Sn particle is of high significance during the growth: in the nucleation stage high In content in the Sn particle has a poisoning effect on the nanowire, once the nanowires are nucleated In has a big contribution in the InAs nanowire growth rate. By employing a two-step growth approach, where the nanowire nucleate at a high V/III ratio and grow at a relatively low V/III ratio, InAs nanowires can be grown with a good trade-off between the nucleation rate and growth rate.

- [1] Sun R, Jacobsson D, Chen I-J, Nilsson M, Thelander C, Lehmann S and Dick K a. 2015 Sn-seeded GaAs nanowires as self-assembled radial p-n junctions *Nano Lett.* 150519161550005
- [2] Jacobsson D, Panciera F, Tersoff J, Reuter M C, Lehmann S, Hofmann S, Dick K A and Ross F M 2016 Interface dynamics and crystal phase switching in GaAs nanowires *Nature* **531** accepted
- [3] Equilibrium T H E 1966 The equilibrium diagram of the system gold-gallium 42–51
- [4] Society R 1964 The equilibrium diagram of the system gold-indium 318–30
- [5] Anon 1992 The Ga-Sn (Gallium-Tin) S y s t e m **13** 181–9
- [6] Villars P and Okamoto H In-Sn Binary Phase Diagram 0-100 at.% Sn: Datasheet from “PAULING FILE Multinaries Edition – 2012” in SpringerMaterials (http://materials.springer.com/isp/phase-diagram/docs/c_0102112)
- [7] Ghasemi M, Selleby M and Johansson J 2017 Thermodynamic assessment and binary nucleation modeling of Sn-seeded InGaAs nanowires *J. Cryst. Growth* **478** 152–8
- [8] Dick K A., Bolinsson J, Messing M E, Lehmann S, Johansson J and Caroff P 2011 Parameter space mapping of InAs nanowire crystal structure *J. Vac. Sci. Technol. B Microelectron. Nanom. Struct.* **29** 04D103



The Starry Night – Sn-seeded nanowires grown in the Big Dipper pattern.